

RATIONAL LOAD RATING OF DECK-GIRDER BRIDGES WITH GIRDER END SHEAR
CRACKS IN REVERSE ORIENTATION

by

ANDREW BERNICA

B.S., Kansas State University, 2014

A THESIS

submitted in partial fulfillment of the requirements for the degree

MASTER OF SCIENCE

Department of Civil Engineering
College of Engineering

KANSAS STATE UNIVERSITY
Manhattan, Kansas

2016

Approved by:

Major Professor
Dr. Hayder Rasheed

Copyright

ANDREW BERNICA

2016

Abstract

Reverse diagonal shear cracking at the supports of many reinforced concrete girders is a phenomenon affecting a number of KDOT's low-volume bridges built in the early-to-mid 1900's. This phenomenon is not addressed in the AASHTO Bridge Design Manual (2002) or ACI specifications. This study investigates the causes of this cracking and creates BRIDGE (Bridge Rating of Inclined Damage at Girder Ends), an Excel-based software to determine the load rating of a user specified bridge exhibiting reverse diagonal shear cracking at the girder supports. A user-interface is created which allows a user to create a grillage model of an existing bridge and to place various rating trucks on the bridge. Equivalent flexibility analysis is used to distribute the truck live loads from within the deck panels to the surrounding girders and diaphragms. Stiffness matrices are utilized to find the nodal displacements then the reactions at the girder supports caused by the truck live loads and bridge dead load. These reactions are checked against RISA software models to test the accuracy of the stiffness matrix application. ABAQUS FE models and Mohr's circle stress distribution is used to find the driving and clamping forces on the crack. These forces are caused by resolving the dead and live load reactions and the friction force generated between the concrete girder and the rusty steel bearing pad along the shear crack orientation. These clamping and driving forces are used, along with the simplified modified compression field theory to determine the shear capacity of each girder at the reverse cracks. A modified version of Equation 6B.4.1 from the Manual for Bridge Evaluation (2011) is used to find the operating and inventory rating factors for the bridge.

Table of Contents

List of Figures	ix
List of Tables	xii
Acknowledgements	xv
Chapter 1 Introduction	1
1.1 Background	1
1.2 Objective	1
1.3 Scope	2
Chapter 2 Literature Review	3
2.1 Load Ratings	3
2.1.1 Dead Load	5
2.1.2 Live Load	5
2.1.2.1 Truck Types	5
2.1.2.2 Truck Placement	6
2.1.2.3 Live Load Reduction	7
2.1.3 Impact Factor	7
2.1.4 Capacity	7
2.1.4.1 Material Capacity	8
2.1.4.1.1 AASHTO	9
2.1.4.1.2 ACI Equations	10
2.1.4.1.3 Simplified Modified Compression Field Theory	12
2.1.4.1.4 Muttoni & Ruiz Equation	15
2.2 Friction Coefficients	16
2.2.1 Steel – to – Concrete	16
2.2.2 Cracked Concrete – to – Cracked Concrete	17
2.2.2.1 ACI	18
2.2.2.2 PCA	18
2.2.2.3 Loov	18
2.2.2.4 Tassios and Vintzeleou	20
2.3 Transformation of Stress	22

2.3.1 Transformation of Stress Block	23
2.3.2 Formulation of Mohr's Circle	24
2.3.3 Principal Stresses & Maximum Shearing Stress.....	25
2.4 Effective Flange Width.....	28
2.5 Previous Studies.....	28
2.6 Poisson's Ratio	30
Chapter 3 BRIDGE Input/Output Interface	31
3.1 Mesh & Alignment Sheet	31
3.1.1 Lane Alignment	32
3.1.2 Bridge Mesh.....	33
3.1.3 Background Functions of the Mesh & Alignment Sheet	35
3.2 Section Geometry and Material Properties Sheet	37
3.2.1 Section Geometry.....	37
3.2.2 Material Properties.....	39
3.2.3 Crack Properties	39
3.2.4 Background Computations of Section Geometry Sheet	40
3.3 Section Properties Sheet	42
3.4 Truck Input Sheet.....	43
3.4.1 Truck Selection and Placement.....	44
3.4.1.1 Truck Type.....	45
3.4.1.2 Lane Number Assignment	46
3.4.1.3 Direction of Travel.....	48
3.4.1.4 Truck Location.....	49
3.4.2 Multiple Lane Presence Factor	49
3.4.3 Background of the Truck Input Sheet.....	50
3.4.4 Create the Bridge & Place Trucks on the Bridge.....	52
3.5 Reaction Input Sheet.....	53
3.6 Results Sheet.....	54
Chapter 4 BRIDGE Functionality.....	56
4.1 Create Mesh	56
4.1.1 Creating Grid and Assigning Member & Node Numbers.....	56

4.1.2 Assigning Coordinates to Nodes and End Nodes to Members	57
4.1.3 Identifying Boundary Members for Panels	58
4.1.4 Determining Truck-Load Paths.....	58
4.1.5 Placing Trucks on Bridge.....	59
4.1.6 Determining Multiple Presence Factor	60
4.1.7 Determining Load Length.....	61
4.2 Place Trucks on Bridge.....	61
4.2.1 Identifying which Panel is under each Load and Location of the Load on the Panel..	61
4.2.2 Distributing each Load to the Members Surrounding the Panel.....	61
4.2.2.1 Finite Element Analysis of Panel.....	62
4.2.2.2 Rigid Slab Analysis of Panel	65
4.2.2.3 Rigid Beam Analysis within the Panel	68
4.2.2.4 Analysis Results and Conclusions	69
4.2.2.5 Aspect Ratio Tables:.....	70
4.2.3 Determining Fixed End Reactions at each Node Caused by Live Loads	74
4.2.4 Determining Reactions at Nodes Caused by Dead Loads.....	75
4.2.5 Printing the k_{ff} & k_{sf} Reactions for the Bridge Matrix.....	76
4.3 Load Rate Bridge	77
4.3.1 Assigning Properties to each Member	77
4.3.2 Creating Assembled Stiffness Matrix for Bridge.....	78
4.3.3 Creating k_{ff} & k_{sf} Matrices	78
4.3.4 Creating k_{ff}^{-1} Matrix	79
4.3.5 Finding the Displacements at each Node.....	79
4.3.6 Finding the Reactions at each Support.....	79
4.3.7 Determining Governing Live Load at each Support.....	79
4.3.8 Calculating the Impact Factor	80
4.3.9 Determining Capacity of the Girders	80
4.3.9.1 Dead & Live Load Approach.....	80
4.3.9.1.1 Method #1	81
4.3.9.1.2 Method #2	82
4.3.9.1.3 Method #3	82

4.3.9.1.4 Method #4	84
4.3.9.2 Friction Load Approach	84
4.3.9.2.1 ABAQUS Study	86
4.3.9.2.1.1 Parameters	86
4.3.9.2.1.2 Model Creation	87
4.3.9.2.1.2.1 Parts	87
4.3.9.2.1.2.2 Properties	87
4.3.9.2.1.2.3 Step	87
4.3.9.2.1.2.4 Interaction	87
4.3.9.2.1.2.5 Load	88
4.3.9.2.1.2.6 Mesh	89
4.3.9.2.1.3 Model Output and Program Incorporation	90
4.3.9.2.1.3.1 Capacity without Clamping Force	92
4.3.9.2.1.3.1.1 SMCFT	92
4.3.9.2.1.3.1.2 ACI Plain Concrete Equation	93
4.3.9.2.1.3.1.3 Muttoni & Ruiz Equation	93
4.3.9.2.1.3.1.4 AASHTO Equation	93
4.3.9.3 Coefficient of Friction of Cracked Concrete	94
4.3.10 Calculating the Rating Factor at each Support	94
Chapter 5 Analysis & Results	95
5.1 Support Reactions: BRIDGE vs. RISA 3D	95
5.2 Capacity: Dead & Live Load Approach	97
5.3 Capacity: Friction Load Approach	97
5.3.1 ABAQUS Setup Confirmation	97
5.3.2 Girder Length vs S/N ratio	100
5.3.3 S/N Relationships	102
5.3.4 Estimation of Crack Propagation Angle	104
5.3.5 Predicted Crack Propagation Angle vs Actual Propagation Angle	104
5.3.6 Capacity without Clamping Force	105
5.4 Analysis of Bridge No. 54-104-15.45	106
Chapter 6 Conclusions	108

References	109
Appendix A - Truck Types	111
Appendix B - Stiffness Matrix	113
Appendix C - Support Reactions: Program vs. RISA.....	114
Appendix D - ABAQUS Models: Shear & Normal Forces.....	139
Appendix E - RF and Truck Ratings for Bridge # 54-104-15.45	142

List of Figures

Figure 1-1: Reverse Diagonal Shear Cracking	1
Figure 1-2: Normal Diagonal Shear Cracking	1
Figure 2-1: Clearance and Load Lane Width.....	6
Figure 2-2: Crack Width at Girder C, Left Side, Pier 1 of Bridge No. 54-104-317.27 (Reprinted from Special Bridge Inspection Report, 2011)	8
Figure 2-3: Shear-Friction Response at Crack Interface.....	11
Figure 2-4: Support Rockers at Pier 4, Left Side, Span 5 of Bridge No. 54-104-317.27 (Reprinted from Special Bridge Inspection Report, 2011)	17
Figure 2-5: Free Body Diagram of Forces Acting at Crack Interface	20
Figure 2-6: General State of Stress at a Point	22
Figure 2-7: Plane Stresses	23
Figure 2-8: Transformed Plane Stresses	23
Figure 2-9: Mohr's Circle of Plane Stresses	25
Figure 2-10: Principal Stresses	26
Figure 2-11: Maximum Shearing Stress	27
Figure 3-1: Bridge Mesh & Alignment User Interface	31
Figure 3-2: No. of Lanes Drop-Down Menu	33
Figure 3-3: 'Median between Lanes' Drop-Down Menu	33
Figure 3-4: 'Check Diaphragms' Error Message.....	34
Figure 3-5: 'Check Diaphragms' Virtual Diaphragm Adequacy Message.....	35
Figure 3-6: Effective and Actual Slab Widths.....	36
Figure 3-7: Numerical Value for User Specified Number of Lanes	36
Figure 3-8: Median Placement Drop-Down Menu Facilitation.....	37
Figure 3-9: Numerical Representation of Median Placement.....	37
Figure 3-10: Section Geometry and Material Properties User Interface	38
Figure 3-11: Angle of Crack Propagation.....	40
Figure 3-12: 'Use Input or Calculated Angle?' Drop-Down Menu.....	40
Figure 3-13: Background of Section Geometry and Material Properties Sheet	41
Figure 3-14: Methods to Calculate the Torsional Constant	41

Figure 3-15: Section Properties Sheet.....	43
Figure 3-16: Truck Input User-Interface.....	44
Figure 3-17: Truck Input and Information Section.....	45
Figure 3-18: ‘Truck Type’ Drop-Down Menu.....	46
Figure 3-19: ‘Lane Number’ Drop-Down Menu	47
Figure 3-20: Warning Message if there are Multiple Trucks in a Lane.....	48
Figure 3-21: ‘Direction of Travel’ Drop-Down Menu	48
Figure 3-22: ‘Truck Location’ Drop-Down Menu.....	49
Figure 3-23: ‘Multiple Lane Presence Factor’ Drop-Down Menu	50
Figure 3-24: Number of Trucks	50
Figure 3-25: Numerical Representation of Truck Placement User-Inputs	50
Figure 3-26: Trucks which Share a Lane.....	51
Figure 3-27: Lanes Occupied by a Truck	51
Figure 3-28: Number of Loaded Lanes.....	51
Figure 3-29: Snapshot of Spacing and Loads on each Truck Axle.....	52
Figure 3-30: First Two Buttons which Run BRIDGE	52
Figure 3-31: Reaction Input User-Interface.....	53
Figure 3-32: ‘Use Calculated or Input Reactions’ Drop-Down Menu	53
Figure 3-33: Results Sheet.....	54
Figure 3-34: Bridge Mesh Graphic	55
Figure 4-1: Bridge Mesh with Labeled Members and Nodes.....	57
Figure 4-2: Member End Nodes and Node Coordinates.....	57
Figure 4-3: Panel List and Surrounding Members.....	58
Figure 4-4: Four Load Paths within each Lane.....	59
Figure 4-5: Truck Load and Placement Information	60
Figure 4-6: Reduction Factor	60
Figure 4-7: Load Length for Impact Factor Calculation.....	61
Figure 4-8: RISA Model of ‘Finite Element Analysis of Panel’ with a 3”x3” Mesh.....	63
Figure 4-9: Reaction at Each Node along Primary Diaphragm	63
Figure 4-10: Reaction at Each Node along Secondary Diaphragm	64
Figure 4-11: Reaction at Each Node along Primary Girder.....	64

Figure 4-12: Reaction at Each Node along Secondary Girder.....	65
Figure 4-13: RISA Model of ‘Rigid Slab Analysis of Panel’ with Pinned Girders and Free Diaphragms	66
Figure 4-14: RISA Model for the ‘Rigid Beam Analysis within the Panel’	69
Figure 4-15: Load Placement on Panel.....	72
Figure 4-16: Fixed-End Moments (FEM) for a Point Load anywhere on the Span	74
Figure 4-17: Fixed-End Moments (FEM) for a Distributed Load	76
Figure 4-18: Snapshot of the k_{ff} Loads in the ‘ k_{ff} Loads’ Sheet	76
Figure 4-19: Snapshot of the k_{sf} Reactions in the ‘ k_{sf} Reactions’ Sheet.....	77
Figure 4-20: Member Properties	78
Figure 4-21: Forces on Crack for the ‘Dead & Live Load Approach’	80
Figure 4-22: Crack Propagation to Either Top of Slab or Edge of Girder.....	82
Figure 4-23: Parameters used to Determine Crack Length.....	83
Figure 4-24: Reaction and Friction Forces Acting on the Reverse Diagonal Crack According to the ‘Friction Load Approach’	85
Figure 4-25: Parameters Varied in the ABAQUS Models.....	86
Figure 4-26: Loading on the ABAQUS Model Girders.....	88
Figure 4-27: Uniformly Distributed Pressure Load on ABAQUS Beams.....	89
Figure 4-28: ABAQUS Model Mesh.....	90
Figure 4-29: Shear-to-Normal Force Ratio Tables	91
Figure 5-1: Support Reaction Comparison #1: RISA 3D Model.....	97
Figure 5-2: Normal Force Distribution in the Girder at the Girder-to-Bearing Pad Interface for Model 12-0.4-10-12	98
Figure 5-3: Shear Force Distribution in the Girder at the Girder-to-Bearing Pad Interface for Model 12-0.4-10-12	99
Figure 5-4: L/h Ratio vs. S/N Ratio for Model 12-0.4-6-L	101
Figure 5-5: L/h Ratio vs. S/N Ratio for Model 18-0.4-6-L	102
Figure B-1: Stiffness Matrix as Function Member Properties.....	113

List of Tables

Table 2-1: Multiple Presence Factor (Adapted from AASHTO, 2002, Article 3.12.1)	7
Table 4-1: Comparison of Load Distribution to Girders and Diaphragms using Different Analysis Methods.....	70
Table 4-2: Comparison of the Centroid of Reaction along Girders and Diaphragms using the Different Analysis Methods	70
Table 4-3: f_D/f_{Dmax} Values for Varying y/b Locations for All Aspect Ratios	72
Table 4-4: f_G/f_{Gmax} Values for Varying x/a Locations and Aspect Ratios	73
Table 4-5: f_D/f_{Dmax} & f_G/f_{Gmax} Values for Varying Load Location on Panel	74
Table 4-6: ABAQUS Parameter Variation	86
Table 5-1: BRIDGE vs. RISA 3D Model Parameter Variations	95
Table 5-2: Support Reaction Comparison #1: BRIDGE Input	96
Table 5-3: Support Reaction Comparison #1: Results.....	96
Table 5-4: S/N Ratios at Bearing Pad for Various L/h Ratios for ABAQUS Models 12-0.4-6-L & 18-0.4-6-L	101
Table 5-5: Load on Corresponding ABAQUS Models, as Shown in Table 5-6 through Table 5-11	102
Table 5-6: S/N Ratio Tables for ABAQUS Models with $b_w = 12''$ & $L/h = 7$	103
Table 5-7: S/N Ratio Tables for ABAQUS Models with $b_w = 12''$ & $L/h = 12$	103
Table 5-8: S/N Ratio Tables for ABAQUS Models with $b_w = 15''$ & $L/h = 7$	103
Table 5-9: S/N Ratio Tables for ABAQUS Models with $b_w = 15''$ & $L/h = 12$	103
Table 5-10: S/N Ratio Tables for ABAQUS Models with $b_w = 18''$ & $L/h = 7$	103
Table 5-11: S/N Ratio Tables for ABAQUS Models with $b_w = 18''$ & $L/h = 12$	104
Table 5-12: Principal Stresses, Max Shear Stress, and Angle of Maximum Shear Plan for 7 ABAQUS Models.	104
Table 5-13: Location and Geometry of 7 Girder Supports for Bridge No. 54-104-317.27-(0005)	105
Table 5-14: Observed Propagation Angles of Reverse Diagonal Crack for 7 Supports for Bridge No. 54-104-317-27-(0005).....	105

Table 5-15: Capacity of Girder with a Height of 41” & Web Width of 15” using different Capacity Eqn’s	106
Table 5-16: Rating Factors for Spans #1 & #5 for 50% & 100% Girder Width	107
Table 5-17: Truck Ratings for Spans #1 & #5 for 50% & 100% Girder Width	107
Table A-1: Truck Axle Loads and Spacings	111
Table C-1: Support Reaction Comparison #2: BRIDGE Input	114
Table C-2: Support Reaction Comparison #2: Results	114
Table C-3: Support Reaction Comparison #3: BRIDGE Input	115
Table C-4: Support Reaction Comparison #3: Results	115
Table C-5: Support Reaction Comparison #4: BRIDGE Input	116
Table C-6: Support Reaction Comparison #4: Results	116
Table C-7: Support Reaction Comparison #5: BRIDGE Input	117
Table C-8: Support Reaction Comparison #5: Results	117
Table C-9: Support Reaction Comparison #6: BRIDGE Input	118
Table C-10: Support Reaction Comparison #6: Results	118
Table C-11: Support Reaction Comparison #7: BRIDGE Input	119
Table C-12: Support Reaction Comparison #7: Results	119
Table C-13: Support Reaction Comparison #8: BRIDGE Input	120
Table C-14: Support Reaction Comparison #8: Results	120
Table C-15: Support Reaction Comparison #9: BRIDGE Input	121
Table C-16: Support Reaction Comparison #9: Results	121
Table C-17: Support Reaction Comparison #10: BRIDGE Input	122
Table C-18: Support Reaction Comparison #10: Results	123
Table C-19: Support Reaction Comparison #11: BRIDGE Input	124
Table C-20: Support Reaction Comparison #11: Results	125
Table C-21: Support Reaction Comparison #12: BRIDGE Input	126
Table C-22: Support Reaction Comparison #12: Results	127
Table C-23: Support Reaction Comparison #13: BRIDGE Input	128
Table C-24: Support Reaction Comparison #13: Results	129
Table C-25: Support Reaction Comparison #14: BRIDGE Input	130
Table C-26: Support Reaction Comparison #14: Results	131

Table C-27: Support Reaction Comparison #15: BRIDGE Input	132
Table C-28: Support Reaction Comparison #15: Results	133
Table C-29: Support Reaction Comparison #16: BRIDGE Input	134
Table C-30: Support Reaction Comparison #16: Results	135
Table C-31: Support Reaction Comparison #17: BRIDGE Input	136
Table C-32: Support Reaction Comparison #17: Results	137
Table C-33: Support Reaction Comparison #18: BRIDGE Input	138
Table C-34: Support Reaction Comparison #18: Results	138
Table D-1: Forces at One Support for ABAQUS Models with a Girder Width of 12 in.	139
Table D-2: Forces at One Support for ABAQUS Models with a Girder Width of 15 in.	140
Table D-3: Forces at One Support for ABAQUS Models with a Girder Width of 18 in.	141
Table E-1: Rating Factors for Spans #2 & #4 for 50% & 100% Girder Width.....	142
Table E-2: Truck Ratings for Spans #2 & #4 for 50% & 100% Girder Width.....	142
Table E-3: Rating Factors for Span #3 for 50% & 100% Girder Width.....	143
Table E-4: Truck Ratings for Span #3 for 50% & 100% Girder Width	143

Acknowledgements

First and foremost, I would like to thank God. Without Him nothing is possible, but through Him, all things are possible.

I would like to thank my advisor Dr. Hayder Rasheed who proposed this project and allowed me to work with him on its development. Without him there would be no project, no BRIDGE program, and no thesis.

Thank you to KDOT for sponsoring this research. Special thanks to John Culbertson, John Jones, Calvin Reed, and Loren Risch for providing valuable feedback and suggestions which kept this project moving forward.

Thank you to Schyler Rohleder for brain storming crack causes which lead to the idea the friction at the girder supports could be causing the reverse diagonal cracking.

Thank you to Rund Almasri for teaching me how to use ABAQUS and for assisting me when issues arose when dealing with ABAQUS.

Thank you to Dr. Asad Esmaily and Kimberly Kramer for accepting a position on my thesis committee.

Chapter 1 Introduction

1.1 Background

The Kansas Department of Transportation (KDOT) as well as several local counties in Kansas own dozens of low traffic bridges built in the early-to-mid 1900s which have developed abnormal reverse diagonal shear cracking at the concrete girder supports, as shown in Figure 1-1. It seems to be a major concern that these cracks might cause a loss of girder bearing support. Normally, diagonal shear cracking propagates from the bottom of the girder at the support toward the slab within the span of the girder, as shown in Figure 1-2. It is hypothesized that the abnormal cracking is caused by friction between the concrete girder and the rusty and locked steel bearing pad. This friction exists because the bearing pad has corroded, preventing the girder from rotating on its rocker. Current bridges are built with rubber bearing pads, which do not corrode when exposed to moisture. However, when these bridges were built, steel bearing pads were used, which corrode when exposed to decades of moisture and deicing salt. This corrosion turns the originally-designed pinned connection into a partially-fixed connection.

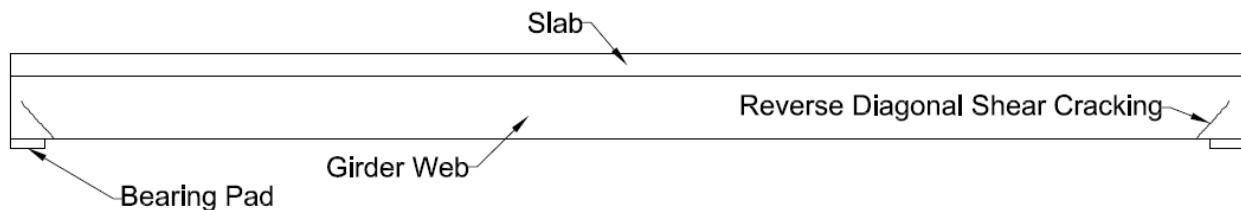


Figure 1-1: Reverse Diagonal Shear Cracking

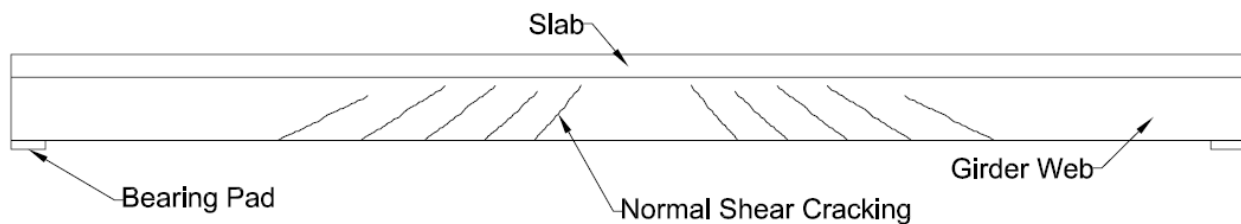


Figure 1-2: Normal Diagonal Shear Cracking

1.2 Objective

The reverse diagonal shear cracking phenomenon is not addressed in the AASHTO Bridge Design Manual (2002) or ACI specifications. The objective of this project is to determine the cause of this phenomenon. KDOT desires to rationally assess the safety of these

bridges, thus, another objective is to determine an accurate method for calculating the capacity and load rating factor for girders experiencing this phenomenon. To this end, an Excel-based program, BRIDGE (Bridge Rating of Inclined Damage at Girder Ends), is developed which analyzes a user-defined bridge span and determines the capacity and rating factor for each girder end.

1.3 Scope

This thesis is composed of six chapters. The first chapter discusses the background and objectives of the project while highlighting the various sections of the thesis. The second chapter reviews the literature used throughout this project, including how to load rate a bridge, various methods for calculating the shear capacity of a concrete beam, various values for the cracked concrete-to-cracked concrete coefficient of friction, and transformation of a stress block. The third chapter discusses the BRIDGE's user interface and the various input options available to the user. The fourth chapter details the functions performed in the background of the program and discusses the various approaches considered to distribute the truck loads between the bridge elements and to find the capacity of the bridge girders. The fifth chapter displays the results of the various approaches considered for calculating the capacity of the bridge girders as well as comparisons between the program and RISA modules to test the program's accuracy and validity. The sixth chapter reviews the conclusions determined throughout this thesis.

Chapter 2 Literature Review

2.1 Load Ratings

Bridge load rating is a method used to determine the safe live load capacities of both new and existing bridges. Only permanent loads (dead loads) and vehicular loads (live loads & impact loads) are considered. “Extreme event” loads, such as earthquake, wind, ice, flood, truck crashes, and fire loads are not typically considered when load rating a bridge and are not considered in this study. This load rating is then used, along with engineering judgement, to determine the need for bridge strengthening or load posting. Load posting is the restriction of truck loads, on a particular bridge, to a fraction of the legal truck load limits. These legal truck loads are discussed in the section 2.1.2.1. When necessary, the structure should be posted at a level which is safe and will not shorten the life of the structure (KDOT Bridge Manual, 2016, Section 4.7). Any bridge which cannot carry a minimum gross live load of 6 kips must be closed (Manual for Bridge Evaluation (MBE), 2011, Article 6B.7.1). MBE (2011) Article 6 outlines three methods to determine load rating: the Load and Resistance Factor Rating (LRFR) method, the Allowable Stress (ASD) method, and the Load Factor (LF) method. MBE (2011) does not distinguish a preferred method and allows bridge owners the choice of which method to use. The Kansas Department of Transportation (KDOT) uses the LF method to load rate their bridges (KDOT Bridge Manual, 2016, Section 4.4), thus this method is used in this study. Therefore, only the LF method is discussed further. MBE (2011) explains that the LF method analyzes the actual loads on the structure multiplied by load factors (A_1 & A_2 , defined in Equation 2-2). Different factors are applied to the dead and live loads based on uncertainty in the load calculations (dead loads are typically calculated with more accuracy than live loads, thus the dead load multiplication factor is smaller than the live load multiplication factors). These factored loads are used in Equation 2-2 to determine the rating of the bridge to ensure that the strength of the various bridge members is not exceeded. The bridges under investigation display unusual reverse diagonal shear cracking at the supports, thus this work focuses on the shear strength capacity at the girder ends.

Two rating levels are required for the LF method, namely: inventory rating and operating rating. The inventory rating describes the load which a bridge can sustain for an indefinite period of time. This rating can be compared to the design load level but also incorporates the deterioration of the bridge. The operating rating describes the absolute maximum live load to

which the bridge may be subjected (MBE, 2011). Frequent loads at the operating level will cause deterioration to the bridge. Each member of the bridge is rated and the lowest is the governing load rating for that bridge. The bridge's rating, as defined by MBE (2011) Equation 6B.4.1-2, is the rating factor (RF) multiplied by the rating vehicle (Equation 2-1):

$$\text{Load Rating} = \text{RF} \times \text{Rating Vehicle Weight} \quad \text{Equation 2-1}$$

The rating vehicle weight is the maximum legal load for a particular type of vehicle. According to the KDOT Bridge Design Manual (2016), Kansas State Statute allows for a gross vehicle weight of 80,000 lbs. on the Interstate and 85,000 lbs. on other highways without a special permit. The program provides the user with 13 standard trucks (discussed in section 2.1.2) with which to load rate the bridge. Each standard truck produces a different live load effect on the bridge, thus the bridge will have a different rating factor and rating for each truck. Any truck which causes a smaller rating than the legal limit will be used for posting (KDOT Design Manual, 2016, Section 15.3). MBE (2011) Equation 6B.4.1-1 defines the rating factor by Equation 2-2:

$$\text{RF} = \frac{\text{Capacity} - A_1 \text{DL}}{A_2(\text{LL} + \text{I})} \quad \text{Equation 2-2}$$

Where:

Capacity	=	Capacity of girder
DL	=	Dead load reaction at support of girder
LL	=	Live load reaction at support of girder
I	=	Impact factor of live load
A ₁	=	Factor for dead loads
	=	1.3
A ₂	=	Factor for live loads
	=	1.3 for operating rating level
	=	2.17 for inventory rating level

When load rating a bridge, the girders are usually assumed to be either a fixed or a pinned support. However, with integral abutments, it is sometimes advisable to analyze the girders as partially fixed (KDOT Design Manual, 2016, Section 15.5)

2.1.1 Dead Load

The dead load of the bridge is determined based on the existing conditions, geometry, and material properties at the time of analysis (MBE, 2011, Article 6B.6). The overlay thickness, which is typically measured at the time of inspection, should also be considered in the dead load of the bridge.

2.1.2 Live Load

Truck loads, axle configurations, and truck placement for load rating bridges are discussed in this section. A discussion of live load reductions and when these reductions are applicable is also included.

2.1.2.1 Truck Types

MBE (2011) Article 6B.6.2 states that the extreme live load used in Equation 2-2 is governed by AASHTO Standard Specifications (AASHTO, 2002). MBE (2011) Article 6B.7.2 states that eight standard trucks (Type 3, Type 3S2, Type 3-3, SU4, SU5, SU6, SU7, and Notional Rating Load (or NRL) should be analyzed to load rate a bridge in addition to any truck configurations specified by the bridge owners. AASHTO (2002) Article 3.7.5 specifies two classes of loading; H and HS loading. H loading is caused by a 2-axle truck and is designated with an 'H' followed by the gross tonnage of the truck. HS loading is caused by a tractor truck towing a semitrailer and is designated with an 'HS' followed by the gross tonnage of the tractor truck only. In addition to the H & HS trucks specified by AASHTO (2002) and the eight additional trucks specified by MBE (2011), KDOT, the bridge owner, states that any legal truck configuration which causes a higher stress on a bridge should be used for rating (KDOT Design Manual, 2016, Section 15.3). There are eight standard trucks rated by KDOT, most of which are already specified by AASHTO (2002) or MBE (2011). In addition, the KDOT Design Manual (2016) specifies that the T130, T170, and Heavy Equipment Transport (HET) trucks are used to load rate bridges. In total, 13 standard trucks are load rated in this program. Appendix A

displays these vehicles, their axle spacing, and weight in table form. On the Kansas highway system, the maximum load allowed on one axle is 20 kips for a single axle and 34 kips for a dual axle with a maximum total truck weight of 85.5 kips. Some of the truck axle loads in Appendix A exceed the maximum allowable load, thus, when these trucks are posted these axles are posted at the legal limit while the other axles on the truck are posted for proportionately reduced loads (KDOT Design Manual, 2016, Section 15.3).

2.1.2.2 Truck Placement

AASHTO (2002) should be followed when determining the number of loaded lanes and the placement of wheel lines (MBE, 2011, Article 6B.6.2.2). MBE (2011) Article C6B.6.2.2 recommends that in certain circumstances it is necessary to consider multiple trucks in the same lane. It recommends that a minimum of 30 ft. clear space be used between trucks in the same lane when the loading per truck is less than 12 tons. The truck loads are to be placed in such a way within their respective load lanes so as to produce the maximum stress in the member being analyzed (AASHTO, 2002, Articles 3.6.4 & 3.11.2). As shown in Figure 2-1, the standard truck's axles are spaced 6 ft. apart and the truck occupies a 10 ft. wide load lane (AASHTO, 2002, Article 3.6.1). This means that the truck will occupy the space 2 ft. to either side of the wheel loads.

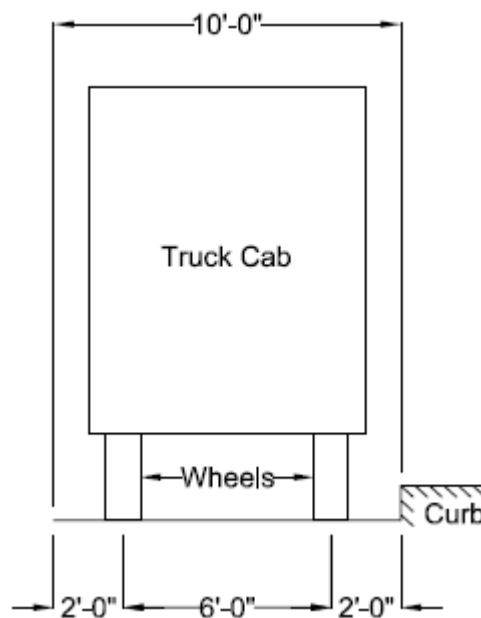


Figure 2-1: Clearance and Load Lane Width

2.1.2.3 Live Load Reduction

A reduction in live load if multiple lanes are loaded simultaneously is allowed due to the improbability of coincident maximum loading in multiple lanes (AASHTO, 2002, Article 3.12.1). These live load reduction factors are described in **Table 2-1**:

Table 2-1: Multiple Presence Factor (Adapted from AASHTO, 2002, Article 3.12.1)

Number of Loaded Lanes	Multiple Presence Factor
1 or 2	1
3	0.9
4 or more	0.75

2.1.3 Impact Factor

MBE (2011) specifies that AASHTO (2002) Equation 3.1 be used for the impact factor in Equation 2-2. This factor is shown in Equation 2-3. The impact factor accounts for the dynamic effects caused by a truck, such as the bounce, sway, and momentum of the vehicle. Dynamic effects also include the response of wheels impacting pavement surface discontinuities, such as joints, cracks, and potholes. L is limited to the smallest of either the truck length or bridge length because this gives a higher impact load coefficient, which is conservative.

$$I = \frac{50}{125 + L} < 0.3 \quad \text{Equation 2-3}$$

Where:

$$\begin{aligned} L &= \text{Length of loaded part of bridge (ft.)} \\ &= \min \begin{cases} \text{Truck Length} \\ \text{Bridge Length} \end{cases} \end{aligned}$$

2.1.4 Capacity

Field investigations are the basis of the rating of an older bridge for its load-carrying capacity. Any feature of a bridge which affects its capacity should be carefully evaluated and any damage, deterioration, and loss of cross-sectional area should be noted (MBE, 2011, Article

6.1.2). MBE (2011) also specifies that certain bridges are subject to unique geometry, loadings, and deterioration. The load rating procedure for these bridges should be augmented where needed to suit the unique characteristics of the bridge. The BRIDGE program developed in the present study is tailored to analyze bridges which are experiencing unusual reverse diagonal shear cracking at the supports. These diagonal cracks begin at the bottom edge of the girder close to the support and propagate toward the end of the girder. Normally, shear cracks propagate diagonally toward the center of the girder. The capacity of these girders at the supports is governed by the shear capacity of the girder at these cracks. It is believed that this capacity is a function of two parameters: the material shear strength of the girder and the friction force between the two faces of the crack caused by clamping forces on either side of the crack.

2.1.4.1 Material Capacity

Figure 2-2 is a photo from an Inspection Report of Kansas Bridge No. 54-104-317.27 taken in 2011. In the photo, the claw of a hammer is wedged into a shear crack at a girder support. This shows that, at the crack interface, parts of the girder have spalled off, indicating that not all of the width of the girder is providing shear resistance.



Figure 2-2: Crack Width at Girder C, Left Side, Pier 1 of Bridge No. 54-104-317.27 (Reprinted from Special Bridge Inspection Report, 2011)

MBE (2011) Article 6B.5.3 states that capacity calculations should account for observable effects of deterioration in the girder while Article C6.1.2 explicitly states that the member cross section used to determine the capacity is the gross cross section less the deteriorated section of the member. To account for the kind of deterioration shown in Figure 2-2, the program allows the user to decrease the width of girder used in the material shear capacity calculations by a certain percentage to be estimated during inspection.

The ultimate shear strength, V_u , of the section is described by AASHTO (2002) Equation 8-46, rewritten here as Equation 2-4:

$$V_u = \phi V_n \quad \text{Equation 2-4}$$

Where:

V_u	=	Ultimate shear strength of the beam (lbs.)
V_n	=	Nominal shear strength of the beam (lbs.)
ϕ	=	Shear strength reduction factor
	=	0.85 for reinforced concrete (AASHTO, 2002, Section 8.16.1.2.2)

The nominal shear capacity, V_n , is given by Equation 2-5 (AASHTO, 2002, Equation 8-47):

$$V_n = V_c + V_s \quad \text{Equation 2-5}$$

Where:

V_c	=	Shear capacity provided by concrete (lbs.)
V_s	=	Steel shear strength (ksi)

A number of shear capacity models are discussed further below.

2.1.4.1.1 AASHTO

AASHTO (2002) Article 8.16.6.2.1 specifies that for LF design the shear capacity of beams subjected to shear and flexure be computed by either Equation 2-6 or Equation 2-7

(equations 8-48 or 8-49) When a more detailed calculation is used to find the shear capacity, the shear capacity should not exceed Equation 2-8.

$$V_c = \left(1.9\sqrt{f'_c} + 2,500\rho_w \frac{V_u d}{M_u} \right) b_w d \quad \text{Equation 2-6}$$

$$V_c = 2\sqrt{f'_c} b_w d \quad \text{Equation 2-7}$$

$$V_c = 3.5\sqrt{f'_c} b_w d \quad \text{Equation 2-8}$$

Where:

f'_c	=	Concrete compressive strength (psi)
b_w	=	Width of beam web (in.)
d	=	Depth of tensile reinforcement (in.) = 0.9h
h	=	Height of girder (through slab) (in.)
V_u	=	Factored shear force at section under consideration (lbs.)
M_u	=	Factored moment at section under consideration (lb.-in.)
ρ_w	=	Reinforcement ratio equal to flexural area of steel normalized by b_w and d

Article 8.16.6.4 states that in cases where it is appropriate to consider shear transfer across a given plane, such as at an existing or potential crack, that shear-friction theory and equations be used to determine the capacity of a beam. These theories and equations are the same as those specified by American Concrete Institute's Building Code Requirements for Structural Concrete (ACI 318-14) and are discussed in the following section.

2.1.4.1.2 ACI Equations

ACI 318-14 Section 22.9 is applicable when shear transfer across an existing or potential crack is considered and is appropriate when analyzing the interactions at a crack interface in monolithic concrete. This section uses the shear-friction concept to derive shear capacity equations. This concept assumes that a crack will form and that reinforcement is provided across the crack to resist relative displacements at the crack interface (ACI 318-14 Section R22.9.1.1). When shear is present at a crack one side of the crack interface will slip relative to the other.

This relative displacement (s in Figure 2-3) causes a separation of the crack interfaces, which causes tensile stress, σ_s , in the reinforcement crossing the crack. This tensile force transfers to the surrounding concrete causing a compressive clamping stress, σ_c , at the crack interface. The clamping force causes friction between the crack interfaces as protruding aggregates on either side of the crack, along with dowel action of the reinforcement, resist shear stress, τ . Figure 2-3 helps explain the force transfer assumed in the shear-friction concept.

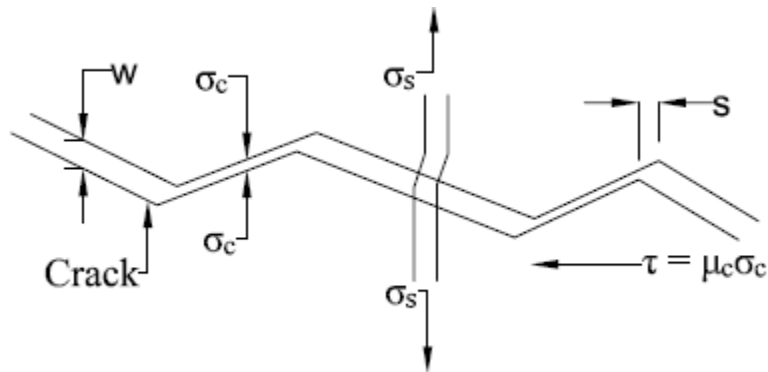


Figure 2-3: Shear-Friction Response at Crack Interface

ACI 318-14 Equation 22.9.4.3, shown below as Equation 2-9, provides a conservative estimate of the shear-transfer strength when the shear force produces tension in the reinforcement. If the shear force produces compression in the reinforcement, shear friction does not apply and V_n is 0. The coefficient of friction, μ_c , is found in ACI 318-14 Table 22.9.4.2 and is discussed in section 2.2.2.

$$V_n = A_v f_y (\mu_c \sin \alpha + \cos \alpha) \quad \text{Equation 2-9}$$

Where

A_v	=	Area of shear-friction reinforcement (in. ²)
f_y	=	yield strength of reinforcement (kips)
μ_c	=	Coefficient of friction between crack interfaces
α	=	Angle between shear-friction reinforcement and shear plane

ACI 318-14 Table 22.9.4.4 specifies the use of Equation 2-10 as upper limits of Equation 2-9 for the nominal cracked shear capacity.

$$V_n = \min \begin{cases} 0.2f'_c A_{cr} \\ 0.8A_{cr} \end{cases} \quad \text{Equation 2-10}$$

Where:

A_{cr} = Area of concrete resisting shear transfer (in.²)

ACI 318-14 Table 14.5.5.1 provides Equation 2-11 as the shear capacity of an un-cracked, plain concrete section subject to one-way shear. Section R14.5.5.1 explains that shear failure in plain concrete will occur as a diagonal tension failure when the principal tensile stress near the centroidal axis becomes equal to the tensile strength of concrete.

$$V_{c, \text{un-cracked}} = \frac{4}{3} \sqrt{f'_c} b_w h \quad \text{Equation 2-11}$$

Where:

$V_{c, \text{un-cracked}}$ = Nominal concrete shear strength of plain, un-cracked section (lb.)

In addition to these shear strength equations, ACI 318-14 also suggests using Equation 2-7 (ACI 318-14 Equation 22.5.5.1) to find the concrete shear capacity, V_c , of non-prestressed beams without axial force.

2.1.4.1.3 Simplified Modified Compression Field Theory

The Simplified Modified Compression Field Theory (SMCFT) was developed by Bentz et al. (2006) as an abbreviated and simpler-to-implement form of the Modified Compression Field Theory (MCFT). The MCFT is a model for reliably finding the shear capacity of reinforced concrete sections and was proposed in the 1980's. Before the MCFT, shear capacity calculations in various codes, including ACI codes, were extremely inconsistent and inaccurate. The ACI code found the shear strength as the load causing diagonal shear cracking at a 45° angle plus the axial load effect (subtracted capacity if member was in axial-tension and added strength

if member was in axial-compression). Bentz et al. (2006) explains that, on average, the ACI calculated capacity was 40% more conservative than experimental shear capacities and the coefficient of variation (COV) was 46.7%.

The MCFT was introduced to create a more effective method for calculating the shear capacity of a section. Bentz et al. (2006) and Abouelleil (2015) explain the assumptions made by Vecchio and Collins (1982) to derive the MCFT. First, the MCFT calculates the diagonal crack angle based on strain conditions present in the section instead of assuming an angle of 45° (with respect to the bottom of the beam). It also accounts for the fact that tensile stresses exist in the concrete between the cracks and uses the average stresses and strains over large areas (covering multiple cracks) in the beam. Also assumed is that each strain state corresponds to one stress state, that the longitudinal and transverse steel is distributed uniformly across the element, and that there is a perfect bond between the steel and concrete. The shear capacity calculated by the MCFT is, on average, just 1% greater than the experimental shear failures and has a COV of only 12.2%. Clearly the MCFT is a much more accurate predictor of shear capacity than previous methods. Unfortunately, this model is mathematically very complex, requiring the 15 equations shown in Bentz et al. (2006) to be solved iteratively through computer modeling. Bentz et al. (2006) simplified the MCFT in order for engineers to better understand the calculations so ‘back of the napkin’ calculations could be made.

The SMCFT assumes that the direction of principal compressive stress remains constant, as an average, over the effective shear depth, d_v , and that shear stresses are uniformly distributed over the width of the web and d_v . It also assumes that by considering the biaxial stress conditions at one location in the section web the shear strength of the section is calculated (AASHTO LRFD Bridge Design Specifications, 2014, Article C5.8.3.4.2). According to Bentz et al. (2006), this method predicts shear capacities only 11% larger than experimental shear capacities and has a COV of 13%, which is reasonably accurate. AASHTO (2014) incorporates the SMCFT into their procedure to find the nominal shear capacity of a section and is described with the following equations (Equations 5.8.3.3-1 through 5.8.3.4.2-5 of AASHTO, 2014):

$$V_c = \beta \sqrt{f'_c} b_v d_v \quad \text{Equation 2-12}$$

$$V_s = \frac{A_v f_y d_v (\cot \theta + \cot \alpha) \sin \alpha}{s} \quad \text{Equation 2-13}$$

$$\beta = \begin{cases} \frac{4.8}{(1 + 750\varepsilon_s)} & \text{contains } \geq \text{ min. shear reinf.} \\ \frac{4.8}{(1 + 750\varepsilon_s)} \frac{51}{(39 + s_{xe})} & \text{contains } < \text{ min. shear reinf.} \end{cases} \quad \text{Equation 2-14}$$

$$\theta = 29 + 3500\varepsilon_s \quad \text{Equation 2-15}$$

$$\varepsilon_s = \frac{\frac{M}{d_v} + 0.5N + V_n}{A_s E_s} \quad \text{Equation 2-16}$$

$$s_{xe} = s_x \frac{1.38}{a_g + 0.63} \quad \text{Equation 2-17}$$

Where:

β	=	Factor indicating ability of diagonally cracked concrete to transmit tension and shear
b_v	=	Effective web width (in.)
	=	minimum web width within the depth d_v
d_v	=	Effective shear depth, measured perpendicular to the neutral axis between the tensile resultant and compressive flexure forces. Is the greater of that depth defined here, $0.9d$ and $0.72h$ (in.)
s	=	spacing of transverse steel (in.)
A_v	=	Area of shear reinforcement within a distance s (in. ²)
α	=	Angle of transverse reinforcement to longitudinal axis (degrees)
θ	=	Angle of inclination of diagonal compressive stresses (degrees)
ε_s	=	Strain in longitudinal steel
N	=	Axial force. Positive if tensile, negative if compressive (kips)
M	=	Absolute value of moment (kips)
A_s	=	Area of longitudinal steel on flexural tension side of member (in. ²)
s_{xe}	=	Crack spacing parameter
s_x	=	Lesser of d_v and the maximum distance between layers of longitudinal crack control reinforcement (in.)
a_g	=	Maximum aggregate size (in.)

First, a shear strength, V_n , is assumed and Equation 2-16 is used to determine the steel strain, ϵ_s . Equation 2-17 is then used to find s_{xe} . This s_{xe} and ϵ_s are used in Equation 2-14 and Equation 2-15 to determine β and θ respectively. β and θ are used in Equation 2-12 and Equation 2-13 to find V_c and V_s respectively. Equation 2-5 is then used to find a new V_n . The process is then repeated until convergence of V_n . The shear at this convergence is the final shear capacity of the section

2.1.4.1.4 Muttoni & Ruiz Equation

Muttoni & Ruiz (2008) note that empirical or semi-empirical expressions have mainly been used to analyze the shear strength in a beam. The MCFT has been successfully used to evaluate the shear strength of a beam without shear reinforcement. However, using these kinds of methods are complicated as they often involve complex computer modeling and there is still no generally accepted method of finding the shear strength of a member without shear reinforcing. Muttoni & Ruiz (2008) developed a physical model which accurately describes the shear strength of 285 beams. They theorize that shear is initially resisted by three separate components: cantilever action, aggregate interlock, and dowel action from the flexural reinforcement traversing a crack. As a critical shear crack forms a fourth shear resisting effect, arching action, develops because of the effects of aggregate interlock. As this arching action becomes stronger, the effects of cantilever action and dowel action reduce and are eventually eliminated. The aggregate interlock and arching action are functions of the estimated crack width in the critical shear region, the roughness of the crack, and the compressive strength of the concrete. Tests by Muttoni and Thurlimann (1986) showed elbow-shaped struts forming in unreinforced beams loaded in shear, which were consistent with the arching action predicted by Muttoni & Ruiz (2008). Equation 2-18 describes their model. The equation assumes an elastic modulus of concrete of: $E_c = 276f_c^{1/3}$ (ksi). This is similar to ACI 318-14 Equation 19.2.2.1.b which describes the elastic modulus of concrete for normal weight concrete: $57f_c^{1/2}$ (ksi).

$$V_u = \frac{4b_w d \sqrt{f_c}}{1 + 120 \frac{\epsilon d}{\frac{5 \text{ in}}{8} + d_g}} \quad \text{Equation 2-18}$$

Where:

V_u = Shear capacity of girder (lbs.)
 d_g = Aggregate diameter (in.)
 ϵ = Strain in the control depth

Muttoni & Ruiz (2008) further simplified this equation by assuming that the depth of the compression zone, c , is equal to $0.35d$, that the reinforcement strain, ϵ_s , is proportional to the bending moment, m_{Ed} , and by estimating the flexural strength of the beam, m_{Rd} . Safety factors for concrete (ϕ_c) and steel (ϕ_s) were also introduced as 0.67 and 0.9 respectively, 29,700 ksi was used as the modulus of elasticity of steel (E_s), 70 ksi was used as the yielding stress of steel (f_y), and 5/4 in. was assumed as the aggregate diameter. With these assumptions and values, Equation 2-19 is calculated, which has been adopted into the Swiss Code for structural concrete.

$$V_u = \frac{2.3b_w d \sqrt{f'_c}}{1 + 0.056d \frac{m_{Ed}}{m_{Rd}}} \quad \text{Equation 2-19}$$

Where:

m_{Ed} = Bending moment in girder (lb.-in.)
 m_{Rd} = Flexural strength in girder (lb.-in.)

2.2 Friction Coefficients

2.2.1 Steel – to – Concrete

Steel bearing pads were used to build the bridges analyzed by the present study. Rubber was not yet used as a material for bearing pads when these bridges were built in the 1920's to 40's. As seen in Figure 2-4 from the Inspection Report for Kansas Bridge No. 54-104-317.27 (2011), steel rockers can get heavily corroded, limiting the ability of the rockers to rotate. This

prevents the girders from rotating at the supports, as designed. The girder locks on the plate and a friction force at the girder-steel boundary is produced. It is necessary to have a coefficient of friction for this interface to estimate the friction forces at the girder supports.



Figure 2-4: Support Rockers at Pier 4, Left Side, Span 5 of Bridge No. 54-104-317.27 (Reprinted from Special Bridge Inspection Report, 2011)

Rabbat & Russell (1985) conducted tests to determine the static coefficient of friction between concrete and steel for both dry and wet interface conditions. It is assumed that the superstructure of the bridges shelter the girder-bearing pad interface from most rain water, so dry interface conditions are assumed in this study. Rabbat & Russell (2008) tested a set of concrete specimens, with dry interfaces, at a normal stress of 60 psi. From these tests, a static coefficient of friction of 0.57 is recommended for normal compressive stresses between 20 and 100 psi. This value was implemented in the current study.

2.2.2 Cracked Concrete – to – Cracked Concrete

Several methods were investigated as possible sources to find the coefficient of friction of cracked concrete-to-cracked concrete.

2.2.2.1 ACI

ACI 318-14 Table 22.9.4.2 recommends a coefficient of friction, μ_c , of 1.4λ for concrete placed monolithically. For normal weight concrete λ is 1 and for lightweight concrete λ is 0.75. As stated in section 2.1.4.1.2, ACI 318-14 Section 22.9 assumes the shear-friction concept is used to determine the shear capacity of the beam. In this concept, it is assumed that shear reinforcement crosses the crack and friction between the crack faces produces all of the shear resistance. Therefore, ACI 318-14 recommends artificially high values of the coefficient of friction so the calculated shear strengths will agree with test results (ACI 318-14 Section R22.9.4.2). AASHTO (2002) Article 8.16.6.4, which outlines the shear-friction process, reflects the values of μ_c referenced in ACI 318-14.

2.2.2.2 PCA

Portland Cement Association's (PCA) Concrete Masonry Handbook (2008) Appendix A recommends using a coefficient of friction, μ_c , between cast-in-place concrete to cast-in-place concrete of 0.4 when designing a building using concrete masonry. This value is based on a safety factor of 2, thus the actual μ_c is 0.8 between cast-in-place-concrete – to – cast-in-place-concrete.

2.2.2.3 Loov

Loov (1998) uses shear friction to formulate equations to model the shear capacity of reinforced concrete beams. Clause 11.1.3 in the CSA A23.3-94 code (Canadian Standards Association, 1994) provides that shear friction must be used to design “interfaces between elements such as webs and flanges, between dissimilar materials, and between concretes cast at different times or at existing or potential major cracks along which slip can occur”. Loov (1998) postulates that beams have “innumerable locations for ‘potential major cracks along which slip can occur’”, thus shear friction can be used for predicting the shear capacity of beams. Equation 2-20, first proposed by Loov (1978), is used as the basis for shear friction equations derived by Loov (1998). This equation, with a k of 0.6, was compared to push-off tests conducted by Kumaraguru (1992) and the results are shown in Loov (1998). Equation 2-20, with a k of 0.6, is consistent with these push-off tests. As explained by Loov (1998), a k of 0.6 is conservative for un-cracked sections but is un-conservative for cracked sections. Loov (1998) asserts that a k of

0.6 is appropriate for beams because the beam will likely be cracked along part of a shear plane but will remain un-cracked along the rest of the shear plane, particularly that portion in the compression zone.

$$v = k\sqrt{\sigma f'_c} \leq \begin{cases} 0.25f'_c & \text{for } f'_c \leq 4 \text{ ksi} \\ 7 & \text{for } f'_c > 4 \text{ ksi} \end{cases} \quad \text{Equation 2-20}$$

To which:

$$\sigma = \frac{R}{A} \quad \text{Equation 2-21}$$

$$v = \frac{S}{A} \quad \text{Equation 2-22}$$

$$\mu_c = \frac{S}{R} \quad \text{Equation 2-23}$$

Where:

σ	=	Average normal stress on shear failure plane
v	=	Average shear stress on shear failure plane
k	=	Factor for relating shear strength and normal strength
	=	Determined from experiments
R	=	Normal force acting on shear failure plane – Figure 2-5
S	=	Shear force acting on shear failure plane – Figure 2-5
A	=	Area of cracked surface
	=	$(b_w h)/\sin\theta$ – Figure 2-5

Where:

θ	=	Angle of crack with respect to horizontal
----------	---	---

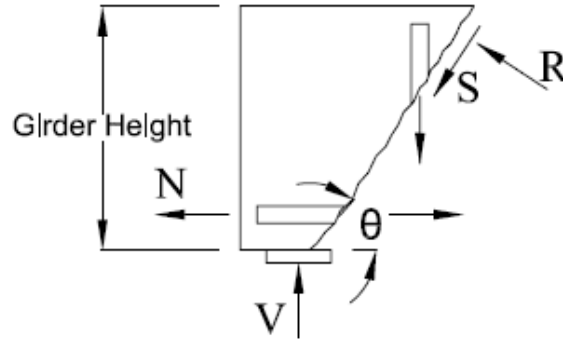


Figure 2-5: Free Body Diagram of Forces Acting at Crack Interface

Equation 2-21, Equation 2-22, and Equation 2-23 are substituted into Equation 2-20 to yield Equation 2-24 for the coefficient of friction, μ_c , between the cracked surfaces of the concrete beam:

$$\mu_c = k \sqrt{\frac{f'_c A}{R}} \quad \text{Equation 2-24}$$

Loov (1998) continues to derive shear-friction equations to find the shear strength of concrete beams. The ACI shear capacity equations, discussed earlier, are based on shear-friction models. Because shear-friction is already considered as a method to find the shear capacity of a beam, the shear strength equations derived by Loov (1998) will not be discussed further.

2.2.2.4 Tassios and Vintzeleou

Tassios & Vintzeleou (1987) analyzed and presented the results of tests to study the behavior of rough interfaces of plain concrete subject to imposed shear displacements. Shear is transferred across a crack through concrete aggregate interlock when there is a normal compressive stress at the crack interface. This compressive stress is caused by either external forces or from reinforcing bars crossing the crack.

Referring to Figure 2-3, when a crack is subject to a small shear displacement, s , some deformation and cut-off occurs in the concrete aggregates on either side of the crack. This causes an increase in the local crack width, w , which in turn produces a stress in the reinforcing steel crossing the crack producing a force equal to $A_s \sigma_s$, which is the area of the reinforcing bar

times the stress in the bar. This tensile force is equal to a compressive force in the concrete around the bar equal to $A_c\sigma_c$, which is the area of concrete surrounding the reinforcing bar times the stress in the concrete. Therefore, Equation 2-25 is proposed. Alternatively, an external compressive force can cause a shear stress in the concrete at the crack interface.

$$\sigma_c = \rho\sigma_s \quad \text{Equation 2-25}$$

Where:

σ_c	=	Stress in concrete in vicinity of reinforcing bar (psi)
σ_s	=	Stress in reinforcing bar (psi)
ρ	=	Steel to concrete ratio

In the tests analyzed by Tassios & Vintzeleou (1987), concrete blocks with reinforcing anchors were precracked to obtain natural cracks. Displacements, s , were then induced in specimens using various constant normal compressive stresses (0.5, 1, and 2 MPa) and varying concrete compressive strengths (16, 30, and 40 MPa). The crack width was then recorded. Since the anchorage of the reinforcing bars in the test specimens were known, the tensile stress in the bar, σ_s , was determined. Then, using Equation 2-25, the normal stress in the concrete at the crack, σ_c , was determined. From this stress and the shear displacement, the shear stress and the frictional response at the crack interface was found.

It was found that the maximum shear stress transferred by the crack interface increased with increasing normal force but was not proportional to this force. It is postulated in Tassios & Vintzeleou (1987) that at lower normal stresses the failure of the aggregate interlocking mechanism occurs when the peaks of the aggregate and cement paste particles protruding from the crack interface are ‘cut off’ by the shear force. At higher normal stresses, the aggregate protrusions are so tightly interlocked that the tensile strength of the concrete matrix is weaker than the shear strength of the aggregate, thus failure occurs in the matrix. This type of failure was observed in the test specimens subject to higher normal stresses.

From the results of these tests, Equation 2-26 was introduced to describe the maximum friction coefficient between the crack interfaces. It should be noted that in these tests, the initial

crack width was less than 0.1 mm, so no free slip at the crack interface was recorded. Thus, this equation is not applicable to cases of larger initial crack widths.

$$\mu_c = 0.44 \left(\frac{\sigma_c}{f'_c} \right)^{-2/3} \quad \text{Equation 2-26}$$

The compressive stress in the concrete is equal to the normal force at the crack divided by the area of the concrete interface: $\sigma_c = R/A$. Substituting this into Equation 2-26 yields Equation 2-27, which is very similar to Equation 2-24 derived by Loov (1998).

$$\mu_c = 0.44 \left(\frac{R}{f'_c A} \right)^{-2/3} \quad \text{Equation 2-27}$$

2.3 Transformation of Stress

The stresses on a finite cube of an element, centered at Q, are described by the 6 stress components in Figure 2-6. σ_x , σ_y , and σ_z represent the normal stresses on the faces of the cube while τ_{xy} , τ_{yz} , and τ_{zx} represent the shear stress on the element faces. When two of the faces of the cubic element do not experience any stresses, as is the case on the surface of a structural element that is not subject to external forces, the remaining stresses are called plane stresses. If the faces perpendicular to the z-axis in Figure 2-6 are free of stress, the resulting plane stresses are displayed in Figure 2-7.

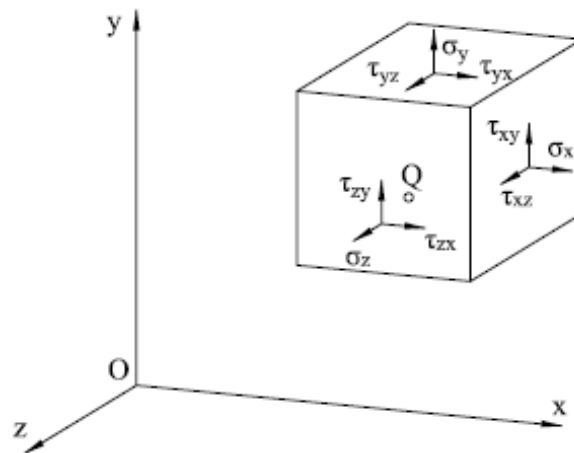


Figure 2-6: General State of Stress at a Point

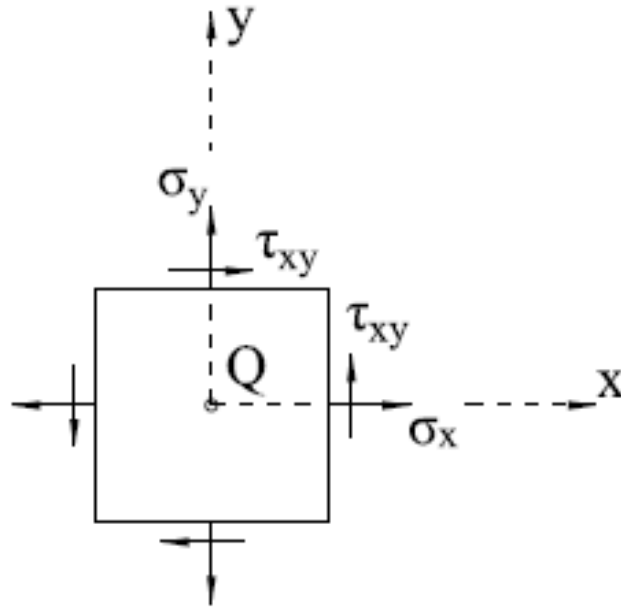


Figure 2-7: Plane Stresses

2.3.1 Transformation of Stress Block

If Figure 2-7 is rotated about its z-axis by an angle, θ , the stresses at the faces of the cube change to $\sigma_{x'}$, $\sigma_{y'}$, and $\tau_{x'y'}$, as shown in Figure 2-8. Beer et al. (2012) Section 7.2 derives Equation 2-28, Equation 2-29, and Equation 2-30 which define these transformed stresses.

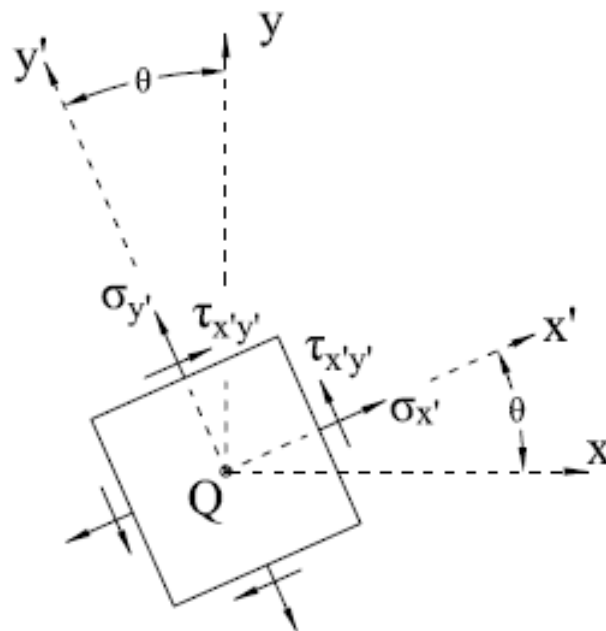


Figure 2-8: Transformed Plane Stresses

$$\sigma_{x'} = \frac{\sigma_x + \sigma_y}{2} + \frac{\sigma_x - \sigma_y}{2} \cos 2\theta + \tau_{xy} \sin 2\theta \quad \text{Equation 2-28}$$

$$\sigma_{y'} = \frac{\sigma_x + \sigma_y}{2} - \frac{\sigma_x - \sigma_y}{2} \cos 2\theta - \tau_{xy} \sin 2\theta \quad \text{Equation 2-29}$$

$$\tau_{x'y'} = -\frac{\sigma_x - \sigma_y}{2} \sin 2\theta + \tau_{xy} \cos 2\theta \quad \text{Equation 2-30}$$

Where:

σ_x	=	Normal stress normal to x-axis (psi)
σ_y	=	Normal stress normal to y-axis (psi)
τ_{xy}	=	Shear stress perp. to z-axis & parallel to either x- or y- axis (psi)
θ	=	Angle of Transformation ($^\circ$)
$\sigma_{x'}$	=	Normal stress normal to x'-axis (psi)
$\sigma_{y'}$	=	Normal stress normal to y'-axis (psi)
$\tau_{x'y'}$	=	Shear stress perp. to z'-axis & parallel to either x' - or y' - axis (psi)

2.3.2 Formulation of Mohr's Circle

Mohr's Circle of plane stress was introduced by German engineer Otto Mohr and is displayed in Figure 2-9. As Beer et al. (2012) explains, Mohr's Circle is derived from Equation 2-28 and Equation 2-30, which are the parametric equations of a circle. For any given value of θ , the point of abscissa, $\sigma_{x'}$, and ordinate, $\tau_{x'y'}$, defines a point, F, which lies on a circle displayed in Figure 2-9. When $(\sigma_x + \sigma_y)/2$ is subtracted from each side of Equation 2-28, both sides of Equation 2-28 and Equation 2-30 are squared, and finally Equation 2-28 and Equation 2-30 are added together, Equation 2-31 is formed.

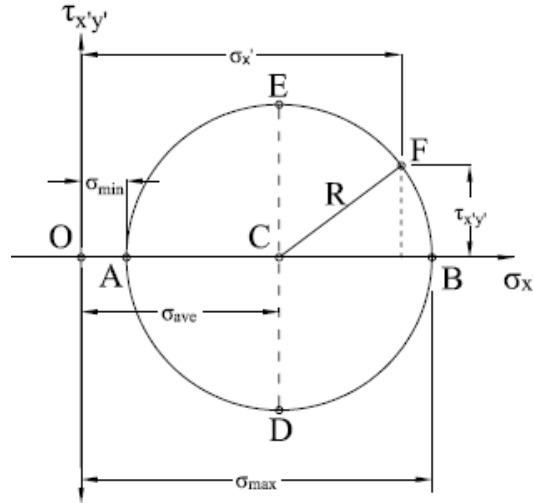


Figure 2-9: Mohr's Circle of Plane Stresses

$$\left(\sigma_{x'} - \frac{\sigma_x + \sigma_y}{2}\right)^2 + \tau_{x'y'}^2 = \left(\frac{\sigma_x - \sigma_y}{2}\right)^2 + \tau_{xy}^2 \quad \text{Equation 2-31}$$

Finally, substituting Equation 2-32 and Equation 2-33 into Equation 2-31 yields Equation 2-34, which is the equation of a circle with radius, R , and center, point C . Figure 2-9 shows that C is at abscissa σ_{ave} and ordinate 0.

$$\sigma_{ave} = \frac{\sigma_x + \sigma_y}{2} \quad \text{Equation 2-32}$$

$$R = \sqrt{\left(\frac{\sigma_x - \sigma_y}{2}\right)^2 + \tau_{xy}^2} \quad \text{Equation 2-33}$$

$$(\sigma_{x'} - \sigma_{ave})^2 + \tau_{x'y'}^2 = R^2 \quad \text{Equation 2-34}$$

Where:

σ_{ave} = Stress at center of Mohr's Circle (psi)

R = Radius of Mohr's circle (psi)

2.3.3 Principal Stresses & Maximum Shearing Stress

Points A & B of Figure 2-9 represent the minimum, σ_{min} , and maximum, σ_{max} , value of the normal stress, $\sigma_{x'}$, respectively. As seen from Figure 2-9, $\tau_{x'y'}$ equals 0 at these points.

Substituting $\tau_{x'y'} = 0$ into Equation 2-30 and rearranging yields Equation 2-35 which finds the angle, θ_p , of the principal planes of stress at point Q. The maximum & minimum normal stresses, σ_{\max} & σ_{\min} , are called the principal stresses at point Q and act normal to the principal planes of stress. Equation 2-35 defines two values of θ_p which are 90° apart. As shown in Figure 2-10 one value is the angle from the x-axis to the x' -axis, which is perpendicular to maximum principal plane. The other value is the angle from the x-axis to the y' -axis, which is perpendicular to the minimum principal plane. No shear stresses are present on the principal planes.

$$\theta_{p \max, \min} = \frac{\tan^{-1} \left[\frac{2\tau_{xy}}{\sigma_x - \sigma_y} \right]}{2} \quad \text{Equation 2-35}$$

Where:

$\theta_{p \max, \min}$ = Transformed angles to the principal planes of stress ($^\circ$)

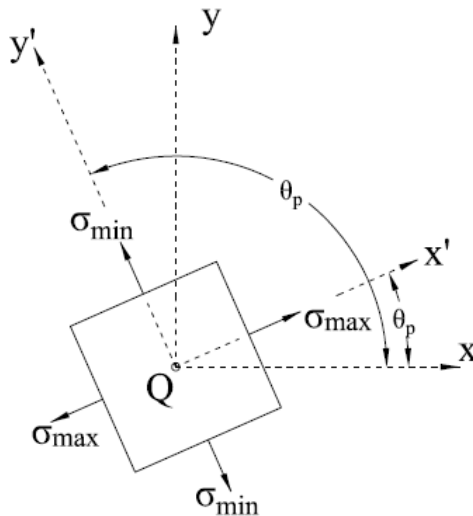


Figure 2-10: Principal Stresses

From Figure 2-9 it is seen that $\sigma_{\max, \min} = \sigma_{\text{ave}} \pm R$. Thus, substituting Equation 2-32 & Equation 2-33 yields Equation 2-36 which defines the maximum and minimum stresses. It is necessary to substitute the θ_p values from Equation 2-35 into Equation 2-28 to determine which θ_p corresponds to which principal stress.

$$\sigma_{\max,\min} = \frac{\sigma_x + \sigma_y}{2} \pm \sqrt{\left(\frac{\sigma_x - \sigma_y}{2}\right)^2 + \tau_{xy}^2} \quad \text{Equation 2-36}$$

Where:

$\sigma_{\max,\min}$ = Maximum and minimum principle stresses (psi)

Points D and E from Figure 2-9 correspond to the points of maximum shearing stress, τ_{\max} . The abscissa of these points is σ_{ave} . Substituting σ_{ave} from Equation 2-32 as $\sigma_{x'}$ in Equation 2-28 and rearranging yields Equation 2-37 which defines two angles, θ_s , which are 90° apart. As shown in Figure 2-11, either of these θ_s values correspond to the orientation of the cubic element which yields the maximum shearing stress at point Q. The angles θ_s are 45° less than their corresponding θ_p values.

$$\theta_s = \frac{\tan^{-1}\left(-\frac{\sigma_x - \sigma_y}{2\tau_{xy}}\right)}{2} \quad \text{Equation 2-37}$$

Where:

θ_s = Transformed angles to the planes of maximum shear stress ($^\circ$)

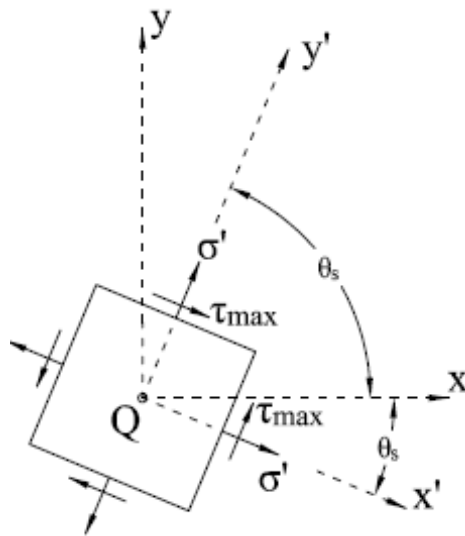


Figure 2-11: Maximum Shearing Stress

The planes of maximum shear stress, defined by the angles θ_s and displayed in Figure 2-11, are subject to the same shear stress, τ_{\max} . As shown in Figure 2-9, τ_{\max} is equal to the radius of Mohr's Circle, R. Thus Equation 2-33 also yields the maximum shear stress, which is redefined as Equation 2-38.

$$\tau_{\max} = \sqrt{\left(\frac{\sigma_x - \sigma_y}{2}\right)^2 + \tau_{xy}^2} \quad \text{Equation 2-38}$$

2.4 Effective Flange Width

AASHTO (2014) Article C4.6.2.6.1 defines the effective flange width as the “Width of the deck over which the assumed uniformly distributed longitudinal stresses result approximately in the same deck force and member moments calculated from elementary beam theory assuming plane sections remain plane, as are produced by the non-uniform stress distribution.” AASHTO (2002) Article 8.10 specifies that the total effective flange width for a T-Girder should not exceed one-quarter of the span length of the girder & that the effective flange width overhang on each side of the web should not be more than six times the thickness of the slab or half the clear distance to the adjacent girder web. The effective overhanging flange width for exterior girders with a slab only on one side of the web should be the lesser of 1/12 of the span length, 6 times the thickness of the slab, or half the clear distance to the adjacent girder web

2.5 Previous Studies

Al-Mahaidi et al. (2000) compared calculated load distributions and shear strengths to the measured load distribution and shear strength displayed by Baranduda Bridge, which is a T-Girder bridge built around 1916 in Victoria, Australia, and was load tested to failure. The 4 girder-continuous 3-span bridges consisted of girders with 280 mm wide flanges, an overall depth (through slab) height of 610 mm, and a slab thickness of 150 mm. The concrete had a compressive strength of 27 MPa and a Young's Modulus of 21 GPa. The flexural reinforcement consisted of 6 28.6 mm diameter bars in positive bending with 3 28.6 mm bars over the supports. The girders had 3 sets of 6.4 mm diameter stirrups ranging from 400-500 mm apart. The steel had a Young's Modulus of 195 GPa. Al-Mahaidi et al. (2000) predicted the girder displacement

using both grillage analysis and a finite element analysis. The resulting displacement from these two methods were extremely close to each other and were slightly more conservative than the actual displacements of the girders displayed during the test, indicating that a grillage analysis adequately distributes point loads to the surrounding members. Al-Mahaidi et al. (2000) then calculated the shear force in the beam using the MCFT and a non-linear finite element model analysis (NLFEM). These two methods yielded shear strengths which were lower than the measured shear strength, but which were relatively close to the measured shear strength and to each other. This shows that the MCFT calculates reasonable shear strength for concrete girder T-beams.

Commander and Shultz (1997) load-tested 6 reinforced-concrete Illinois Bulletin Slab (IBS) bridges in Kansas by slowly moving a truck with known weight and axle spacing over the bridge and constantly recording the strain at the top and bottom of the deck slab and curbs. These bridges are typically continuous for three or more spans and the spans do not exceed 45 ft. It was found that the stiffness of the bridge was nearly the same at both positive and negative moment regions, that cracks had little effect on the flexure or load transfer in the bridge, and that the pier column bases acted as fixed supports. Commander and Shultz (1997) then load rated the bridges for both inventory and operating levels using both allowable stress and load factor designs. It was assumed that the live load distributed similarly to the dead load, however, the authors questioned this assumption based on the resulting load ratings. In every case, the load rating at negative moment regions controlled because the calculated dead load moments at these locations nearly equaled the inventory capacities.

Azizinamini et al. (1994a, 1994b) performed an ultimate load test on a five-span concrete slab bridge built in 1938 which was 8 m. wide, and a maximum span length of 11.4 m. and a maximum slab thickness of 43 cm. According to AASHTO provisions of the time, the bridge had a load rating of 0.671, so the bridge was decommissioned. Azizinamini et al. (1994a, 1994b) found that, at ultimate failure, the bridge was equivalently loaded with 7 AASHTO HS20 trucks, or 10.4 times the inventory rating calculated using AASHTO provisions. To determine a more accurate method for determining the load rating of the bridge, Azizinamini et al. (2004) developed a rating method which is based on determining the probability of failure of the bridge using the load effect on the bridge and the resistance of the bridge. Based on their method, Azizinamini et al. (2004) rated the same bridge and found that trucks weighing up to 50 tons

could safely cross the bridge, which was much more accurate than the rating calculated using the AASHTO provisions.

Ranasinghe and Gottshall (2002) developed a method to load rate compression members which are specifically tailored for deck-filled arches composed of non-slender, rectangular, reinforced concrete members in uni-axial bending, which are sometimes used in bridge construction. In this method, analysis software is used to measure the applied loads and moments on a compression member. Then, the developed equations can be used in a spreadsheet application, such as Excel, in order to find the load rating of the compression member. This method was tested on the Bulkeley Arch Bridge in Hartford, Connecticut and compared to an interaction diagram created from an exact solution. The method created by Ranasinghe and Gottshall (2002) agrees very well with this interaction diagram. This proposed method can be manipulated for compression members experiencing bi-axial bending, members which are slender, and deteriorated members.

2.6 Poisson's Ratio

When a stress is applied on a material in one direction the material typically deforms in the other two orthogonal directions as well. This deformation is described by the Poisson's ratio of the material. When an axial load is applied to a material, the Poisson's ratio, ν , is described by Equation 2-39.

$$\nu = - \frac{\text{Lateral Strain}}{\text{Axial Strain}} \quad \text{Equation 2-39}$$

Where:

ν = Poisson's ratio

AASHTO (2002) Article 8.7.3 defines Poisson's ratio as 0.2 for reinforced concrete.

Chapter 3 BRIDGE Input/Output Interface

An excel-based program named Bridge Rating of Inclined Damage at Girder Ends, or BRIDGE, was created to allow a user to model a simply supported bridge span composed of concrete girders, diaphragms, and a deck slab. The user then loads the bridge with the desired truck loading. BRIDGE uses the user-input data to analyze the bridge and loading to determine the rating factor for each girder support.

3.1 Mesh & Alignment Sheet

The Mesh & Alignment sheet displays the Bridge Mesh and Lane Alignment options in the corresponding boxes shown in Figure 3-1. The user input data is provided in the white boxes next to the respective parameters.

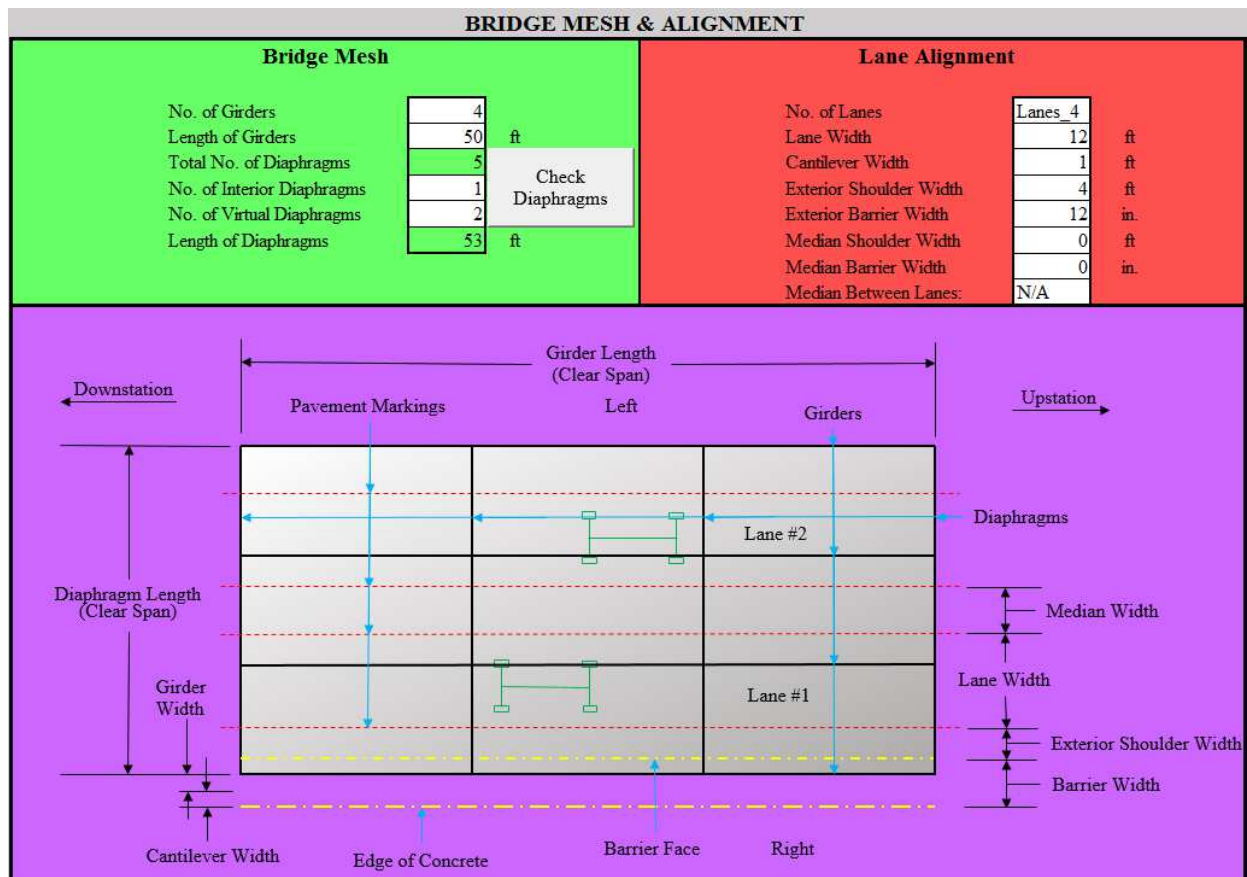


Figure 3-1: Bridge Mesh & Alignment User Interface

3.1.1 Lane Alignment

The input parameters for the Lane Alignment section, as seen in Figure 3-1, are:

- Number of Lanes (NL)
- Lane Width (LW) (ft.)
- Cantilever Width (CW) (ft.)
- Exterior Shoulder Width (ESW) (ft.)
- Exterior Barrier Width (EBW) (in.)
- Median Shoulder Width (MSW) (ft.)
- Median Barrier Width (MBW) (in.)
- Median Placement ('Median Between Lanes')

The user selects the number of lanes from a drop-down menu, as shown in Figure 3-2 which ranges from 1 to 4 ('Lanes_1' to 'Lanes_4'). The lane width is assumed equal for all lanes. The cantilever width is the distance from the outside face of the exterior girder to the edge of the slab and is displayed in the graphic in Figure 3-1. It is assumed that the cantilever width, exterior shoulder width, and exterior barrier width are equal for both sides of the bridge. The median shoulder width is assumed equal on both sides of the median barrier if median barriers and shoulders exist. When one or two lanes are selected the 'Median between Lanes' drop-down menu is disabled and "N/A" is displayed in this field. This is because the BRIDGE assumes that no medians exist on bridges with only one lane and if a median exists on a two lane bridge then it is between the two lanes. When there are three lanes the 'Median between Lanes' drop-down menu, as shown in Figure 3-3, allows the user to place the median either between lanes '1 and 2' or between lanes '2 and 3'. When there are 4 lanes the 'Median between Lanes' drop-down menu is again disabled and 'N/A' is displayed as the program assumes the median, if one is present, is between lanes two and three. As shown in Figure 3-1, the program assumes lane #1 is the closest lane to the bottommost girder of Figure 3-1. The number of lanes increases until the last lane is closest to the topmost girder.

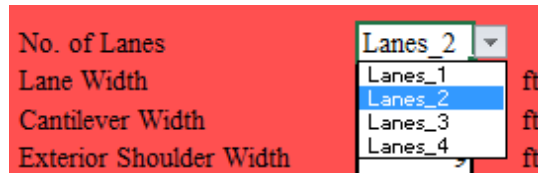


Figure 3-2: No. of Lanes Drop-Down Menu

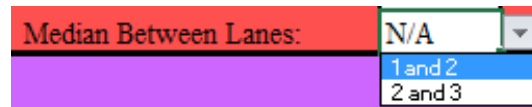


Figure 3-3: 'Median between Lanes' Drop-Down Menu

3.1.2 Bridge Mesh

The input parameters for the Bridge Mesh section, as seen in Figure 3-1, are:

- Number of Girders (NG)
- Length of Girders (GL) (ft.)
- Number of Interior Diaphragms
- Number of Virtual Diaphragms

The girders, as shown in the graphic of Figure 3-1, refer to the bridge beams which run parallel to the bridge span. The girder length input is defined as the clear span between the exterior diaphragms, or the distance from inside face-to-inside face of the exterior diaphragms (NOT the center-to-center distance between the exterior diaphragms). The choice of using the clear span length is for user convenience, per KDOT request. In our meetings with KDOT in Fall 2014 and Spring 2015 it was stated that the majority of bridge plans call out the “clear span” spacing of the diaphragms, thus, it is convenient for users to simply input the clear span girder length as described in the bridge plans.

Diaphragms are the bridge beams which run perpendicular to the span length and the girders. Exterior diaphragms are those at the outside edges of the bridge span being analyzed. BRIDGE automatically assumes there are two exterior diaphragms; one on either side of the span. Interior diaphragms are an optional user input. Interior diaphragms are real diaphragms between the two exterior diaphragms. The program assumes these interior diaphragms are spaced uniformly between the exterior diaphragms. Virtual diaphragms are also an optional user input. Virtual

diaphragms are ‘imaginary’ diaphragms within the bridge which have a total depth equal to the depth of the slab, thus, virtual diaphragms have no web.

If any virtual diaphragms are incorporated, BRIDGE automatically spaces them uniformly between the real end and interior diaphragms. Their inclusion increases the number of nodes and members used in the analysis. This makes the analysis more accurate, especially when the distance between real diaphragms is large. In order for the program to work properly there must be the same number of virtual diaphragms between each pair of real diaphragms. For example, if there is 1 interior diaphragm, there must be an even number of virtual diaphragms. If there are 2 interior diaphragms, the number of virtual diaphragms must be divisible by ‘3’. If there are no interior diaphragms, there are no limitations to the number of virtual diaphragms. The ‘Check Diaphragms’ button runs the ‘Verify_Deck_Width’ macro which checks to make sure that the number of virtual diaphragms is compatible with the number of real diaphragms. If the number of virtual diaphragms is incompatible an error message will appear, as shown in Figure 3-4. If this message appears, the user should select ‘OK’ on the error message box and adjust the number of virtual diaphragms until Equation 3-1 is satisfied, then reselect the ‘Check Diaphragms’ button. If Equation 3-1 is satisfied the message box shown in Figure 3-5 appears. The user can then select ‘OK’ and continue with the BRIDGE program.

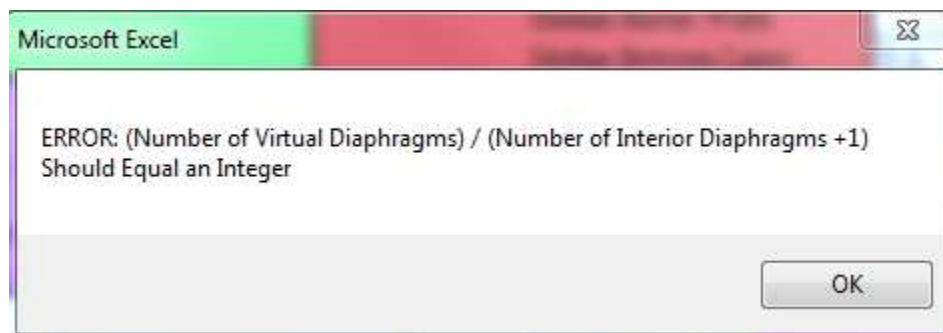


Figure 3-4: ‘Check Diaphragms’ Error Message

$$\# \text{ Virtual Diaphragms} = n(\# \text{ Interior Diaphragms} + 1) \quad \text{Equation 3-1}$$

Where:

n = Any integer

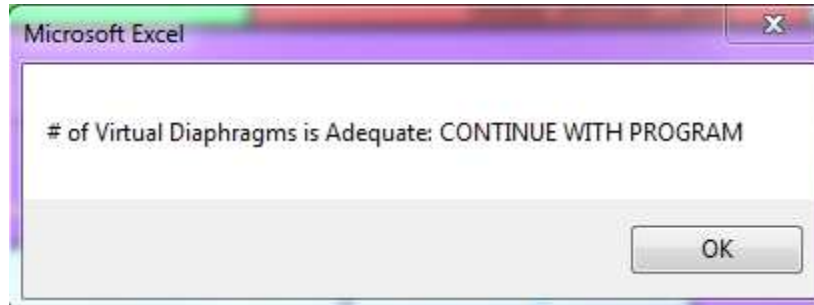


Figure 3-5: 'Check Diaphragms' Virtual Diaphragm Adequacy Message

The total number of diaphragms and diaphragm length are automatically calculated within the program and are dependent upon the user inputs. The total number of diaphragms is two (exterior diaphragms which are automatically assumed as part of the bridge) plus the number of interior and virtual diaphragms. The diaphragm length, displayed in the program and shown in the graphic of Figure 3-1, is the clear distance between the interior faces of the two exterior girders. Like the girder length, the use of clear span length is based upon KDOT request. The diaphragm length is defined by Equation 3-2.

$$DL = (NL \times LW) + (2 \times ESW) + (2 \times MSW) + \left(\frac{MBW}{12}\right) + \left(\frac{2 \times EBW}{12}\right) - (2 \times CW) - \left(\frac{2 \times GW}{12}\right) \quad \text{Equation 3-2}$$

Where:

DL = Diaphragm Length (ft.)

GW = Girder Width (in.) (Described in section 3.2.1)

3.1.3 Background Functions of the Mesh & Alignment Sheet

Outside of the user input screen view, shown in Figure 3-1, is a table which calculates the actual and effective slab flange widths for each interior and exterior girder and diaphragm. The actual slab width of the girders is used to calculate the dead load of the structure. This actual slab width is that portion of the slab which is tributary to a girder and consists of the girder web width plus half the distance to the adjacent girder web on either side of the web. For dead load calculation purposes, the entire slab is accounted for in the actual tributary widths of the girders,

therefore the actual tributary width of the diaphragms is unnecessary and is not calculated. The effective slab width of the girders is in accordance with AASHTO (2002) Article 8.10 and follows the guidelines outlined in section 2.4. AASHTO (2002) Article 8.10, however, does not specify an effective flange width for diaphragms, therefore the actual tributary width of the diaphragms is used as the effective slab width. The tributary width of each diaphragm consists of the diaphragm web width plus half the distance to the adjacent diaphragm webs on either side of the web. These effective slab widths are used in the Section Properties sheet to determine girder and diaphragm section properties. The table of the actual and effective slab widths are shown in Figure 3-6:

	Effective Width of Slab	Actual Width of Slab	
Interior Girder	83.75	83.75	in.
Exterior Girder	60.875	60.875	in.
Interior Diaphragm	612		in.
End Diaphragm	310.5		in.

Figure 3-6: Effective and Actual Slab Widths

Outside of the user screen, BRIDGE determines and prints the number of lanes which the user specifies. Since the ‘Median between Lanes’ drop-down menu is dependent upon the ‘No. of Lanes’ drop-down menu excel will not allow just numbers to populate the “No. of lanes” drop-down menu. Thus, this cell, shown in Figure 3-7, determines the numerical number of lanes from the available drop-down menu options.

of Lanes:
4

Figure 3-7: Numerical Value for User Specified Number of Lanes

The table in Figure 3-8 is used to facilitate the drop-down menu for the ‘Median between Lanes’ user input since it is dependent upon the selected number of lanes. The lane number options are printed in the first row of the table while the ‘Median between Lanes’ options for each ‘No. of Lanes’ option is printed in the columns.

Facilitates Drop-Down Menus			
Lanes_1	Lanes_2	Lanes_3	Lanes_4
N/A	N/A	1 and 2	N/A
N/A	N/A	2 and 3	N/A

Figure 3-8: Median Placement Drop-Down Menu Facilitation

Figure 3-9 displays the box which reads the user selection for ‘Median between Lanes’ and displays a numerical value dependent upon the selection. If the user selects “1 and 2” then the box will display the number ‘1’. If the user selects ‘2 and 3’ then this box will display the number ‘2’. If the user does not have the option to specify where the median is located and ‘N/A’ is selected then this box will display a ‘0’. The number displayed in this box, along with the number of lanes, is used within the program to correctly place the median if one exists.

Median Placement:
0

Figure 3-9: Numerical Representation of Median Placement

3.2 Section Geometry and Material Properties Sheet

The Section Geometry and Material Properties user interface, shown in Figure 3-10, allows the user to input girder, diaphragm, slab, and wearing surface geometry. In addition, the user can input concrete material properties and crack width properties. All user-input boxes are displayed with a white background.

3.2.1 Section Geometry

This sheet allows the user to input the height (in.) and width (in.) of the girders and diaphragms as well as the deck slab thickness (in.). Per KDOT request, BRIDGE defines the height of the girders and diaphragms as from the bottom of the element through the top of the slab. This height definition should allow the user to more conveniently input the girder and diaphragm properties directly from the bridge design plans. If the user desires either the girder or diaphragm to not have a ‘web’ section, the user may simply make the height of the girder or diaphragm equal to the deck slab thickness and the web width equal to any number. The

program will work correctly and assume there is no web for the girder or diaphragm. Per KDOT permission, the girders and diaphragms are assumed rectangular as this is the only beam shape used in the bridges targeted by this program. The program allows the user to specify different dimensions for the interior and exterior diaphragms. However, the program assumes that all exterior diaphragms have the same dimensions and all interior real diaphragms have the same dimensions. If, in the Mesh & Alignment sheet, the user specifies that there are no interior diaphragms then the user may set the interior diaphragm user-input cells in the Section Geometry and Material Properties sheet to anything – BRIDGE knows to ignore these inputs. No user input for the virtual diaphragms is necessary as the program already assumes that the virtual diaphragms, discussed in section 3.1.2, have a height equal to the deck slab thickness and have a tributary width equal to the interior diaphragm effective slab width, as displayed in Figure 3-6.

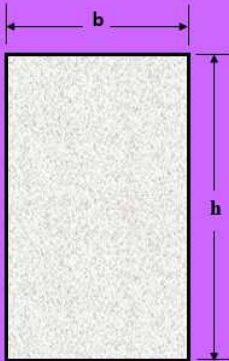


SECTION GEOMETRY AND MATERIAL PROPERTIES		
<p>Girder</p> <p>Height (through deck) (h) <input type="text" value="41"/> in.</p> <p>Width (web) (b) <input type="text" value="15"/> in.</p> 	<p>Diaphragms</p> <p>Exterior:</p> <p>Height (through deck) (h) <input type="text" value="21"/> in.</p> <p>Width (web) (b) <input type="text" value="9"/> in.</p> <p>Interior:</p> <p>Height (through deck) (h) <input type="text" value="0"/> in.</p> <p>Width (web) (b) <input type="text" value="0"/> in.</p> 	<p>Deck Slab</p> <p>Thickness (t) <input type="text" value="6.5"/> in.</p> 
		<p>Wearing Surface</p> <p>Thickness <input type="text" value="2"/> in.</p> <p>Unit Weight <input type="text" value="150"/> pcf</p>
		<p>Material Properties</p> <p>Concrete Strength (f'_c) <input type="text" value="3000"/> psi</p> <p>Concrete Unit Weight (γ_c) <input type="text" value="150"/> pcf</p>
		<p>Crack Properties</p> <p>% Cracked Girder Width Used <input type="text" value="100"/> %</p> <p>Angle of Crack Propagation (θ) <input type="text" value="50"/> °</p> <p>Use Input or Calculated Angle? <input type="text" value="Calculated"/></p> <p>Aggregate Diameter <input type="text" value="1"/> in.</p>

Figure 3-10: Section Geometry and Material Properties User Interface

Additionally, the user may input a wearing surface thickness (in.) along with the wearing surface unit weight (pcf). The wearing surface properties are used strictly for bridge dead load

calculations and do not contribute to the girder or diaphragm cross sectional properties or the bridge stiffness.

3.2.2 Material Properties

Per KDOT request, the user specifies the concrete compressive strength, f'_c (psi), as well as the concrete unit weight, γ_c (pcf), which is used to determine the bridge's dead load weight. The concrete strength is a user input, however, if the user does not know the specified design concrete strength, it is recommended that a value of 3000 psi be used. 3000 psi was a common compressive strength for concrete in the early 1900's when most of the bridges affected by reverse diagonal cracking were built.

3.2.3 Crack Properties

In this sheet, the user specifies the crack properties and the condition of the girders near the supports. As discussed in section 2.1.4.1 and shown in Figure 2-2, the crack width of the reverse diagonal shear cracks are sometimes so severe that a portion of the crack faces are no longer in contact with each other and, thus, do not provide any shear capacity. Based on inspection reports and engineering judgement, the user should determine the percent of the girder width which maintains full contact between crack faces and thus transfers shear across the crack. This percent is entered for the "% Cracked Girder Width Used". The less girder width used the smaller the shear capacity and more conservative the load rating. The user may also specify the angle of crack propagation, θ , of the reverse diagonal crack. The orientation of this angle is shown in Figure 3-11. As discussed in section 4.3.9.2, the program calculates a predicted crack angle based on the effects of friction forces at the girder-to-bearing pad interface. The user can choose to either use their manually-entered crack angle, θ , or use the program calculated crack angle. To use the manually-entered angle the user should select "Manual" from the "User Input or Calculated Angle?" drop-down menu, as shown in Figure 3-12. Otherwise, the user should select "Calculated" for the analysis to use the calculated crack angle. The user may also specify the diameter of the aggregate used in the girder concrete in the 'Aggregate Diameter' input box. If this parameter is unknown, it is recommended that the user input an aggregate diameter of 1". The larger the aggregate diameter specified, the larger and less conservative the rating factor.

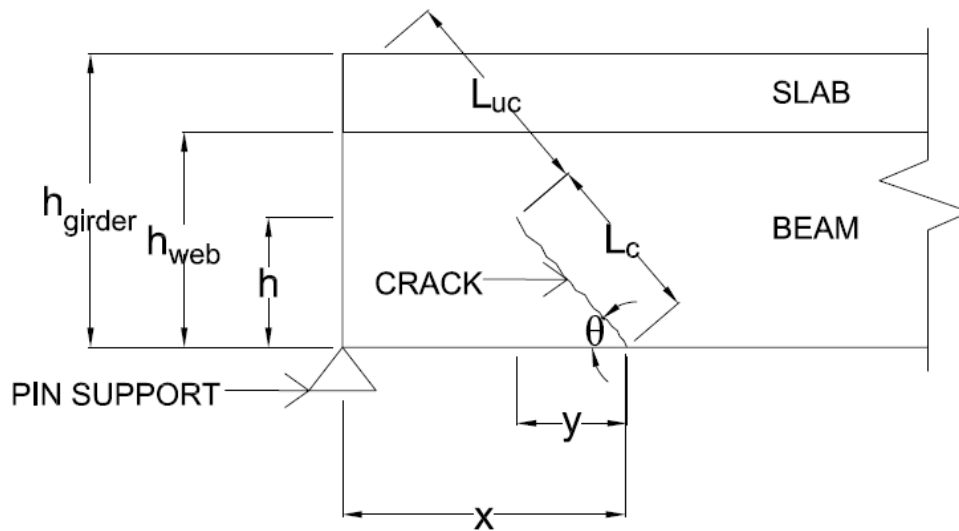


Figure 3-11: Angle of Crack Propagation

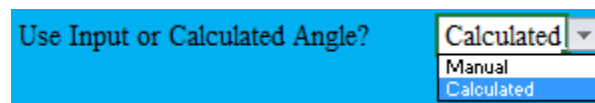


Figure 3-12: 'Use Input or Calculated Angle?' Drop-Down Menu

3.2.4 Background Computations of Section Geometry Sheet

Two tables, shown in Figure 3-13, are located in the background of this sheet. The first table displays the web area of the girders and diaphragms. It also displays the distance from the top of the slab to the centroid of the girder or diaphragm web (assuming the slab thickness is NOT part of the girders and diaphragms). These are used later to find other geometric properties for the bridge members. The other table displays the torsion constants, J , for each interior, exterior, real, and virtual girder and diaphragm and its corresponding effective slab. If interior or virtual diaphragms do not exist in the run, then no J is calculated for those members. The slab/girder or slab/diaphragm element is broken into simpler rectangular sections in order to calculate the torsional constant. There are two ways to break the elements, shown as 'Method 1' and 'Method 2' in Figure 3-14. For each method, the torsional constant for each cut-up section is computed using Equation 3-3. These torsional constants are then added together to find the overall torsional constant of the shape for each method. The virtual diaphragms are composed entirely of a slab element. Therefore, the torsional constant (J) of only a single rectangular

section is calculated. BRIDGE uses the larger of the calculated torsional constants (using Method 1 or Method 2) in the analysis because it is closer to the actual value.

	X-Centroid (from top of deck) (in.)				
	Area (in ²)				
Girder	504	22			
Ext. Diaphragm	192	16			
Int. Diaphragm	192	16			
	Interior Girder & Deck	Exterior Girder & Deck	Interior Diaphragm & Deck	End Diaphragm & Deck	Virtual Diaphragm & Deck
J (Method 1)	69046	54027	30228	18196	25252
J (Method 2)	80467	69073	31836	20664	

Figure 3-13: Background of Section Geometry and Material Properties Sheet

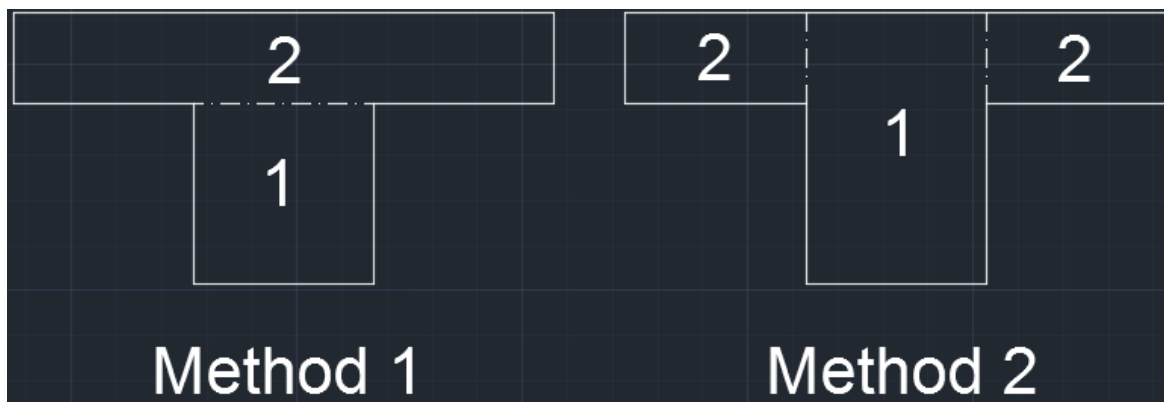


Figure 3-14: Methods to Calculate the Torsional Constant

$$J = \sum b^3 h \left(\frac{1}{3} - 0.21 \frac{b}{h} \left[1 - \frac{1}{12} \left(\frac{b}{h} \right)^4 \right] \right) \quad \text{Equation 3-3}$$

Where

- J = Torsional constant (in.⁴)
- b = Smaller dimension of rectangles in Figure 3-14 (in.)
- h = Larger dimension of rectangles in Figure 3-14 (in.)

3.3 Section Properties Sheet

The Section Properties sheet is not a user input sheet. However, the user may view this sheet in order to gain a better understanding of the analysis being conducted by the program or to help them perform hand checks. The area, A , y-centroid from top of deck, C_y , x-centroid from center of the girder/diaphragm web, C_x , and the moments of inertia in both the x & y directions about the section centroid is calculated for each interior, exterior, real, and virtual girder and diaphragm web and effective tributary slab width. These properties are displayed in the table shown in Figure 3-15. The torsional constant, J , for each section is calculated in the background of the Section Geometry sheet and the governing J is displayed in the table in Figure 3-15. The parallel axis theorem is used to find the moments of inertia about the centroid of each section. The moment of inertia does not include barriers, per KDOT request. Since the barriers would increase the stiffness of the sections, their exclusion is conservative. A cross-sectional view of each real element, including the effective deck section, with the general centroid location, is also included in this sheet, as shown in Figure 3-15. Steel reinforcement does not contribute to these section properties, which is a conservative simplification.

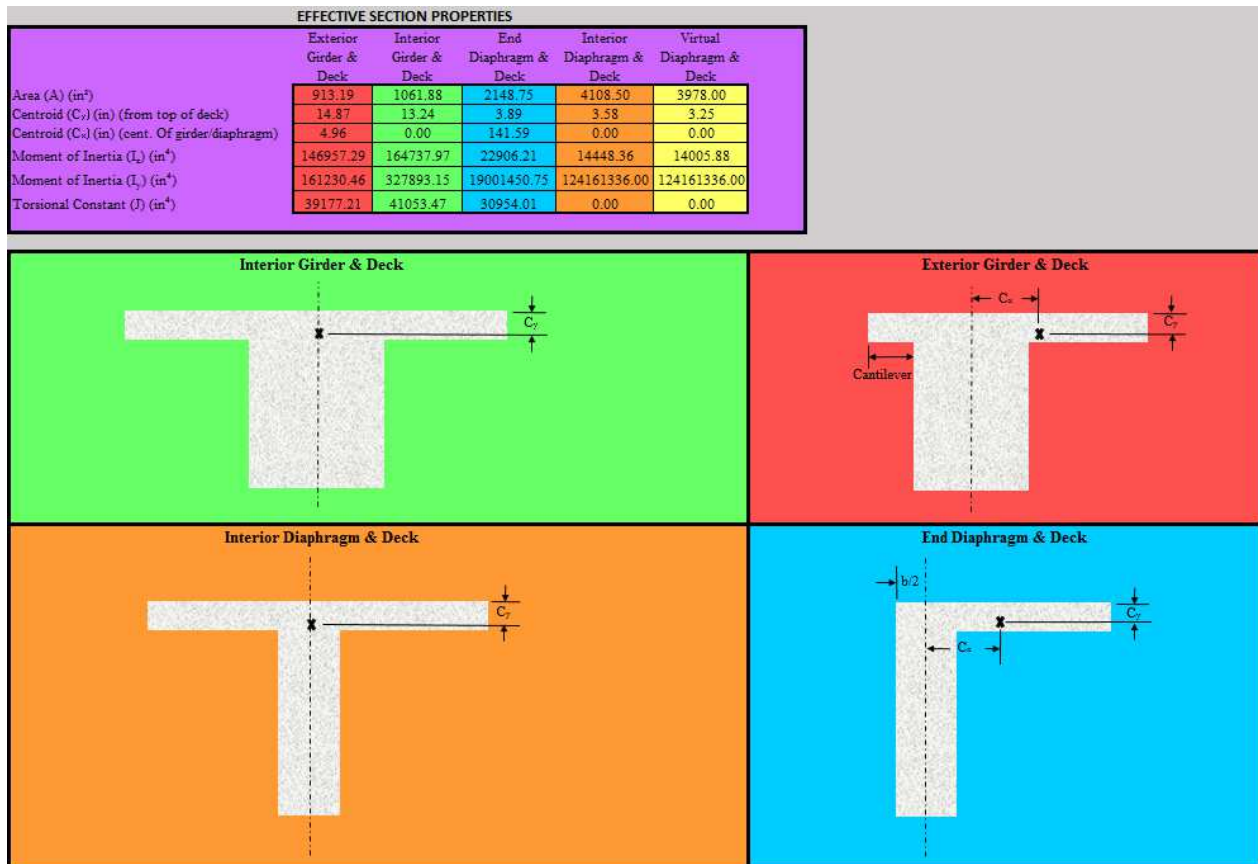


Figure 3-15: Section Properties Sheet

3.4 Truck Input Sheet

The Truck Input user interface, shown in Figure 3-16, allows the user to place between one and four trucks on the bridge. All user input boxes are displayed with a white background. As seen in Figure 3-16, the information for Truck #1 is displayed in the upper-left section, Truck #2 in the upper-right section, Truck #3 in the lower-left section, and Truck #4 in lower-right section. The display options are the same for each truck. If the user desires only one truck placed on the bridge then the 'Truck #1' section MUST be filled out while all of the other truck sections MUST display 'None' in the 'Truck Type' user input box. This configuration is displayed in Figure 3-16. As long as the 'Truck Type' user input displays 'None' it does not matter what the other user-input boxes display for that truck. If a second truck is added to the bridge, it MUST be entered into the 'Truck #2' section and so forth.

Truck #1			
Truck Type:	H Unit		
Gross Vehicle Weight (tons):	20		
Number of Axles:	2		
Lane #	2		
Direction of Travel	Up-Station		
Truck Location	Entering Bridge		
Load Length (ft)	14		

Axle #	Distance Behind Front (1st) Axle (ft):	Weight on Axle (tons):	Weight on Axle (lbs)
1	0	4	8000
2	14	16	32000

Truck #2			
Truck Type:	None		
Gross Vehicle Weight (tons):			
Number of Axles:			
Lane #			
Direction of Travel	Down-Station		
Truck Location	Exiting Bridge		
Load Length (ft)	14		

Axle #	Distance Behind Front (1st) Axle	Weight on Axle (tons):	Weight on Axle

Truck #3			
Truck Type:	None		
Gross Vehicle Weight (tons):			
Number of Axles:			
Lane #			
Direction of Travel	Up-Station		
Truck Location	Entering Bridge		
Truck Position	Rightmost		
Load Length (ft)	14		

Axle #	Distance Behind Front (1st) Axle (ft):	Weight on Axle (tons):	Weight on Axle (lbs)

Truck #4			
Truck Type:	None		
Gross Vehicle Weight (tons):			
Number of Axles:			
Lane #			
Direction of Travel	Down-Station		
Truck Location	Entering Bridge		
Truck Position	Rightmost		
Load Length (ft)	14		

Axle #	Distance Behind Front (1st) Axle	Weight on Axle (tons):	Weight on Axle

Use Multiple Lane Presence Factor from AASHTO Standard Specifications (2002) Article 3.12? ☐ YES

Create Mesh (SELECT 1st)

Place Trucks on Bridge (SELECT 2nd)

Figure 3-16: Truck Input User-Interface

3.4.1 Truck Selection and Placement

Further discussion of the Truck Input user interface will focus on the ‘Truck #1’ section, shown for more clarity in Figure 3-17.

Truck #1

Truck Type:	H Unit ▼
Gross Vehicle Weight (tons):	20
Number of Axles:	2
Lane #	2
Direction of Travel	Up-Station
Truck Location	Entering Bridge
Load Length (ft)	14

Axle #	Distance Behind Front (1st) Axle (ft):	Weight on Axle (tons):	Weight on Axle (lbs)
1	0	4	8000
2	14	16	32000

Figure 3-17: Truck Input and Information Section

3.4.1.1 Truck Type

When the ‘Truck Type’ user interface box is selected a drop-down menu appears (Figure 3-18) which lists all of the 13 truck types which the user can place on the bridge (discussed in section 2.1.2.1) along with the ‘None’ option discussed previously. For rating purposes, all trucks on the bridge should be the same type. Once a truck type is selected the ‘Gross Vehicle Weight (tons)’ and ‘Number of Axles’ sections will populate automatically to display the information unique to the truck type selected. The table at the bottom of the ‘Truck #1’ section will also populate automatically. The ‘Axle #’ column lists the number of axles on the truck type. Axle #1 is always the axle closest to the front of the truck. The ‘Distance behind Front (1st) Axle’ column displays the location (ft.) of each axle relative to the truck’s front axle. For example, as shown in Figure 3-17, the 2nd axle of an H Unit truck is 14 ft. behind the front-most axle. As shown in the figures in Appendix A, the 3rd axle of the HS Unit Truck is permitted to vary between 14 and 30 ft. behind the 2nd axle while the 2nd axle of the Notional Rating Load (NRL) is permitted to vary between 6 and 14 ft. behind the 1st axle. For simplicity, the user is not given an option to choose the location of these axles. BRIDGE assumes the smallest axle

spacing permitted (14 ft. for the HS Unit Truck and 6 ft. for the NRL) because this configuration leads to the truck loads being less distributed over the length of the bridge. This more concentrated load pattern leads to larger live load reactions at supports close to the truck which lowers the rating factor, thus, this is a conservative approach. The ‘Weight on Axle (tons)’ and ‘Weight on Axle (lbs.)’ columns display the gross weight on each axle in the corresponding units. This information is displayed to give the user confidence that the program is using the correct data which is taken from the AASHTO (2002), MBE (2011), and KDOT (2016) figures displayed in Appendix A.

Truck #1	
Truck Type:	H Unit
Gross Vehicle Weight (tons):	None
Number of Axles:	H Unit
Lane #	Type 3 Unit
Direction of Travel	HS Unit
Truck Location	Type 3S2 Unit
	Type 3-3 Unit
	Type T130 Unit
	Type T170 Unit
Load Length (ft)	14

Figure 3-18: ‘Truck Type’ Drop-Down Menu

There is a glitch in the program which occurs when a new truck type is selected for Truck #1. The ‘Gross Vehicle Weight’ box, ‘Number of Axles’ box, and the Truck #1 table does not repopulate to display the information for the new truck selection. However, the problem is entirely cosmetic as the user-selected truck is placed on the bridge and analyzed if the ‘Create Mesh’ and ‘Place Trucks on Bridge’ buttons are selected. To adjust for this malfunction, it is suggested that the user reset Truck #2 to the desired truck type after adjusting Truck #1. When Truck #2 is reset the page refreshes to display the correct information for Truck #1.

3.4.1.2 Lane Number Assignment

When the ‘Lane #’ user interface box is selected a drop-down menu appears, as shown in Figure 3-19. The drop down menu displays only the number of lanes which the user defined in the ‘Mesh & Alignment’ sheet. As stated in section 3.1 and shown in the graphic of Figure 3-1, ‘Lane #1’ is the lane closest to the bottom girder. The lane numbers progressively increase

toward the top girder, as shown in Figure 3-1. BRIDGE allows the user to place multiple trucks in the same lane. As stated in section 2.1.2.2, MBE (2011) specifies that to load rate bridges, this is sometimes necessary. When the user specifies two trucks occupying the same lane the ‘Lane #’ user interface boxes turn red and a warning message with red text appears, as shown in Figure 3-20. The text reads **“Multiple trucks are in the same lane! Ensure they do not overlap! Trucks in the same lane should have the same ‘Direction of Travel’ and opposite ‘Truck Locations’!”**. While the program allows the user to place multiple trucks in the same lane, it is the user’s responsibility to place the trucks in such a way that the trucks do not occupy the same space or ‘overlap’. To ensure that two trucks in the same lane do not overlap the following three criteria **MUST** be met:

1. Both trucks must be traveling in the ‘Up-Station’ direction or both be traveling in the ‘Down-Station’ direction
2. One truck must be in the ‘Entering Bridge’ location while the other must be in the ‘Exiting Bridge’ location
3. The sum of the extreme axle spacings (last number in the ‘Distance behind Front (1st) Axle’ column) of the two trucks must not exceed the ‘Girder Length’ specified by the user in the ‘Bridge Mesh & Alignment’ sheet.
 - a. An additional 30 ft. of clearance is recommended by MBE (2011) Article C6B.6.2.2.

Truck #1	
Truck Type:	H Unit
Gross Vehicle Weight (tons):	20
Number of Axles:	2
Lane #	2
Direction of Travel	1 2
Truck Location	Entering Bridge
Load Length (ft)	14

Figure 3-19: ‘Lane Number’ Drop-Down Menu

Multiple trucks are in the same lane! Ensure they do not overlap! Trucks in the same lane should have same 'Direction of Travel' and opposite 'Truck Location'!

Create Mesh (SELECT 1st)

Place Trucks on Bridge (SELECT 2nd)

Figure 3-20: Warning Message if there are Multiple Trucks in a Lane

3.4.1.3 Direction of Travel

When the 'Direction of Travel' user interface box is selected a drop-down menu appears, as shown in Figure 3-21. The user is given two options: 'Up-Station' and 'Down-Station'. As shown in the graphic of Figure 3-1, 'Up-Station' refers to the direction right of the bridge. Therefore, all trucks heading toward the 'right' of the bridge should be specified as traveling in the 'Up-Station' direction while all trucks heading toward the 'left' of the bridge should be specified as traveling in the 'Down-Station' direction. Trucks in the same lane should travel in the same direction which is why the 'Direction of Travel' must be the same for all trucks placed in the same lane. This connotation is used in BRIDGE because most bridge design sheets are orientated in such a way that the roadway stationing increases from left to right on the sheet. Thus 'Up-Station' is in the direction of increasing station numbers while 'Down-Station' is in the direction of decreasing station numbers.

Truck #1	
Truck Type:	H Unit
Gross Vehicle Weight (tons):	20
Number of Axles:	2
Lane #	2
Direction of Travel	Up-Station ▼
Truck Location	<div style="border: 1px solid black; padding: 2px;"> Up-Station Down-Station </div>
Load Length (ft)	14

Figure 3-21: 'Direction of Travel' Drop-Down Menu

3.4.1.4 Truck Location

When the ‘Truck Location’ user interface box is selected a drop-down menu appears, as shown in Figure 3-22. The user is given two options: ‘Entering Bridge’ and ‘Exiting Bridge’. BRIDGE conservatively places the entire truck on the bridge as this will produce a larger live load at the girder supports (compared to the same truck only half on the bridge), thus producing a smaller rating factor. When the ‘Entering Bridge’ option is selected the program places the truck’s last axle on the center of the end diaphragm with the rest of the truck on the bridge. When the ‘Exiting Bridge’ option is selected the program places the truck’s first axle on the center of the end diaphragm (the opposite end diaphragm referenced for the ‘Entering Bridge’ option) with the rest of the truck on the bridge. When two trucks are placed in the same lane and both are given the same ‘Truck Location’, the program assumes the user is placing these trucks directly on top of each other which is not realistic and should be avoided.

Truck #1	
Truck Type:	H Unit
Gross Vehicle Weight (tons):	20
Number of Axles:	2
Lane #	2
Direction of Travel	Up-Station
Truck Location	Entering Bridge
	Entering Bridge
	Exiting Bridge
Load Length (ft)	14

Figure 3-22: ‘Truck Location’ Drop-Down Menu

3.4.2 Multiple Lane Presence Factor

AASHTO (2002) Article 3.12 allows reduction of the live loads by the factors specified in Table 2-1. BRIDGE allows the user to choose whether or not to use this reduction. When the ‘Use Multiple Lane Presence Factor’ user interface box is selected a drop-down menu will appear, as shown in Figure 3-23. When the user selects ‘YES’ the program will apply the reduction factors to all truck loads placed on the bridge (When only one or two lanes contain trucks this factor is ‘1’ and the load is not reduced). When the user selects ‘NO’ the program will NOT apply the reduction factors to any trucks and the bridge is analyzed for the full gross weight of all the trucks placed on the bridge. Selecting ‘NO’ is conservative, as it creates a

larger live load reaction at the girder supports thus causing a smaller rating factor at those supports.

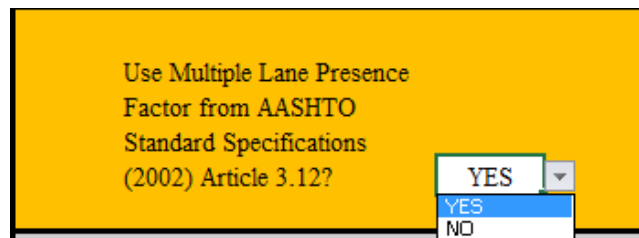


Figure 3-23: 'Multiple Lane Presence Factor' Drop-Down Menu

3.4.3 Background of the Truck Input Sheet

The background of the Truck Input sheet contains many tables which are used within the program to properly assign a magnitude and location to each truck load. The first table, shown in Figure 3-24, calculates and displays the number of user-specified trucks used in the analysis.

of Trucks:
2

Figure 3-24: Number of Trucks

The second table, shown in Figure 3-25, gives numerical values to the user inputs. For the 'Direction' of each truck, a '1' signifies 'Up-Station' while a '2' signifies 'Down-Station'. For the 'Entering or Exiting' row, a '1' signifies that the truck is entering the bridge while a '2' signifies that the truck is exiting the bridge. The 'Direction' and 'Entering or Exiting' rows may contain a value for a truck that is not placed on the bridge. The 'Lane #' row indicates which lane each truck is in while a blank value indicates that there is no truck selected.

	Truck #1	Truck #2	Truck #3	Truck #4
Direction:	1	2	1	2
Entering or Exiting:	1	2	1	1
Lane #:	1	2		

Figure 3-25: Numerical Representation of Truck Placement User-Inputs

The third table, shown in Figure 3-26, describes which trucks are sharing a lane with another truck. A '0' indicates that the truck is sharing a lane with another truck while a '1' indicates that the truck is not.

	Multiple Truck in Lane?			
Truck #	Truck #1	Truck #2	Truck #3	Truck #4
YES/NO	1	1	1	1

Figure 3-26: Trucks which Share a Lane

The table shown in Figure 3-27 indicates which lanes contain a truck. A '1' indicates that the specified lane contains a truck while a '0' indicates that either that lane is empty or there is no corresponding lane. The table shown in Figure 3-28 displays the number of lanes which contain a truck and is simply the sum of the values in Figure 3-27.

Lane 1	Lane 2	Lane 3	Lane 4
1	1	0	0

Figure 3-27: Lanes Occupied by a Truck

Loaded Lanes
2

Figure 3-28: Number of Loaded Lanes

The background of this sheet contains a list of the axle spacings and the weight on each axle for every truck. A sample of this list is shown in Figure 3-29. This list is used to display the automatically generated information in this sheet to use within the program to place the truck loads on the bridge.

	Distance Behind Front (1st) Axle (ft):	Weight on Axle (tons):
H Unit	0	4
	14	16
Type 3 Unit	0	8
	15	8.5
	19	8.5
HS Unit	0	4
	14	16
	28	16
Type 3S2 Unit	0	5
	11	7.75
	15	7.75
	37	7.75
	41	7.75

Figure 3-29: Snapshot of Spacing and Loads on each Truck Axle

3.4.4 Create the Bridge & Place Trucks on the Bridge

Once the user inputs in the ‘Mesh & Alignment’, ‘Section Geometry’, and ‘Truck Input’ sheets are completed the program is ready to create the bridge and place truck loads on the bridge. To do this the user simply selects the ‘Create Mesh’ and ‘Place Trucks on Bridge’ buttons, shown in Figure 3-30. The user MUST select the ‘Create Mesh’ button BEFORE the ‘Place Trucks on Bridge’ button. It should take no more than a few seconds for each of these buttons to perform their respective functions. The more and larger the trucks placed on the bridge the more time required to run the ‘Place Trucks on Bridge’ function. The amount of data needed to perform the tasks completed by these two buttons is too big to fit into one module. Therefore, they are divided into two modules and two buttons are required to run these two modules. The functions performed by these buttons are described in sections 4.1 and 4.2.

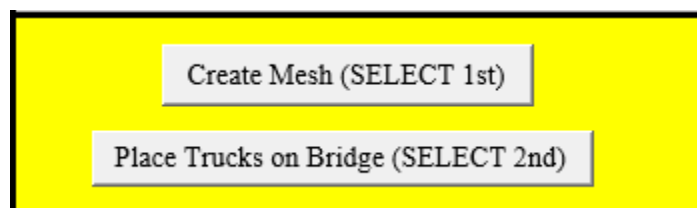


Figure 3-30: First Two Buttons which Run BRIDGE

3.5 Reaction Input Sheet

The Reaction Input user interface, shown in Figure 3-31 allows the user to choose either the girder support reactions calculated by BRIDGE or their own reactions calculated externally by any other software in determining the rating factor for the bridge. To enter a reaction the user simply inputs both the dead and live load reactions (kips) in the appropriate column and row, shown in Figure 3-31. Each ‘Support Node #’ represents a girder support. A graphic illustrating the support corresponding to each ‘Support Node #’ is shown in the Results sheet and in Figure 3-34.

Support Node #:	Reaction at Support Caused By:	
	Dead Load (kips):	Live Load (kips):
1	5.00	16.00
3	5.00	8.00
4	7.00	16.00
6	7.00	8.00
7	7.00	16.00
9	7.00	8.00
10	5.00	16.00
12	5.00	8.00

Use Calculated or Input Reactions:

CALCULATED

Load Rate Bridge

Figure 3-31: Reaction Input User-Interface

When the ‘Use Calculated or Input Reactions’ user-input box is selected, a drop-down menu appears which displays two options: ‘CALCULATED’ and ‘INPUT’, as shown in Figure 3-32. When ‘CALCULATED’ is selected, the rating factor is based on the program-calculated reactions. When ‘INPUT’ is selected the rating factor is based on the user-input reactions.

Use Calculated or Input Reactions:

CALCULATED

CALCULATED

INPUT

Figure 3-32: ‘Use Calculated or Input Reactions’ Drop-Down Menu

When the ‘Load Rate Bridge’ button is selected the load rating is calculated and displayed in the ‘Results’ sheet. The functionality of this button is described in section 4.3.

3.6 Results Sheet

The Results sheet displays both the operating (left column) and inventory (right column) minimum load ratings at each support caused by the truck-load placement combination which caused the largest live load at each support. This sheet is NOT a user-input sheet and only displays the program results. Like in the Reaction Input sheet, each ‘Support Node #’ represents a girder support, which is graphically shown in Figure 3-34. When ‘N/A’ is shown as the rating factor at a support, there is very little or no live load reaction at that support. This leads to a rating factor which is either very large or undefined (due to the rating factor equation being divided by ‘0’). If this is the case, the rating factor at this support will not govern the rating factor of the bridge, thus it is inconsequential and ‘N/A’ is printed. The ‘Governing Load Rating’ table displays the absolute minimum operating and inventory load ratings for the bridge. These load ratings are used to assess the condition of the bridge and to determine if the bridge needs posting.

Support Node #:	Minimum Load Rating		Governing Load Rating:	
	Operating	Inventory		
1	1.26	0.76	1.10	0.66
3	N/A	N/A		
4	1.10	0.66		
6	2.13	1.28		
7	1.12	0.67		
9	1.44	0.86		
10	1.17	0.70		
12	1.42	0.85		

Figure 3-33: Results Sheet

Also in this tab is a graphical representation of the bridge mesh, shown in Figure 3-34, which is created when the ‘Create Mesh’ button is selected. This graphic illustrates the number

or girders (horizontal members) and diaphragms (vertical members) and shows how each member and node is labeled by the program. When the 'Show Node Numbers' circle is selected, the graph only displays the node labels which, in Figure 3-34, are the numbers by the member intersections that are not boxed. When 'Show Member Numbers' is selected, the graph only displays the member labels which, in Figure 3-34, are the boxed numbers adjacent to their respective members. When 'Show Node & Member Numbers' is selected, both node and member labels are displayed on the graphic. The graphic can illustrate up to 12 girders and any number of diaphragms. End, real interior, and virtual interior diaphragms are illustrated in the graphic.

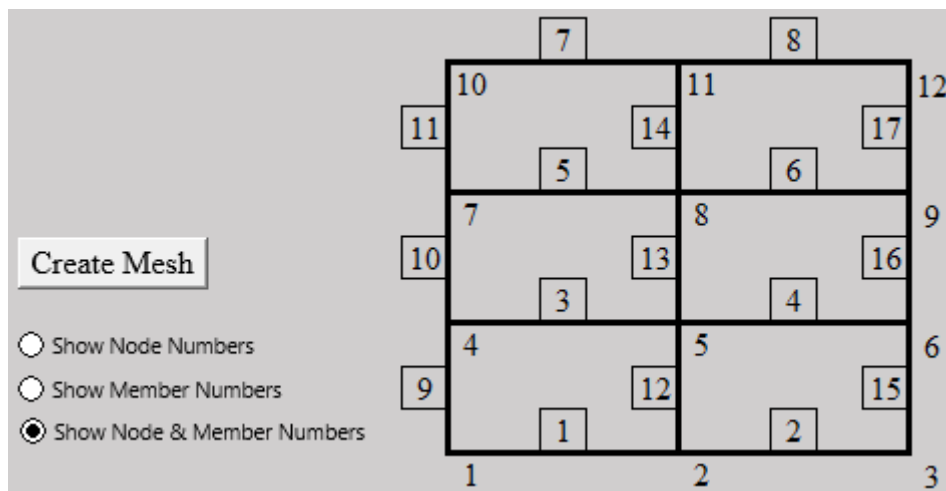


Figure 3-34: Bridge Mesh Graphic

Chapter 4 BRIDGE Functionality

4.1 Create Mesh

The 'Create Mesh' button initializes the 'Load_Path_Locations' module within the program. When this module is ran BRIDGE performs the following tasks:

4.1.1 Creating Grid and Assigning Member & Node Numbers

This module creates a grid composed of the bridge girders and diaphragms and assigns a number to each member and node (member ends) within the grid. The grid of a bridge with 4 girders and 3 diaphragms is shown in Figure 4-1. The numbers in boxes represent member numbers while the numbers not boxed represent node numbers.

If the number of girders is greater or equal to the number of diaphragms, the numbering of the nodes begins at the bottom left corner of the bridge and increases along the bottom girder until all the diaphragm-girder connecting points are assigned a number. When the end of the first girder is reached, the successive node is on the far left end of the adjacent girder. The node numbering then increases along the girder until all of the nodes on this girder are assigned. This continues with each successive girder until all of the diaphragm-girder connecting nodes are assigned, as shown in Figure 4-1. Then the members are numbered, starting at the bottom leftmost girder and increasing across the girder before moving to the girder above, as shown in Figure 4-1. After all the girder members are labeled, the diaphragm members are numbered starting at the bottom leftmost diaphragm member and increasing along the left diaphragm before starting with the next diaphragm, as shown in Figure 4-1.

When the number of diaphragms is greater than the number of girders, the numbering of the nodes and members is similar to when the number of girders is greater than the number of diaphragms except the numbering first increases along the diaphragms beginning at the leftmost diaphragm before progressing to the girders.

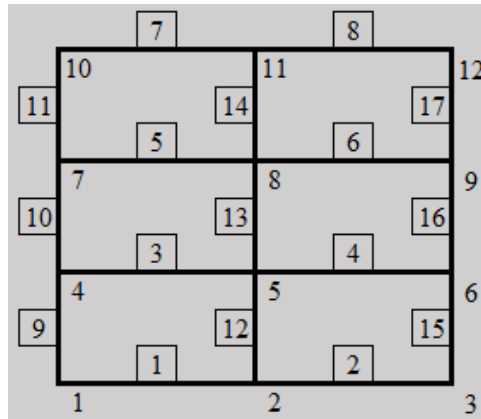


Figure 4-1: Bridge Mesh with Labeled Members and Nodes

4.1.2 Assigning Coordinates to Nodes and End Nodes to Members

Coordinates (in.) are assigned to each node based on the user input from the Mesh & Alignment sheet. Nodes are also assigned to the ends of each member. The assignments are displayed in the Node & Member Assignment sheet, as shown in Figure 4-2. For the node coordinates, the 'x' axis is parallel to the bridge span and girders while the 'y' axis is parallel to the diaphragms. End node 'i' is the node to the left of a girder member or bottom of a diaphragm member while the 'j' node is on the opposite end of the member.

Node	Node Coordinates		Member	End Nodes	
	x	y		i	j
1	0	0	1	1	2
2	306	0	2	2	3
3	612	0	3	4	5
4	0	171.333	4	5	6
5	306	171.333	5	7	8
6	612	171.333	6	8	9
7	0	342.667	7	10	11
8	306	342.667	8	11	12
9	612	342.667	9	1	4
10	0	514	10	4	7
11	306	514	11	7	10
12	612	514	12	2	5
			13	5	8
			14	8	11
			15	3	6
			16	6	9
			17	9	12

Figure 4-2: Member End Nodes and Node Coordinates

4.1.3 Identifying Boundary Members for Panels

The grid creates ‘panels’, which are rectangles surrounded above and below by girders and to the left and right by diaphragms. These panels are numbered by the program starting with ‘1’ for the bottom leftmost panel in Figure 4-1 and increases numerically first to the right then to the top. The panel numbers and the number of each surrounding member are displayed in a table in the Node & Member Assignments sheet, as shown in Figure 4-3.

Panel #	Member # Above	Member # Below	Member # Left	Member # Right
1	3	1	9	12
2	4	2	12	15
3	5	3	10	13
4	6	4	13	16
5	7	5	11	14
6	8	6	14	17

Figure 4-3: Panel List and Surrounding Members

4.1.4 Determining Truck-Load Paths

BRIDGE determines the truck paths in each lane. Standard truck axles are spaced 6 ft. apart and the truck encroaches an additional 2 ft. past the centerline of each wheel load, making the entire truck clearance 10 ft., as explained by Figure 2-1. AASHTO (2002) states that the truck should be placed in its lane so as to produce the maximum live load reaction at the girder supports. This would require the creation of influence lines to determine the exact truck placement combination which creates the maximum live load for each girder support. This type of analysis is computationally expensive to create as it would result in much longer run times for the program. As a simplified alternative, the program places each truck in four load paths across their respective lane. The exterior wheels in the first and fourth load paths are placed 2 ft. from the edge of the barrier or lane-dividing line, as shown by the exterior trucks in Figure 4-4. The other two truck-load paths (interior trucks in Figure 4-4) are spaced uniformly between the two exterior loading paths at a spacing labeled ‘Load Path Spacing’ in Figure 4-4. The ‘Load Path Spacing’ is unique for each lane depending upon the lane width and shoulder widths adjacent to

that lane. The shoulder widths are considered part of the adjacent lane, thus the truck is allowed to encroach upon the shoulder width. Truck-load paths are assumed straight across the length of the bridge.

To determine the extreme live load at each girder support the program places Truck #1 in its first load path and incrementally moves all the other trucks throughout their load paths. Truck #1 is then moved to its second load path and the process is repeated until all possible truck placement combinations, and the girder support reactions caused by each combination, are analyzed. For example, if there are two trucks on the bridge there will be 16 separate load combinations analyzed by the program. If there are three trucks, there will be 64 total load combinations.

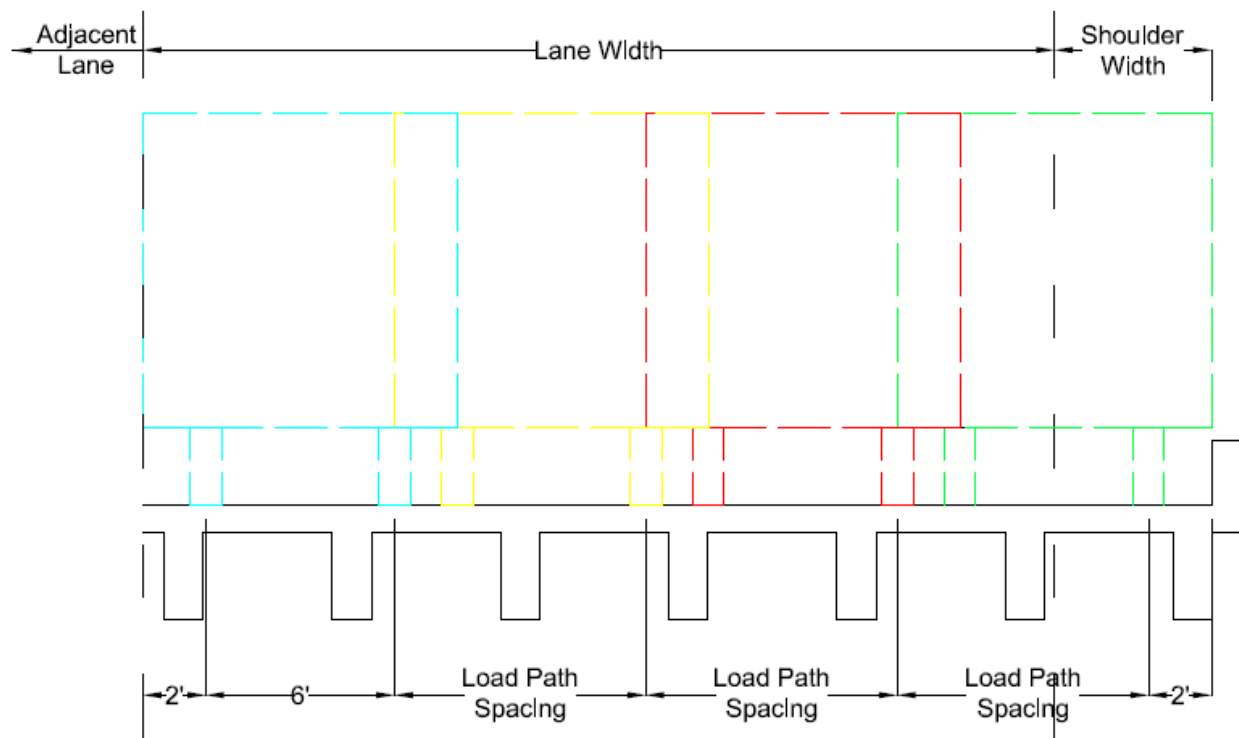


Figure 4-4: Four Load Paths within each Lane

4.1.5 Placing Trucks on Bridge

The program uses the tables in the background of the Truck Input sheet to place the truck loads in the appropriate user-specified locations. Each wheel load is assigned a number. The loads from Truck #1 are labeled first followed by Truck #2 and so on. The location of each

wheel load is then identified. The x-coordinate of each load is measured from the center of the far left diaphragm while the y-coordinate of each load is measured from the center of the bottom exterior girder. There are four y-coordinates corresponding to each load which represent the positions of the four truck-load paths discussed in the previous section. The “Rightmost” load path refers to the load path closest to the bottom girder while the “Leftmost” load path refers to the load path furthest from the bottom girder. The load magnitude and location of each load is displayed in the Node & Member Assignments sheet, as shown in Figure 4-5.

Load #	Load on Wheel (tons)	x-dist from cent. far left diaphragm (in.)	y-dist from cent. of bottom girder for each "load path" (in.)			
			"Rightmost"	"Right"	"Left"	"Leftmost"
1	4	168	17	65	113	161
2	4	168	89	137	185	233
3	16	0	17	65	113	161
4	16	0	89	137	185	233
5	4	0	281	329	377	425
6	4	0	353	401	449	497
7	16	168	281	329	377	425
8	16	168	353	401	449	497
9	16	336	281	329	377	425
10	16	336	353	401	449	497

Figure 4-5: Truck Load and Placement Information

4.1.6 Determining Multiple Presence Factor

BRIDGE reads whether or not the user chooses to use the live load reduction factor for loads in multiple lanes described by AASHTO (2002) Article 3.12. If the user chooses not to use the reduction factors, the program sets the reduction factor to 1. If the user does choose to use the reduction factors, the program will read the background of the Truck Input sheet to determine how many lanes are loaded and assign a reduction factor based on Table 2-1. The program then prints the reduction factor into the background of the Truck Input sheet, as shown in Figure 4-6.

Reduction Factor
1

Figure 4-6: Reduction Factor

4.1.7 Determining Load Length

The program determines the length of each truck, which is defined by the program as the distance between the 1st and last axles. This length (ft.) is then printed in the 'Load Length' section in the user-input section of the Truck Input sheet, shown in Figure 3-17. The overall load length used for determining the impact factor in Equation 2-3 is then found and printed in the background of the Truck Input sheet, as shown in Figure 4-7. This length is the smallest of either the shortest truck length on the bridge or the bridge length because this gives the highest impact load coefficient, which is conservative.

Load Length:
14

Figure 4-7: Load Length for Impact Factor Calculation

4.2 Place Trucks on Bridge

The 'Place Trucks on Bridge' button initializes the 'Truck_Placement' module. When this module is ran BRIDGE performs the following tasks:

4.2.1 Identifying which Panel is under each Load and Location of the Load on the Panel

This module reads the location of each load and determines which panel the load is on. The relative location of each load on the panel is then determined. The 'x'-distance of the load is measured from the center of the diaphragm on the left edge of the panel while the 'y' distance is measured from the center of the girder on the bottom edge of the panel.

4.2.2 Distributing each Load to the Members Surrounding the Panel

Each load is then distributed to the girders and diaphragms on the edges of each panel. The portion of each load distributed to the various edge members is dependent upon the length of the edge diaphragms and girders as well as the location of the load on the panel. Three methods were investigated to find the most appropriate method of distributing the truck wheel point loads from the panels to the surrounding girders and diaphragms. The three methods are the 'Finite

Element Analysis of panel', the 'Rigid Slab Analysis of panel', and the 'Rigid Beam Analysis within the panel'.

4.2.2.1 Finite Element Analysis of Panel

To investigate the 'Finite Element Analysis of Panel' method a RISA model was created which represented a panel surrounded by 8 ft. long diaphragms and 12 ft. long girders. The RISA model is shown in Figure 4-8. This panel is assumed flexible and consisted of an 8 in. thick plate of 4 ksi normal weight concrete, which is a reasonable representation of bridge deck slab thicknesses and material strength. To improve the accuracy of the model, the plate was divided using a 1'x1' mesh. A 10 kip load was placed 3 ft. from the origin along the girder and 2 ft. from the origin along the diaphragm. If the origin is at the bottom-left corner of the plate and the entire plate lies in the first quadrant with the bottom girder along the x-axis then the load is placed at the coordinates (3', 2'), as shown in Figure 4-8. Each node along the boundary girders and diaphragms was set as a pinned reaction and the model was ran. The reaction at each node of the boundary elements was recorded and the sum of the reactions equaled 10.242 kips. This differentiated from the 10 kip original point load more than desired so the plate's mesh was further refined to a 3"x3" mesh. Keeping the load in the same location, the model was again ran. This time, the sum of the reactions at the boundary elements was 9.997 kips, which is very close to the original 10 kip point load, thus, the 3"x3" mesh was deemed to produce adequately accurate results. The reactions along each boundary member are shown in Figure 4-9, Figure 4-10, Figure 4-11, and Figure 4-12. The 'primary diaphragm' is the diaphragm closest to point load while the 'secondary diaphragm' is the diaphragm furthest from the point load. Likewise for the girders. The total load on each edge member is shown in Table 4-1.

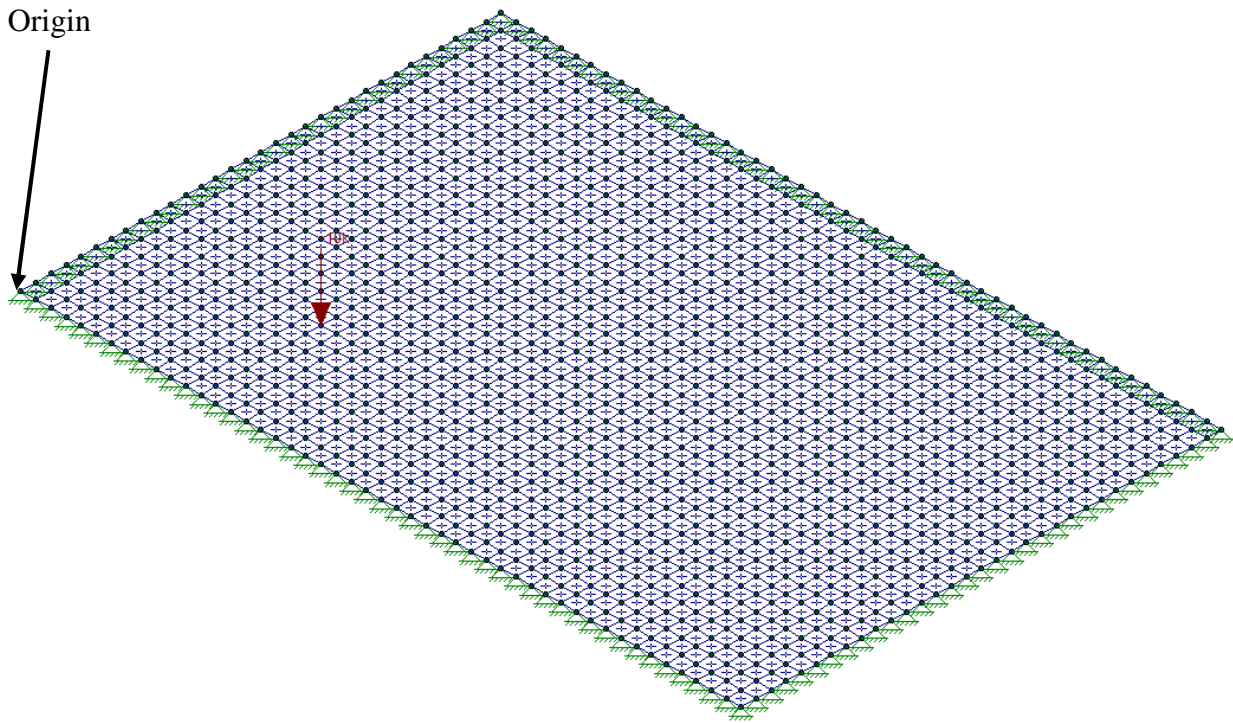


Figure 4-8: RISA Model of 'Finite Element Analysis of Panel' with a 3"x3" Mesh

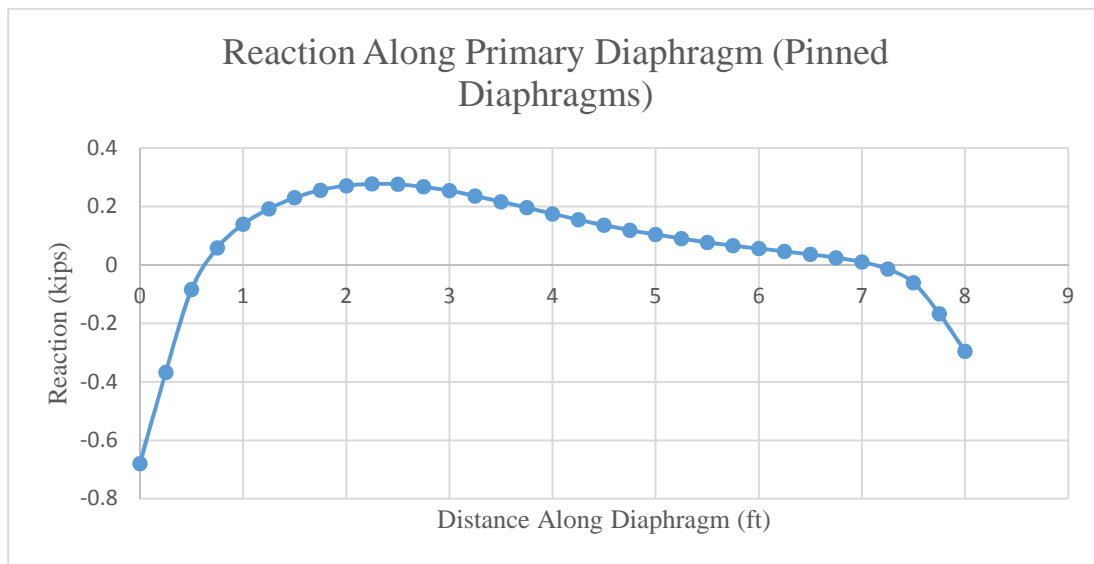


Figure 4-9: Reaction at Each Node along Primary Diaphragm

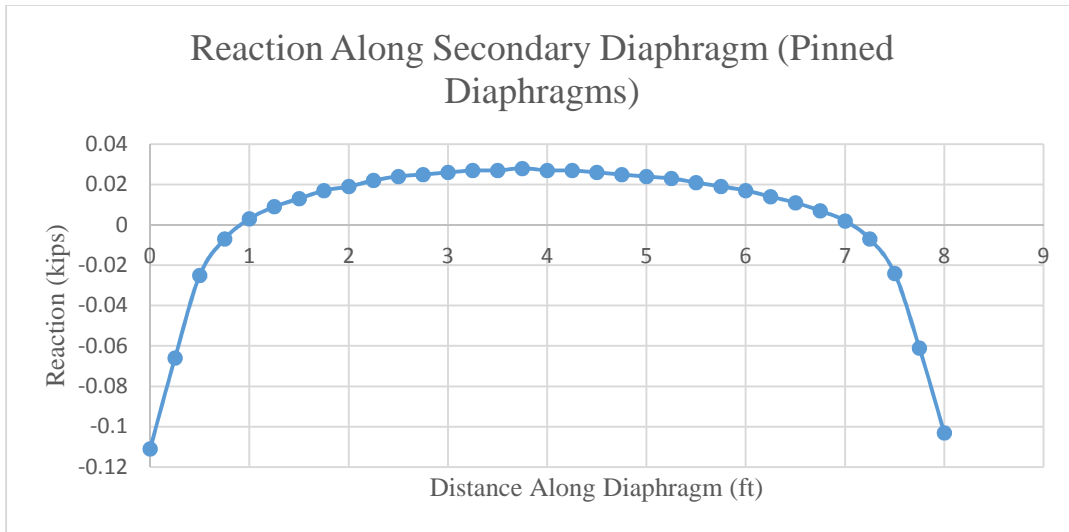


Figure 4-10: Reaction at Each Node along Secondary Diaphragm

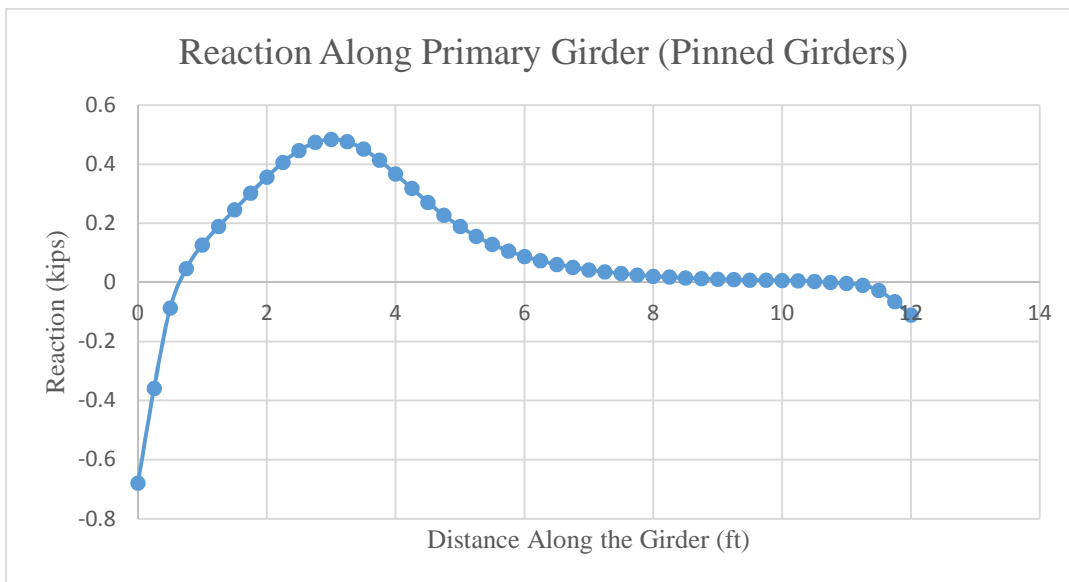


Figure 4-11: Reaction at Each Node along Primary Girder

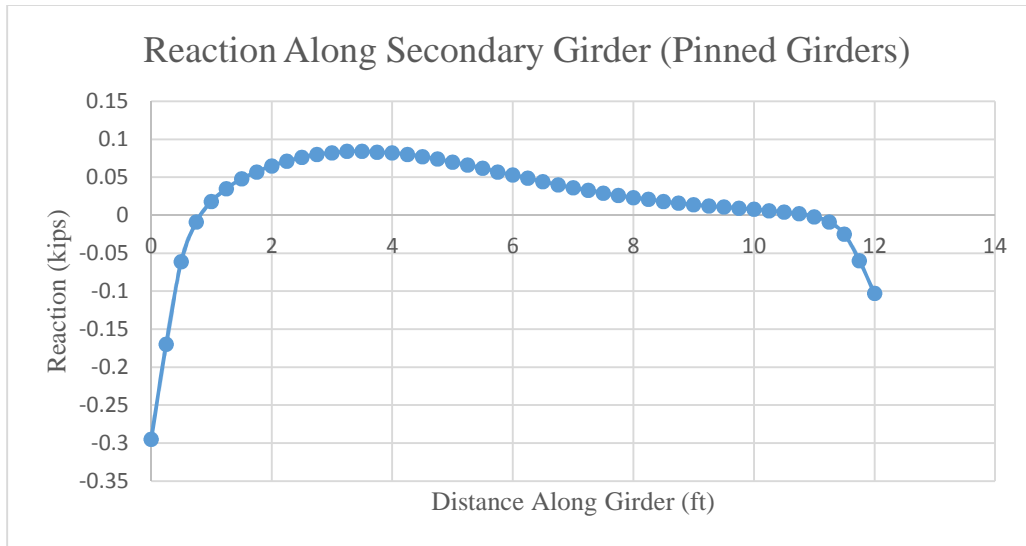


Figure 4-12: Reaction at Each Node along Secondary Girder

It was seen that the loads along each girder and diaphragm were centered near the location of the load, thus it was desired to determine if the portion of load distributed to each member can act as a single point load along the member at the location of the load. Further, if this method is used in the program, a finite element analysis would need to be conducted for each panel on the bridge to find the loads on each surrounding girder and diaphragm. This is very time consuming and complicated, thus, it was desired to determine if other distribution methods yield reasonable results.

4.2.2.2 Rigid Slab Analysis of Panel

For the 'Rigid Slab Analysis of Panel' a RISA model of the same panel from section 4.2.2.1 was analyzed, except the diaphragms' end nodes were freed so only the girder nodes were pinned and the slab acted in one way action between the girders, as shown in Figure 4-13. The load and load location remained the same and the deflection of the slab at the location of the load (Δ_d) was found. Next, the girder nodes were freed and the diaphragm nodes were pinned so the slab acted in one way action between the diaphragms. The load and load location remained the same and the deflection at the location of the load (Δ_g) was found. These deflections were used, along with the applied load, to determine how the load distributed to each of the end diaphragms and girders. The slab, for these calculations, was assumed rigid. The calculations to distribute the load are derived below. Equation 4-1 is substituted to create Equation 4-2 while

Equation 4-3 is substituted into Equation 4-4 to yield Equation 4-5 and Equation 4-6. Equation 4-1 and Equation 4-2 are then substituted into Equation 4-6 to yield Equation 4-7.

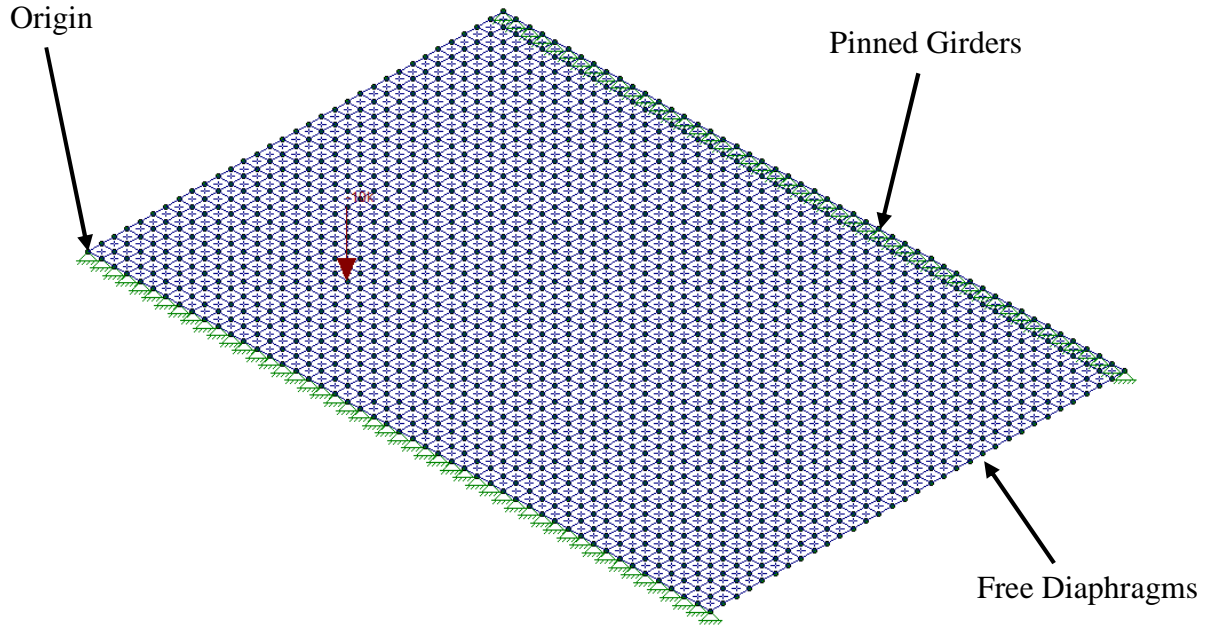


Figure 4-13: RISA Model of ‘Rigid Slab Analysis of Panel’ with Pinned Girders and Free Diaphragms

Derivation:

$$K_G = \frac{P}{\Delta_G} \text{ \& \; } K_D = \frac{P}{\Delta_D} \quad \text{Equation 4-1}$$

$$K_{\text{sum}} = K_G + K_D = \frac{P}{\Delta_G} + \frac{P}{\Delta_D} \quad \text{Equation 4-2}$$

$$\Delta = \frac{P_G}{K_G} = \frac{P_D}{K_D} \quad \text{Equation 4-3}$$

$$K_{\text{sum}} = \frac{P}{\Delta} \rightarrow \Delta = \frac{P}{K_{\text{sum}}} \quad \text{Equation 4-4}$$

$$\frac{P_G}{K_G} = \frac{P}{K_{\text{sum}}} \text{ \& \; } \frac{P_D}{K_D} = \frac{P}{K_{\text{sum}}} \rightarrow \quad \text{Equation 4-5}$$

$$P_G = K_G \frac{P}{K_{\text{sum}}} \text{ \& \; } P_D = K_D \frac{P}{K_{\text{sum}}} \rightarrow \quad \text{Equation 4-6}$$

$$P_G = \frac{P}{\Delta_G} \left(\frac{P}{\left(\frac{P}{\Delta_G} + \frac{P}{\Delta_D} \right)} \right) \quad \& \quad P_D = \frac{P}{\Delta_D} \left(\frac{P}{\left(\frac{P}{\Delta_G} + \frac{P}{\Delta_D} \right)} \right) \quad \text{Equation 4-7}$$

Where:

P	=	Load Applied to Slab
K _G	=	Stiffness of the slab when acting as a girder (kip/in.)
K _D	=	Stiffness of the slab when acting as a diaphragm (kip/in.)
Δ _G	=	Deflection of slab when acting as a girder (in.)
Δ _D	=	Deflection of slab when acting as a diaphragm (in.)
K _{sum}	=	Sum of slab stiffness when acting as girder and diaphragm (kip/in.)
P _G	=	Total load transferred to diaphragms (slab acts as girder) (kips)
P _D	=	Total load transferred to girders (slab acts as diaphragm) (kips)

For this analysis the Δ_G and Δ_D were 0.029 in. and 0.009 in. respectively while the applied load, P, was 10 kips. Therefore, P_G and P_D were 2.39 kips and 7.63 kips respectively, as shown in Equation 4-8 and Equation 4-9:

$$P_G = \frac{10}{0.029} \left(\frac{10}{\left(\frac{10}{0.029} + \frac{10}{0.009} \right)} \right) = 2.39 \text{ kip} \quad \text{Equation 4-8}$$

$$P_D = \frac{10}{0.009} \left(\frac{10}{\left(\frac{10}{0.029} + \frac{10}{0.009} \right)} \right) = 7.63 \text{ kip} \quad \text{Equation 4-9}$$

The loads on each girder and diaphragm are then determined in a similar method as used to determine the reactions of a simply supported beam caused by a point load on the beam, as shown in Equation 4-10 and Equation 4-11. The point loads transferred to each member using the ‘Rigid Slab Analysis’ are displayed in Table 4-1.

$$P_{\text{distributed to diaphragm}} = P_G \frac{a}{L_G} \quad \text{Equation 4-10}$$

$$P_{\text{distributed to girder}} = P_D \frac{a}{L_D} \quad \text{Equation 4-11}$$

Where:

$P_{\text{dist. to diaphragm}}$	=	Point load on each diaphragm
$P_{\text{dist. to girder}}$	=	Point load on each girder
a	=	Distance between point load and girder/diaphragm analyzed
L_G	=	Length of girders
L_D	=	Length of diaphragms

4.2.2.3 Rigid Beam Analysis within the Panel

It was then desired to see, with what accuracy, the slab could be modeled as two beams. In the ‘Rigid Beam Analysis’ a RISA model was created which consisted of two beams, each 1 ft. wide and 8 in. thick. The ‘girder’ beam was 2 ft. from the origin while the ‘diaphragm’ beam was 3 ft. from the origin, so that the intersection of the two beams was at the coordinates (3’, 2’). The 10 kip point load was applied at this location, just like the previous models. This setup is shown in Figure 4-14. The girder beam was deleted, leaving the diaphragm beam with both ends pinned. The deflection of the beam, Δ_D , at the location of the load was determined. The girder beam was then added and the diaphragm beam was deleted. The deflection of the girder beam, Δ_G , at the location of the load was then found. Equation 4-7 and Equation 4-10 were then used to find the load transferred to each diaphragm and girder.

For this analysis the Δ_G and Δ_D were 0.19 in. and 0.057 in. respectively while the applied load, P , was 10 kips. Therefore, P_G and P_D were 2.308 kips and 7.69 kips respectively, and the load transferred to each girder and diaphragm are as shown in Table 4-1.

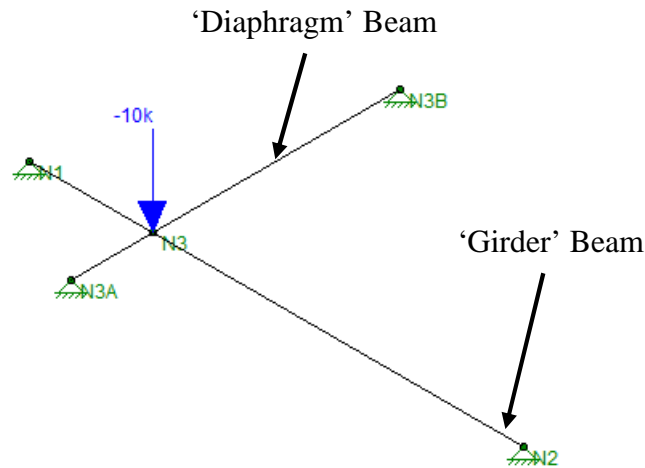


Figure 4-14: RISA Model for the 'Rigid Beam Analysis within the Panel'

4.2.2.4 Analysis Results and Conclusions

As seen in Table 4-1, the 'Rigid Slab Analysis of Panel' and 'Rigid Beam Analysis within the Panel' distribute loads similarly to the more accurate 'Finite Element Analysis of Panel', especially for the primary girder, which receives the majority of the load. Based on these results, it was concluded that the 'Rigid Beam Analysis of Panel' can distribute loads to the girders and diaphragms with reasonable accuracy.

The centroid of reaction along each girder and diaphragm for each method are shown in Table 4-2. The area under the curves of Figure 4-9 through Figure 4-12 were analyzed to find the reaction location for the 'Finite Element Analysis' while a similar process was used for the 'Rigid Slab Analysis'. For the 'Rigid Beam Analysis' the load was assumed to transfer to the girders and diaphragms at the point along the member corresponding to the location of the concentrated load. The centroid of the reaction for the 'Rigid Slab Analysis' was extremely close to the location along the girders and diaphragms of the concentrated load. The centroid of reactions along the girders and diaphragms for the 'Finite Element Analysis' were further away from the location of the concentrated load. However, for the primary girder, which carries the majority of the load, the centroid of reaction was at a distance of 3.7 ft. from the origin, which is close to the center of reaction for the 'Rigid Beam Analysis'. For the other diaphragms and girders, the centroid of reaction is 1.25-2 ft. away from the reactions of the 'Rigid Beam Analysis'. This was considered insignificant since less load is transferred to these members. Therefore, it was concluded that the 'Rigid Beam Analysis' transfers the load to the girders and diaphragms with reasonable accuracy. Thus, this load distribution method is incorporated into BRIDGE.

Table 4-1: Comparison of Load Distribution to Girders and Diaphragms using Different Analysis Methods

ANALYSIS METHOD:	Load Transferred to:			
	Diaphragm		Girder	
	Primary	Secondary	Primary	Secondary
Finite Element	2.783	0.186	5.758	1.27
Rigid Slab	1.776	0.592	5.723	1.908
Rigid Beam	1.731	0.577	5.769	1.923

Table 4-2: Comparison of the Centroid of Reaction along Girders and Diaphragms using the Different Analysis Methods

ANALYSIS METHOD:	Centroid of Reaction from Origin (ft.):			
	Diaphragm		Girder	
	Primary	Secondary	Primary	Secondary
Finite Element	3.25	3.99	3.70	4.99
Rigid Slab	2.27	2.35	3.10	3.28
Rigid Beam	2	2	3	3

4.2.2.5 Aspect Ratio Tables:

The ‘Rigid Beam Analysis’ method was then ran for a series of girder-to-diaphragm length ‘aspect ratios’. In the analysis, each ‘diaphragm’ beam was 1 ft. wide, 8 in. thick, and 10 ft. long. Each ‘girder’ beam was 1 ft. wide and 8 in. deep while the length of the beam varied. For an aspect ratio of ‘1’ the beam length was 10 ft. For each incremental ‘0.1’ increase of the aspect ratio the length of the ‘girder’ beam increased by 1 ft. Therefore, for an aspect ratio of 1.5, the girder length was 15 ft. The aspect ratio is the girder-length-to-diaphragm-length ratio of a panel.

The f_D/f_{Dmax} & f_G/f_{Gmax} values were calculated for various x/a and y/b load locations for each aspect ratio combination. The f_D/f_{Dmax} & f_G/f_{Gmax} values are used to find the flexibility of the panel in each bending direction and are described by Equation 4-12 through Equation 4-15. These values are multiplied by the f_{Dmax} and f_{Gmax} for the actual panel being analyzed by the program to obtain the flexibility of the diaphragm and girder panel beams, f_D and f_G ,

respectively. f_D is the flexibility of the panel beam acting as a diaphragm (spanning between the girders and parallel to the diaphragms) while f_G is the flexibility of the panel beam acting as a girder (spanning between the diaphragms and parallel to the girders). These flexibilities are inverted to find the stiffness of each beam, K_D and K_G . These values are then used in Equation 4-7 and Equation 4-10 to distribute the load to the girders and diaphragms. The x/a and y/b ratios describe the location of the load on the panel. As shown in Figure 4-15, 'a' represents the girder length along the panel edge, 'b' is the diaphragm length along the panel edge, 'x' is the position of the load along the girder and 'y' is the position of the load along the diaphragm.

$$f_{Dmax} = \frac{L_D^3}{48EI_D} \quad \text{Equation 4-12}$$

$$f_{Gmax} = \frac{L_G^3}{48EI_G} \quad \text{Equation 4-13}$$

$$f_D = \frac{\Delta_D}{P} \quad \text{Equation 4-14}$$

$$f_G = \frac{\Delta_G}{P} \quad \text{Equation 4-15}$$

Where:

f_{Dmax}	=	Maximum flexibility of the diaphragm beam (in./kip)
f_{Gmax}	=	Maximum flexibility of the girder beam (in./kip)
L_D	=	Length of diaphragm (in.)
L_G	=	Length of girder (in.)
E	=	Modulus of elasticity for concrete
I_D	=	Moment of inertia of diaphragm beam (in. ⁴)
I_G	=	Moment of inertia of girder beam (in. ⁴)
f_D	=	Actual flexibility of the diaphragm beam (in./kip)
f_G	=	Actual flexibility of the girder beam (in./kip)
P	=	Point load placed on beams (kips)
Δ_D	=	Deflection of the diaphragm beam at location of point load (in.)
Δ_G	=	Deflection of the girder beam at location of point load (in.)

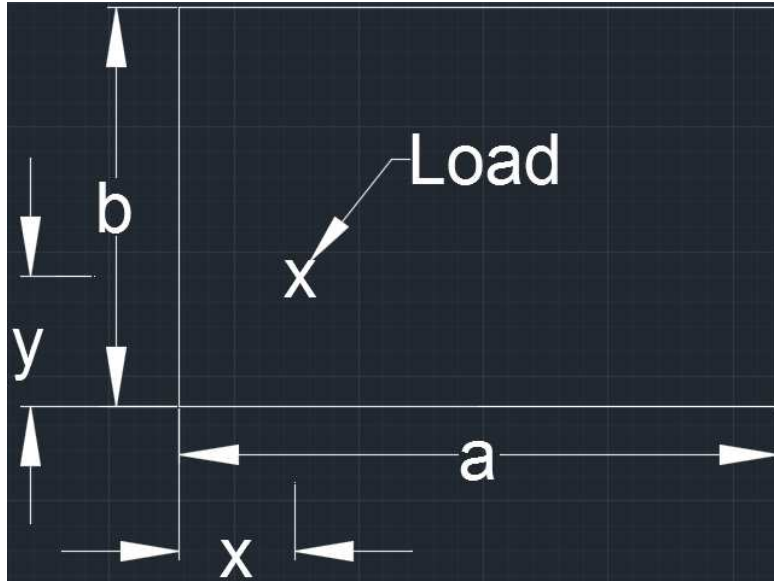


Figure 4-15: Load Placement on Panel

f_D/f_{Dmax} & f_G/f_{Gmax} values are calculated for aspect ratios ranging from 1 to 2 by 0.1 increments. Aspect ratios from 0.5 to 1 use the same values calculated from the aspect ratios 1 to 2, except the load distribution is switched from the girders to the diaphragms and vice versa. For example, the f_D/f_{Dmax} value for an aspect ratio of 0.6 is the same as the f_G/f_{Gmax} value for an aspect ratio of 1.2. When the aspect ratio is below 0.5 the program assumes that the entire load is transferred to the diaphragms. When the ratio is over 2, the program assumes that the entire load is transferred to the girders. If a wheel load is on the cantilever portion of the deck the program automatically transfers the full load to the adjacent girder.

The f_D/f_{Dmax} & f_G/f_{Gmax} values for various x/a and y/b values at different aspect ratios are displayed in Table 4-3 and Table 4-4.

Table 4-3: f_D/f_{Dmax} Values for Varying y/b Locations for All Aspect Ratios

f_D/f_{Dmax}		All Aspect Ratios:
y/b	0	0
	0.2	0.415295601
	0.4	0.922879112
	0.6	0.922879112
	0.8	0.415295601
	1	0

Table 4-4: f_G/f_{Gmax} Values for Varying x/a Locations and Aspect Ratios

f_G/f_{Gmax}		Aspect Ratio										
		1	1.1	1.2	1.3	1.4	1.5	1.6	1.7	1.8	1.9	2
x/a	0	0.0	0.0	0.0	0.0	0.0	0.0	0.0	0.0	0.0	0.0	0.0
	0.2	0.4153	0.4122	0.4095	0.4107	0.4092	0.4086	0.4081	0.4080	0.4079	0.4074	0.4070
	0.4	0.9229	0.9206	0.9198	0.9195	0.9174	0.9176	0.9163	0.9152	0.9152	0.9149	0.9145
	0.6	0.9229	0.9206	0.9198	0.9195	0.9174	0.9176	0.9163	0.9152	0.9152	0.9149	0.9145
	0.8	0.4153	0.4122	0.4095	0.4107	0.4092	0.4086	0.4081	0.4080	0.4079	0.4074	0.4070
	1	0.0	0.0	0.0	0.0	0.0	0.0	0.0	0.0	0.0	0.0	0.0

Table 4-3, shows the f_D/f_{Dmax} values for varying y/b load locations. The ‘diaphragm’ beam length was kept constant, therefore the f_D/f_{Dmax} value was constant for every aspect ratio.

Table 4-4, shows the f_G/f_{Gmax} values for varying x/a load locations. The values did change for varying aspect ratios as the girder became longer. However, for a given x/a the f_G/f_{Gmax} value is extremely close for all aspect ratios. Therefore, for simplicity, the values for an aspect ratio of 1 are used regardless of the actual aspect ratio of the panel. These match the f_D/f_{Dmax} values for different y/b ratios, therefore, Table 4-3 and Table 4-4 are combined into Table 4-5. More values for y/b and x/a were included in this table to increase the accuracy of interpolation within the table. The program uses the x/a and y/b locations of the wheel-load on the panel to interpolate within Table 4-5 to determine an appropriate f_D/f_{Dmax} and f_G/f_{Gmax} for each load. The f_D/f_{Dmax} is found when y/b is used in Table 4-5 and f_G/f_{Gmax} is found when x/a is used. Table 4-5 is displayed in the program’s ‘Tables’ sheet.

Table 4-5: f_D/f_{Dmax} & f_G/f_{Gmax} Values for Varying Load Location on Panel

y/b & x/a		f_D/f_{Dmax} & f_G/f_{Gmax}
All Aspect Ratios	0	0
	0.1	0.133304761
	0.2	0.415295601
	0.3	0.707540653
	0.4	0.922879112
	0.5	0.999785705
	0.6	0.922879112
	0.7	0.707540653
	0.8	0.415295601
	0.9	0.133304761
	1	0

4.2.3 Determining Fixed End Reactions at each Node Caused by Live Loads

The re-distributed load is applied as a point load on the edge girders and diaphragms at a distance along the diaphragm member equal to the load's 'y'-distance on the panel and along the girder member equal to the load's 'x'-distance on the panel. These loads are then converted into fixed-end forces at the member end nodes. The fixed-end moments are defined by Equation 4-16 and Equation 4-17 while Equation 4-18 and Equation 4-19, with reference to Figure 4-16, define the fixed-end shear forces. The fixed-end shear forces are always in the positive 'upward' direction. The fixed-end moments and shears at each end nodes of the member are then summed.

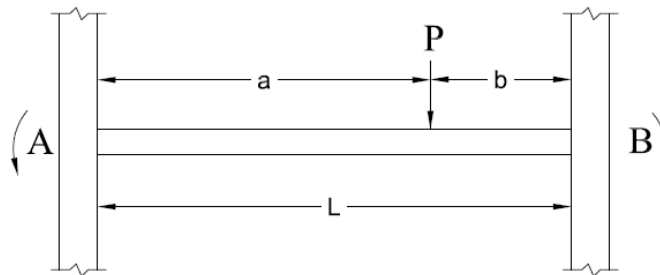


Figure 4-16: Fixed-End Moments (FEM) for a Point Load anywhere on the Span

$$FEM_{AB} = \frac{Pb^2a}{L^2} \quad \text{Equation 4-16}$$

$$FEM_{BA} = \frac{Pa^2b}{L^2} \quad \text{Equation 4-17}$$

$$V_a = \frac{Pb^2}{L^3} [L + 2a] \quad \text{Equation 4-18}$$

$$V_b = \frac{Pa^2}{L^3} [L + 2b] \quad \text{Equation 4-19}$$

Where:

FEM_{AB} = Fixed-End Moment at point 'A' in Figure 4-16

FEM_{BA} = Fixed-End Moment at point 'B' in Figure 4-16

V_a = Vertical reaction at point 'A' in Figure 4-16

V_b = Vertical reaction at point 'B' in Figure 4-16

4.2.4 Determining Reactions at Nodes Caused by Dead Loads

The cross sectional properties and material properties for the girders, slab, and wearing surface, along with the actual effective slab width from the background of the Mesh & Alignment sheet, are used to calculate the uniform dead load, w , along each girder. The weight of the diaphragms and barriers is neglected as insignificant and their inclusion would add a great deal of unnecessary complication to the user input section and dead load calculations. The dead load is transferred to the girders because, typically, the girders are closer together than are the diaphragms. If the diaphragms are closer to each other than are the girders then the load should transfer to the diaphragms. However, it is impractical for the diaphragms to be closer together than the girders, so the program always transfers the dead load to the girders. The fixed-end moments are defined by Equation 4-20, while Equation 4-21, with reference to Figure 4-17, defines the fixed end shear forces. The fixed-end shear forces are always in the positive 'upward' direction.

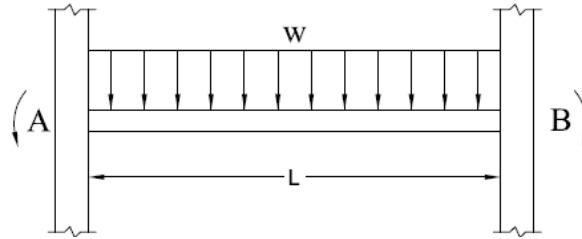


Figure 4-17: Fixed-End Moments (FEM) for a Distributed Load

$$FEM_{AB} = FEM_{BA} = \frac{wL^2}{12} \quad \text{Equation 4-20}$$

$$V_A = V_B = \frac{wL}{2} \quad \text{Equation 4-21}$$

4.2.5 Printing the k_{ff} & k_{sf} Reactions for the Bridge Matrix

The dead and live load fixed-end forces are sorted into the k_{ff} loads and k_{sf} reactions for the bridge mesh. The live k_{ff} loads and k_{sf} reactions for each truck placement combination, discussed in section 4.1.4, are calculated and printed. The dead k_{ff} loads and k_{sf} reactions are kept separate from the live loads because the governing live load combination for each girder is not yet determined. A sample of these reactions are displayed in the k_{ff} Loads and k_{sf} Reactions sheets respectively, as shown in Figure 4-18 and Figure 4-19.

k_{ff} Dead Loads:						
	0.00	-953.14	-37.38	0.00	0.00	0.00
Combination #	k_{ff} Live Loads					
1	-555.77	-175.89	-3.16	-7.59	214.12	0.00
2	-555.77	-175.89	-3.16	-7.59	214.12	0.00
3	-555.77	-175.89	-3.16	-7.59	214.12	0.00
4	-555.77	-175.89	-3.16	-7.59	214.12	0.00
5	-495.54	-98.56	-1.88	-8.45	119.99	0.00
6	-495.54	-98.56	-1.88	-8.45	119.99	0.00

Figure 4-18: Snapshot of the k_{ff} Loads in the ' k_{ff} Loads' Sheet

k_{sf} Dead Reactions:							
-6.5876 -6.58759 -7.5649 -7.5649 -7.5649 -7.5649 -7.5649							
Combination #	k_{sf} Live Reactions:						
1	-12.423	0	-16.39	0	-3.8862	0	-4.0976
2	-12.423	0	-16.39	0	-3.187	0	-3.3984
3	-12.423	0	-16.39	0	-3.187	0	-2.0976
4	-12.423	0	-16.39	0	-3.187	0	-0.7967
5	-7.2195	0	-16.39	0	-9.0894	0	-4.0976
6	-7.2195	0	-16.39	0	-8.3902	0	-3.3984

Figure 4-19: Snapshot of the k_{sf} Reactions in the ‘k_{sf} Reactions’ Sheet

4.3 Load Rate Bridge

When the user selects the ‘Load Rate Bridge’ button the “Stiffness” module is ran which performs the following tasks:

4.3.1 Assigning Properties to each Member

BRIDGE uses the information displayed in the Section Properties sheet, shown in Figure 3-15, along with the concrete strength user-input, and the coordinates of each node to determine the area, length, moment of inertia (I_x), torsional constant (J), shear modulus (G), elastic modulus (E), and angle of rotation (theta = 0 or 90) for each member in the bridge mesh. These properties are displayed in the Member Properties sheet, as shown in

Figure 4-20. Equation 4-22 and Equation 4-23 are used to find the elastic modulus and shear modulus respectively. A Poisson’s ratio (ν) of 0.2 is used. The girders are all oriented at an angle of 0° while the diaphragms are oriented at -90°. The ‘theta’ column in

Figure 4-20 displays these angles in radians.

$$E = 57\sqrt{f'_c} \quad \text{Equation 4-22}$$

$$G = \frac{E}{2(1 + \nu)}$$

Equation 4-23

Member	Area (in ²)	Length (in)	I (in ⁴)	J (in ⁴)	G (ksi)	E (ksi)	theta
1	943.25	306	150991	39601	1301	3122.019	0
2	943.25	306	150991	39601	1301	3122.019	0
3	1122	306	170629	41900	1301	3122.019	0
4	1122	306	170629	41900	1301	3122.019	0
5	1122	306	170629	41900	1301	3122.019	0
6	1122	306	170629	41900	1301	3122.019	0
7	943.25	306	150991	39601	1301	3122.019	0
8	943.25	306	150991	39601	1301	3122.019	0
9	1154.25	171.333333	18652	16948	1301	3122.019	-1.5708
10	1154.25	171.333333	18652	16948	1301	3122.019	-1.5708
11	1154.25	171.333333	18652	16948	1301	3122.019	-1.5708
12	2119.5	171.333333	7834	0	1301	3122.019	-1.5708
13	2119.5	171.333333	7834	0	1301	3122.019	-1.5708
14	2119.5	171.333333	7834	0	1301	3122.019	-1.5708
15	1154.25	171.333333	18652	16948	1301	3122.019	-1.5708
16	1154.25	171.333333	18652	16948	1301	3122.019	-1.5708
17	1154.25	171.333333	18652	16948	1301	3122.019	-1.5708

Figure 4-20: Member Properties

4.3.2 Creating Assembled Stiffness Matrix for Bridge

The program uses the member properties to create the 6x6 stiffness matrix, shown in Appendix B, for each member. The member end nodes are then used to combine these member stiffness matrices into one large assembled stiffness matrix which encompasses the entire bridge.

4.3.3 Creating k_{ff} & k_{sf} Matrices

BRIDGE separates the assembled stiffness matrix into the k_{ff} & k_{sf} matrices. The k_{ff} matrix is square and consists of the matrix elements corresponding to both the unknown nodal displacements and known nodal forces. In this program, the unknown nodal displacements are the translational displacements and rotations at all of the non-support nodes plus the rotations at the support nodes (nodes on the end diaphragms). The translational displacements at each

support are zero and are known. The known nodal forces are all of the forces and moments at the non-support nodes and the moments at the support nodes. The k_{sf} matrix consists of the matrix elements corresponding to both the unknown nodal displacements and unknown nodal forces. The unknown nodal forces consists of all the vertical forces at the support nodes.

4.3.4 Creating k_{ff}^{-1} Matrix

The Gauss-Jordan Elimination method is used to find the k_{ff}^{-1} matrix. To facilitate this method the program creates an identity matrix and the half band-width k_{ff} matrix. The identity matrix is the same size as the k_{ff} matrix and its elements are all 0's except for the diagonal, which are 1's. The k_{ff} matrix is symmetric, thus, to save memory, only half of it, the half band-width matrix, is used to solve for the k_{ff}^{-1} matrix. This half band-width and identity matrix are manipulated using the Gauss-Jordan Elimination method to find the k_{ff}^{-1} matrix. This inverse matrix is displayed in the K_{ff}^{-1} sheet.

4.3.5 Finding the Displacements at each Node

The unknown nodal displacements caused by both dead load and each live load combination are found. These displacements are found by multiplying the k_{ff}^{-1} matrix by the ' P_f ' loads, discussed in section 4.2.2.5.

4.3.6 Finding the Reactions at each Support

Next, the reaction at each support due to the dead load and each live load combination are found. They are found by multiplying the k_{sf} matrix by the displacements found in the previous section then adding the fixed-end forces corresponding to the P_s vector, discussed in section 4.2.2.5.

4.3.7 Determining Governing Live Load at each Support

BRIDGE cycles through the reaction caused by each load combination at every support and identifies the largest live load reaction at each support. This load contributes to the governing rating factor for that support.

4.3.8 Calculating the Impact Factor

The load length from Figure 4-7 is used in Equation 2-3 to find the impact factor used in Equation 2-2.

4.3.9 Determining Capacity of the Girders

As shown in Equation 2-2, the capacity of each girder at its supports is necessary to determine the rating factor of the bridge. Two approaches were considered for determining the capacity of the girders. The first approach assumes that just reactions caused by the live and dead loads act on the crack while the second approach assumes that a frictional force at the concrete girder-to-steel pad interface also acts on the crack.

4.3.9.1 Dead & Live Load Approach

The 'Dead & Live Load' approach assumes that only the reaction at the girder supports caused by live and dead load act on the crack face, as illustrated in Figure 4-21.

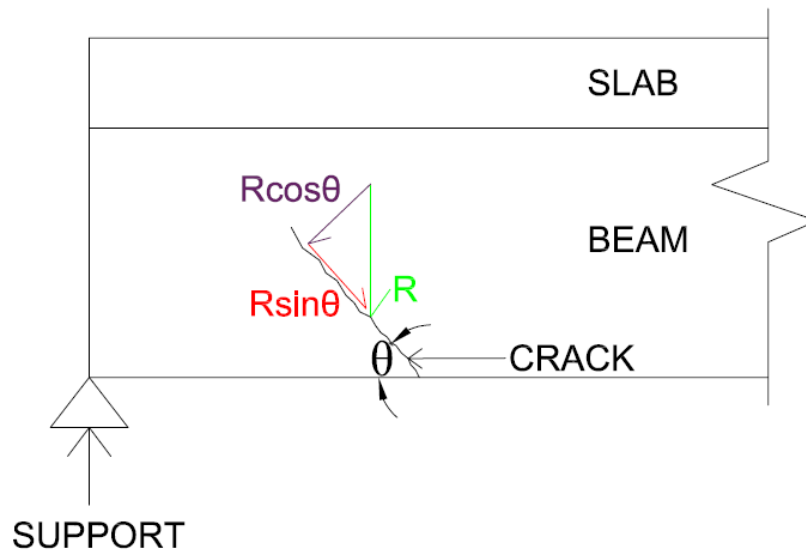


Figure 4-21: Forces on Crack for the 'Dead & Live Load Approach'

As shown in Figure 4-21, the driving force ($R \sin \theta$) and clamping force ($R \cos \theta$) are components of the dead & live load reaction at the support of the girder (R) and are dependent upon the angle the crack makes with the bottom of the beam in the direction of the support, θ . The driving force causes the crack to propagate while the clamping force holds the faces of the

crack together, thus resisting propagation and contributing to the capacity of the shear crack. With this assumption, Equation 2-2 is rewritten as Equation 4-24.

$$RF = \frac{\text{Capacity} - A_1 R_{DL} \sin \theta}{A_2 R_{LL} \sin \theta (1 + IL)} \quad \text{Equation 4-24}$$

Where:

θ	=	Angle between crack and bottom of beam in direction of support
R_{DL}	=	Reaction at support caused by dead loads (kips)
R_{LL}	=	Reaction at support caused by live loads (kips)

Four methods were investigated to determine the capacity of the beam using the Dead & Live Load Approach.

4.3.9.1.1 Method #1

The capacity used in ‘Method #1’ assumes that the crack extends through the entire height and width of the girder web and that the shear capacity of the slab is neglected as insignificant. These are very conservative assumptions because, in reality, the cracks do not necessarily extend through the entire web height and the slab does contribute to the shear capacity of the girder. If the crack does not extend through the entire web of the girder then the un-cracked portion of the girder will provide more capacity than if that portion were cracked. This method also assumes that the entire width of the web contributes to the shear capacity of the girder. This is a slightly un-conservative approach as spalling of the cover concrete could exist in actual beams. However, the earlier conservative assumptions outweighed the un-conservative nature of this assumption.

From these assumptions, the capacity of the beam is calculated as the minimum of Equation 2-10 and Equation 4-25. Equation 4-25 is the shear resistance caused by friction between the two faces of the crack, which is a function of the clamping force and the cracked-concrete-to-cracked-concrete coefficient of friction, μ_c . Equation 2-10 acts as an upper limit to Equation 4-25. The governing equation is then used in Equation 2-4 to determine the capacity, V_n , used in Equation 4-24.

$$V_n = \mu_c (R_{DL+LL}) \cos \theta \quad \text{Equation 4-25}$$

At this point in the program development, it was unclear what μ_c to use, so a value of 1.2 was used, as it is within the range of researched values. This μ_c used was later changed, as discussed in section 4.3.9.3. As explained, the crack is assumed to propagate to either the end of the beam or to the bottom of the slab (through the height of the web), as described in Figure 4-22.

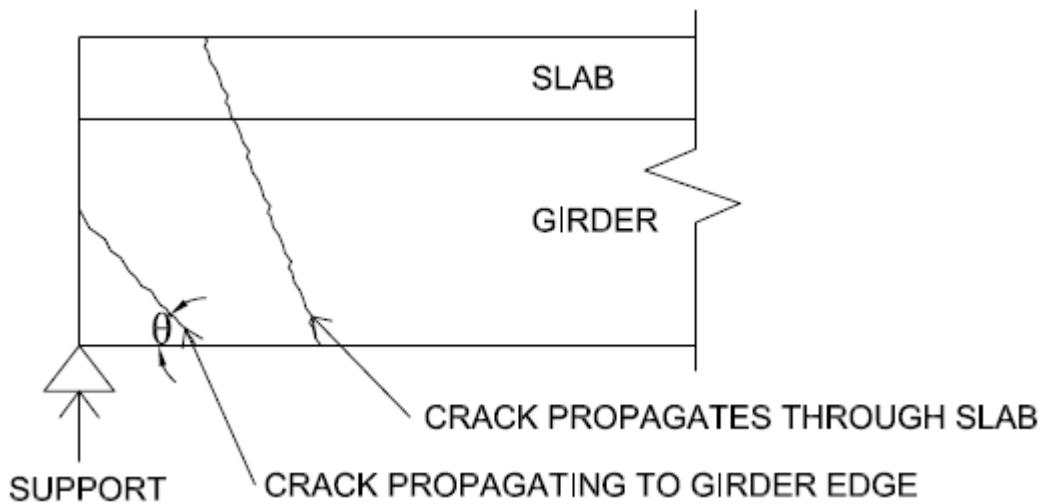


Figure 4-22: Crack Propagation to Either Top of Slab or Edge of Girder

4.3.9.1.2 Method #2

The capacity determined from Method #2 is the same as that obtained from Method #1 except the crack is assumed to extend through the depth of the slab if the crack propagates to the slab. Thus, the thickness of the slab also contributes to the shear capacity of the girder. The tributary width of the slab is assumed to not contribute to the shear capacity.

4.3.9.1.3 Method #3

Method #3 accounts for the shear capacity of the slab, like Method #2, but also accounts for the effects of the un-cracked portion of the girder. Equation 2-10 and Equation 4-25 from Method #1 are modified by adding the un-cracked capacity, based on Equation 2-11, to form Equation 4-26. Since the un-cracked capacity is considered, the cracked capacity portions of

Equation 4-26 are reduced to account for only the shear capacity provided by the cracked portion of the girder. This is done by reducing the cracked area, A_{cr} , in Equation 2-10 (still assuming that the clear cover concrete contributes to the capacity of the beam) and by multiplying Equation 4-25 by the cracked length-to-total propagation length ratio, L_c/L . The total propagation length, L , is the length of the crack if it did extend through the beam, either to the top of the slab, or to the edge of the girder, and is the cracked length, L_c , plus and un-cracked length, L_{uc} , shown in Figure 4-23. When the crack propagates to the bottom of the slab it is assumed that the crack propagates all the way to the top of the slab, which is a conservative assumption and is necessary because it is impossible for a bridge inspector to know how far through the slab the crack propagates. When the crack propagates to the bottom of the slab or to the edge of the girder the un-cracked length, L_{uc} , and un-cracked capacity are both '0' and Method #3 is the same as Method #2.

$$V_n = \min \begin{cases} \frac{L_c}{L} \mu_c (R_{DL+LL}) \cos \theta + \text{uncracked capacity} \\ 0.2f'_c A_{cr} + \text{uncracked capacity} \\ 0.8A_{cr} + \text{uncracked capacity} \end{cases} \quad \text{Equation 4-26}$$

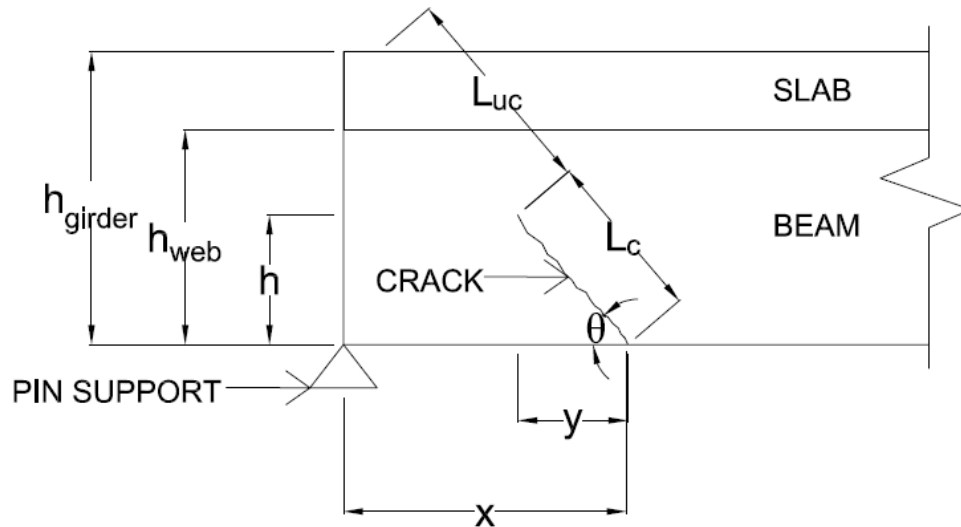


Figure 4-23: Parameters used to Determine Crack Length

Where:

$$\begin{aligned}
 A_{cr} &= \text{Area of crack (in.}^2\text{)} \\
 &= b_w L_c \\
 L_c &= \text{Length of crack (in.), Figure 4-23} \\
 \text{un-cracked capacity} &= \frac{4}{3} \sqrt{f'_c} A_{uc} \text{ (kips)} \\
 A_{uc} &= \text{Area of un-cracked section (in.}^2\text{)} \\
 &= b_w L_{uc} \\
 L_{uc} &= \text{Length of un-cracked section (in.), Figure 4-23} \\
 L &= L_c + L_{uc} \text{ (in.)}
 \end{aligned}$$

4.3.9.1.4 Method #4

In Method #4, Equation 4-26 is modified so the capacity equation dependent upon the reaction is no longer influenced by the un-cracked capacity equation and is instead reliant upon the average coefficient of friction of the cracked, μ_c , and un-cracked, μ_{uc} , sections depending upon the cracked length. This modification is shown in Equation 4-27. Like with the previous methods μ_c is taken as 1.2. μ_{uc} is taken as 1.6. The un-cracked coefficient, logically, should be larger than the cracked coefficient, and this assumption is reasonable considering the cracked-concrete coefficients of friction discussed in section 2.2.2. All other assumption made for Method #3 are applied to Method #4.

$$V_n = \min \left\{ \begin{array}{l} \frac{\mu_c L_c + \mu_{uc} L_{uc}}{L} (R_{DL} + R_{LL}) \cos \theta \\ 0.2 f'_c A_{cr} + \text{un-cracked capacity} \\ 0.8 A_{cr} + \text{un-cracked capacity} \end{array} \right. \quad \text{Equation 4-27}$$

Where:

$$\mu_{uc} = \text{un-cracked concrete coefficient of friction}$$

4.3.9.2 Friction Load Approach

The 'Friction' approach assumes that the friction force between the girder and bearing pad is significant and actually causes the crack to propagate in the reverse diagonal direction. In this approach the dead and live load reaction, R , and friction force, F , act at the crack interface, as shown in Figure 4-24. Corrosion of the bearing pad and rocker prevents the end of the girders from rotating, leading to the friction force, which was not considered in the design of the girders. As the girder is loaded it will deflect downward which creates tension in the bottom of the girder. This causes the girder, at the supports, to try to slide further away from the center of the girder. This movement, however, is prevented by the friction force at the beam-to-pad interface. The friction force in the girder, thus, acts toward the center of the girder, as shown in Figure 4-24. The crack-driving force component of the two forces, shown parallel to the crack in Figure 4-24, act against each other while the crack-clamping forces, shown perpendicular to the crack in Figure 4-24, are additive. The driving and clamping forces are shown as Equation 4-28 and Equation 4-29.

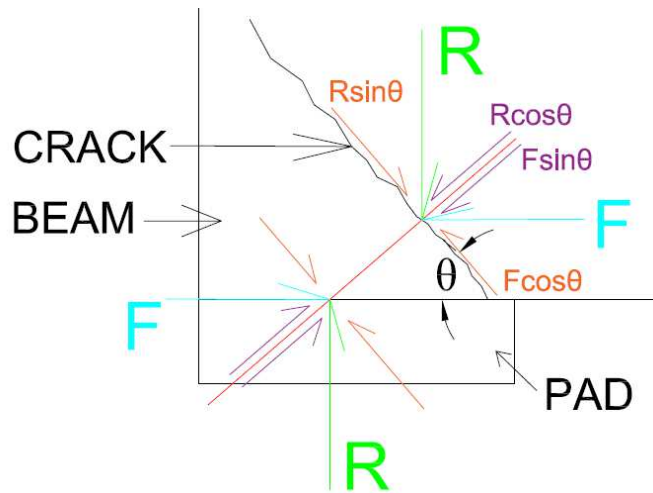


Figure 4-24: Reaction and Friction Forces Acting on the Reverse Diagonal Crack According to the 'Friction Load Approach'

$$\text{Driving Force} = R \sin \theta - F \cos \theta$$

Equation 4-28

$$\text{Clamping Force} = R \cos \theta + F \sin \theta$$

Equation 4-29

4.3.9.2.1 ABAQUS Study

A parametric study using ABAQUS was conducted to test the validity of the Friction Load Approach. Various girder models were created with varying geometric and loading parameters to investigate the reaction-to-friction force relationship at the beam-to-bearing pad interface.

4.3.9.2.1.1 Parameters

Various T-shape girders were created in ABAQUS. The web width, b_w , web width-to-height ratio, b_w/h , slab (flange) thickness, h_s , and beam length-to-girder height ratio, L/h , were varied in each model. These parameters are displayed in Figure 4-25. Also displayed in the figure is how the effective flange width is calculated. The slab extends past the girder web a distance equal to the girder web height ($h-h_s$) on either side of the web, forming a 45° angle with the bottom of the girder web, as shown in Figure 4-25. Table 4-6 displays the variations for each parameter. One variation was changed while all the others were held constant until a model was created for every possible combination.

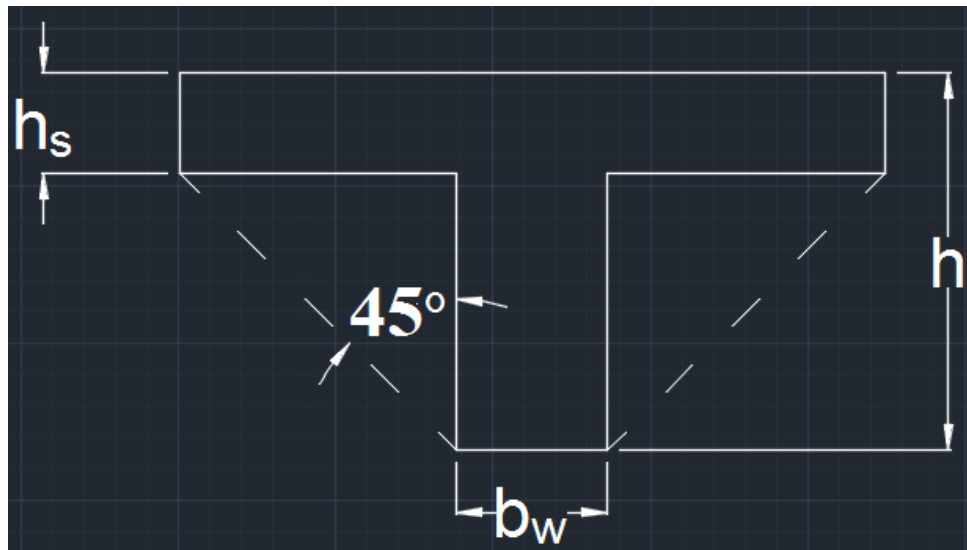


Figure 4-25: Parameters Varied in the ABAQUS Models

Table 4-6: ABAQUS Parameter Variation

Variable Parameter:	Variation:		
b_w (in.)	12	15	18
b_w/h	0.4	0.5	0.6

h_s (in.)	6	8	10
L/h	7	12	17

4.3.9.2.1.2 Model Creation

The following sections discuss the ABAQUS input properties which were consistent for every model.

4.3.9.2.1.2.1 Parts

Three ‘Parts’ are created within ABAQUS: 1 beam and 2 pads. They are deformable have a solid shape, and are an ‘extrusion’ type. Both beam and pad parts have a dependent instance type and the pads are placed on the bottom of the beam web, one on either end of the beam length. The ‘pad’ parts are 1 in. thick, 9 in. long, and have the same width as the beam web. The ‘beam’ part follows the dimension parameters unique to each model, as discussed in section 4.3.9.2.1.1.

4.3.9.2.1.2.2 Properties

The beam sections consist of solid and homogeneous concrete. The concrete is mechanical, elastic, and isotropic, has 0 field variables, a long-term moduli time scale, and a Poisson’s ratio of 0.2. A Young’s modulus, E , of 3,122,019 psi is used. This modulus is calculated using Equation 4-22 and assuming a compressive strength, f'_c , of 3000 psi. The pad sections consist of solid and homogeneous steel. The steel is mechanical, elastic, and isotropic with 0 field variables, a long-term moduli time scale, a Poisson’s ratio of 0.3, and a Young’s modulus of 29,000,000 psi.

4.3.9.2.1.2.3 Step

A ‘step’ is created of the ‘General; Static, General’ type. Everything else is kept as default.

4.3.9.2.1.2.4 Interaction

Two rigid body constraints are created; one for each ‘pad’ part. A reference point is placed on each ‘pad’ part on a bottom-corner node. A contact type interaction property is then created. This interaction property is mechanical with tangential behavior. It is assigned to have

a penalty friction formulation, isotropic directionality, 0 field variables, and a coefficient of friction of 0.57. A surface-to-surface contact (standard) interaction is created with the top surface of the pads as the ‘Master’ surfaces and the bottom face of the beam web as the ‘Slave’ surface. The discretization method for this interaction is ‘surface to surface’.

4.3.9.2.1.2.5 Load

A boundary condition is assigned to the reference point on each ‘pad’ part. The boundary conditions are mechanical with a ‘Symmetry/Antisymmetry/Encastre: ENCASTRE ($U1=U2=U3=UR1=UR2=UR3=0$)’ type. Next, a uniformly distributed pressure type mechanical load is applied to the top surface of the beam slab (flange) with a ramp amplitude.

The HS20 truck is used to estimate the loading on the beams. It is assumed that an entire line of wheel-loads acts on the girder. This is conservative because a wheel-load is typically distributed to multiple girders. It is also assumed that, if the beam is long enough, wheel-loads from multiple trucks are placed on the bridge. As shown in Figure 4-26, a wheel-load of 16 kips (half of the 32 kip axle load) is placed on the right end of the beam. The HS20 truck’s middle wheel-load of 16 kips is placed 14 ft. away while the truck’s front wheel-load of 4 kips is placed 14 ft. away from the middle wheel-load. A 6 ft. buffer region is assumed to separate two trucks, after which another truck’s rear wheel-load is placed. This process continues until no more wheel-loads can fit within the beam span.

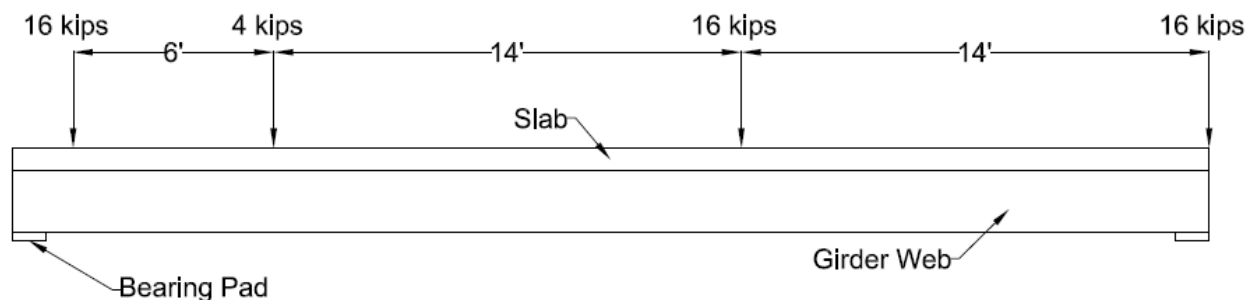


Figure 4-26: Loading on the ABAQUS Model Girders

These truck loads are then applied as a pressure load to the ‘beam’ part using Equation 4-30. This applied pressure on the beam is displayed in Figure 4-27.

$$\text{Pressure (psi)} = \frac{\sum \text{Truck wheel loads (lbs.)}}{\text{Length (in.)} \times \text{Effective Flange Width(in.)}} \quad \text{Equation 4-30}$$

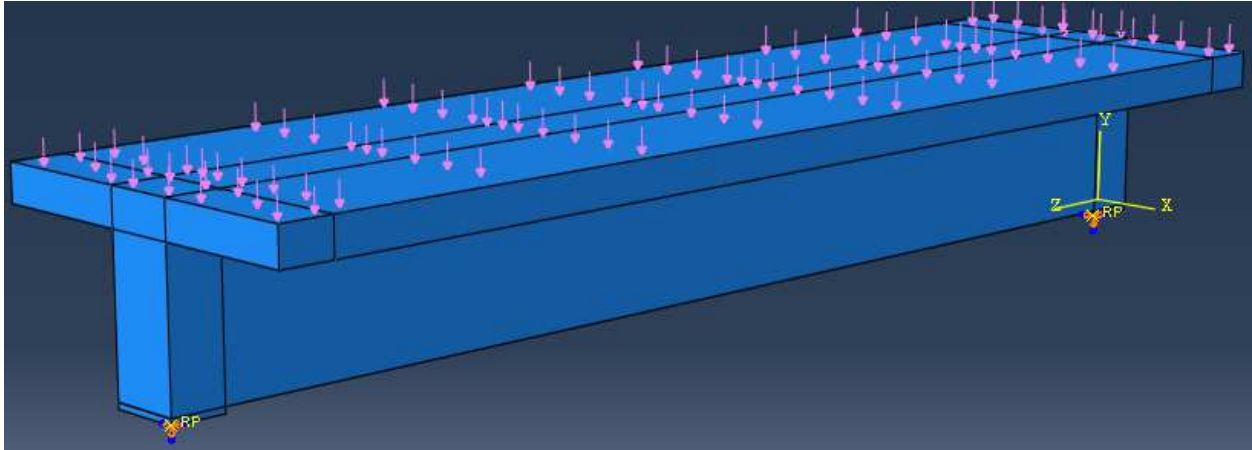


Figure 4-27: Uniformly Distributed Pressure Load on ABAQUS Beams

4.3.9.2.1.2.6 Mesh

To facilitate ABAQUS's finite element analysis, the 'pad' and 'beam' parts are divided into a mesh. The program gives the option to divide parts into either rectangular or tetrahedral meshes. Generally, the rectangular mesh out performs tetrahedral meshes, but tetrahedral meshes are more versatile and better suited for irregular shapes. The 'pad' and 'beam' parts are both uniform regular shapes, thus they are divided using a rectangular mesh.

The focus of these models is to analyze the forces at the beam-to-pad interface. Thus, a smaller mesh was used near this interface to yield more accurate results in the region. The mesh in the interior span of the 'beam' part is larger than at the supports, as shown in Figure 4-28. This larger size mesh in 'non-critical' areas of the beam allows ABAQUS to analyze the models faster. The rectangular mesh at the supports are 3 in. x 3 in. x 3 in. cubes while in the middle span, the prisms are 3 in. x 3 in. x 6 in. The pads are divided into 3 in. x 3 in. x 1 in. prisms. To facilitate the differently sized rectangular meshes, the 'beam' part is partitioned into 12 sections, as shown in Figure 4-27. The geometric order of the mesh is quadratic while the element library is standard. Every other setting is set to the default values.

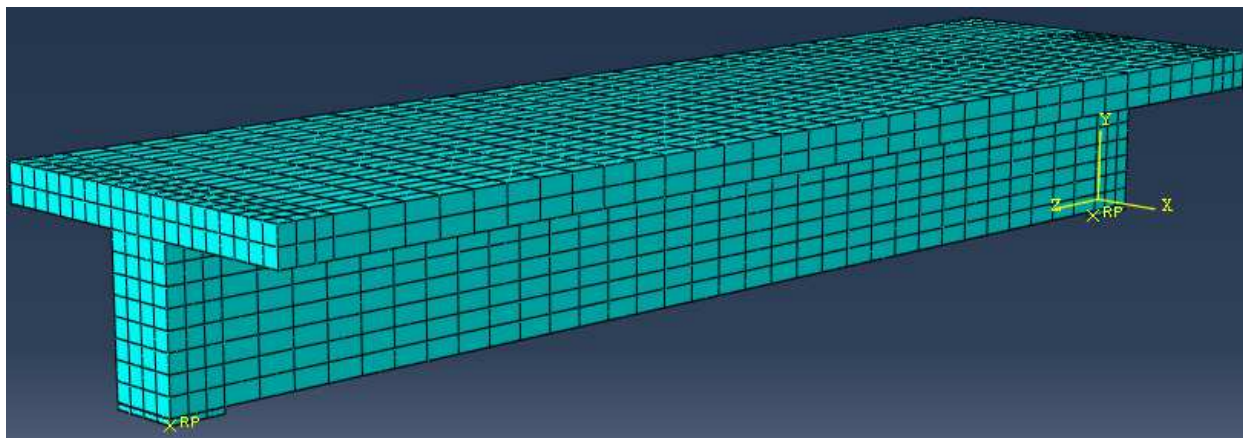


Figure 4-28: ABAQUS Model Mesh

4.3.9.2.1.3 Model Output and Program Incorporation

After a model is analyzed the normal and shear forces in the beam at the beam-to-bearing pad interface are found. The results of these models are discussed further in section 5.3.3. From the results, shear-to-normal force ratios, S/N , were found for each parametric variation. These ratios are displayed in the Tables sheet, as shown in Figure 4-29. BRIDGE uses the girder length, L , girder height, h , slab thickness, h_s , and girder web width, b_w of the user-defined girders to interpolate within the tables in Figure 4-29 to find the S/N ratio corresponding to the girders in the program. This S/N ratio is the predicted ratio of the friction force to normal force between the girder and bearing pad. If the interpolation yields a ratio larger than 0.57 then the program will limit the coefficient of friction to 0.57, as this is the theoretical point at which the girder starts slipping on the pad, which does not occur. The program then finds the friction (shear) force due to live load, dead load, and combined dead and live load at each girder support by multiplying the S/N ratio by the reaction at the support caused by live load, dead load, and combined dead and live load, respectively, as shown in Equation 4-31 through Equation 4-35.

a user-defined bridge. This is because, in the program, the geometry of every girder is the same, therefore, every S/N ratio is the same. This leads to identical θ_s at every girder even if the reactions are dissimilar. The user, in the Section Geometry and Material Properties sheet, has the option to use this calculated angle or a manually-entered crack angle. The chosen angle, along with the friction force calculated in Equation 4-31, and the reaction force calculated within BRIDGE are used in Equation 4-28 and Equation 4-29 to find the clamping and driving forces on the crack at each girder support. These forces are then used to find the rating factor for each girder support, which is described by Equation 4-34.

$$RF = \frac{[Capacity\ w/o\ Clamping\ Force + \mu_c(Clamping_{DL+LL})] - A_1 Driving_{DL}}{A_2 Driving_{LL+IL}} \quad \text{Equation 4-34}$$

Where:

μ_c	=	Concrete-to-concrete coefficient of friction
	=	1.4
$Clamping_{DL+LL}$	=	$\cos\theta R_{DL+LL} + \sin\theta F_{DL+LL}$
$Driving_{DL}$	=	$\sin\theta R_{DL} - \cos\theta F_{DL}$
$Driving_{DL+IL}$	=	$\sin\theta(1+I)R_{LL} - \cos\theta(1+I)F_{LL}$
I	=	Impact Load, Equation 2-3
θ	=	Angle of crack propagation chosen by user

4.3.9.2.1.3.1 Capacity without Clamping Force

Four methods were considered when calculating the shear capacity of the girders without clamping force. The shear capacity is described by Equation 2-4 where V_n is described by one of the four methods below.

4.3.9.2.1.3.1.1 SMCFT

The SMCFT Equation 2-12, described in section 2.1.4.1 was considered and ultimately used in BRIDGE to find the capacity of the girders. This method was chosen because it is consistent with AASHTO shear design specifications and it produces the most conservative rating factor, as shown in section 5.3.6. In addition many studies have proven the accuracy and

validity of the SMCFT, unlike other approaches, especially the Muttoni and Ruiz (2008) equation.

4.3.9.2.1.3.1.2 ACI Plain Concrete Equation

Equation 2-11 was considered to describe the shear capacity of the girder at the support. This equation seemed valid because there is no steel transversing the crack, therefore only concrete resists shearing in the girders. However, this approach was ultimately not used because this equation assumes that the shear plane is uncracked, which is untrue in the girders analyzed by the program.

4.3.9.2.1.3.1.3 Muttoni & Ruiz Equation

The Muttoni & Ruiz method outlined in the section 2.1.4.1 was considered. However, the simplified Equation 2-19 is not applicable to this project and is modified using other assumptions. This project is conducted using LF design. For the LF method, AASHTO (2002) specifies 0.85 for ϕ_c and ϕ_s . The aggregate diameter size was changed to 1", as this is closer to the size of aggregate used in most of the bridges experiencing reverse diagonal cracking and because it yields a more conservative shear strength value. E_s was changed to 29,000 ksi and the f_y was changed to 33 ksi. MBE (2011) Article 6B.5.3.2 recommends using this yield stress for reinforcing steel in bridges which were made prior to 1954, and in which the steel strength is unknown, as is the case with all of the bridges analyzed by this program. Muttoni & Ruiz (2008) explain that m_{Ed}/m_{Rd} can be set to 1 as a conservative value. With these adjusted assumptions, Equation 2-19 becomes Equation 4-35:

$$V_u = \frac{3.06bd\sqrt{f'_c}}{1 + 0.0298d} \quad \text{Equation 4-35}$$

4.3.9.2.1.3.1.4 AASHTO Equation

Equation 2-7 from section 2.1.4.1 was considered because it is a well-known and widely used equation for finding the shear capacity of a beam. However, as shown in section 5.3.6, this equation is less conservative than all the other methods and was not used.

4.3.9.3 Coefficient of Friction of Cracked Concrete

The various values for the coefficient of friction for cracked concrete-to-cracked concrete, μ_c , are detailed in section 2.2.2. Originally it was believed that ACI's recommendation of 1.4 was too high because this value assumes shear reinforcement is traversing the crack. Reinforcing steel, however, does not traverse the reverse diagonal cracks in the girders analyzed by BRIDGE. Reinforcing tension steel may or may not traverse the crack, however it is assumed to not contribute to shear capacity, which is a conservative, and likely accurate, assumption. It was also reasoned that PCA's 0.8 was too low because this describes the coefficient of friction of concrete between smooth faces, not rough cracks. Therefore, a conservative value of 1 or 1.2 was deemed reasonable..

Equation 2-24 and Equation 2-27, developed by Loov (1998) and Tassios & Vintzeleou (1987), respectively, were considered. These equations are dependent upon the clamping force on the crack and, thus, to the reaction at the girder support. Since the reaction varies depending upon the truck loads analyzed, the μ_c calculated by these equations varies with truck loading. It was seen that these μ_c values were very large under some circumstances and were thus un-conservative. Since it was desired that μ_c be a constant material property Equation 2-24 and Equation 2-27 were no longer considered.

Upon further analysis, it was seen that, for the ACI value, it is assumed that tension forces develop in the steel traversing the crack which in turn causes compressive forces in the concrete surrounding the steel at the crack interface. This creates a clamping force between the two faces of the crack, as described in section 2.1.4.1.2. Since the cracked faces are still being clamped together, as explained in section 4.3.9.3, this μ_c value of 1.4 is still applicable and is used in Equation 4-34 to find the rating factor of the bridge.

4.3.10 Calculating the Rating Factor at each Support

The rating factor calculations for the capacity method considered above was discussed in section 4.3.9.

Chapter 5 Analysis & Results

5.1 Support Reactions: BRIDGE vs. RISA 3D

It is desired to test the accuracy of BRIDGE's calculated live load reactions at the support of each girder. Eighteen program and RISA 3D models were created with the various combinations of parameters shown in Table 5-1. The remainder of the bridge parameters, displayed in Table 5-2 and Appendix C, are varied randomly within reasonable and realistic bounds. This was to obtain a wide variety of bridge diversity for the support reaction comparison. At the time of this analysis, the dead load of the bridge was not calculated, the program did not calculate both the inventory and operating levels simultaneously, and the user specified the location of each truck in its respective lane with 'South' referring to the position in the lane closest to the 'bottom-most' girder. None of these changes affected the calculations of the live load reaction at the supports. Figure 5-1 displays the RISA model for Comparison #1 with the truck wheel-loads distributed to each surrounding girder and diaphragm using the 'Rigid Beam Analysis within the Panel' discussed in section 4.2.2.3, which is the method used by BRIDGE to distribute wheel-loads. Both the program and RISA 3D models were ran and the results for Comparison #1 are displayed in Table 5-3. The 'BRIDGE input' and 'results' tables for the other 17 Comparisons are displayed in Appendix C. As shown in the 'results' tables, the live load reaction calculated by BRIDGE and RISA 3D are extremely close. There is usually not more than 0.3% error between the results. When a larger error exists between the two models, it is usually at supports with very small reactions. Thus, even very small differences result in larger percent errors. From these comparisons, it is seen that the program calculates the live load reactions with high accuracy, indicating that the stiffness matrix creation and manipulation within the program is accurate.

Table 5-1: BRIDGE vs. RISA 3D Model Parameter Variations

	Parameter Variations:		
# of Lanes:	---	2	4
# of Girders:	3	4	5
Diaphragm Configuration:	4 Real	4 Real, 3 Virtual	3 Real, 4 Virtual

Table 5-2: Support Reaction Comparison #1: BRIDGE Input

LOADING:				
	Truck #1:		Truck #2:	
Truck Type:	Type T170 Unit		Type T130 Unit	
Lane #:	1		2	
Direction of Travel:	Up-station		Down-station	
Truck Location:	Entering Bridge		Exiting Bridge	
Position in Lane:	South Edge		North Edge	
Analysis Level:	Inventory		Inventory	
LANE ALIGNMENT:		SECTION GEOMETRY:		
# of Lanes:	2	Girders	Height (in.):	60
Lane Width (ft.):	11		Width (in.):	18
Cantilever Width (ft.):	0.083333	Exterior Diaphragms	Height (in.):	24
Ext. Shld. Width (ft.):	3		Width (in.):	18
Ext. Barrier Width (in.):	11	Interior Diaphragms	Height (in.):	12
Median Shld. Width (ft.):	0		Width (in.):	8
Median Barrier Width (in.):	0	Slab Thickness (in.):		6
BRIDGE MESH:				
# of Girders:	3	# of Interior Diaphragms:		1
Length of Girders (ft.):	60	# of Virtual Diaphragms		4
Tot. # of Diaphragms:	7	Diaphragm Length (ft.):		36
MATERIAL PROPERTIES:		Concrete Strength (psi)		4000

Table 5-3: Support Reaction Comparison #1: Results

Reactions at Supporting Nodes: Program vs RISA			
Node:	Program (k)	RISA (k)	% Difference:
1	87.595	87.721	-0.1434%
2	122.985	122.735	0.2039%
3	64.621	64.746	-0.1923%
19	73.373	73.457	-0.1149%
20	101.957	101.786	0.1676%
21	55.469	55.555	-0.1550%

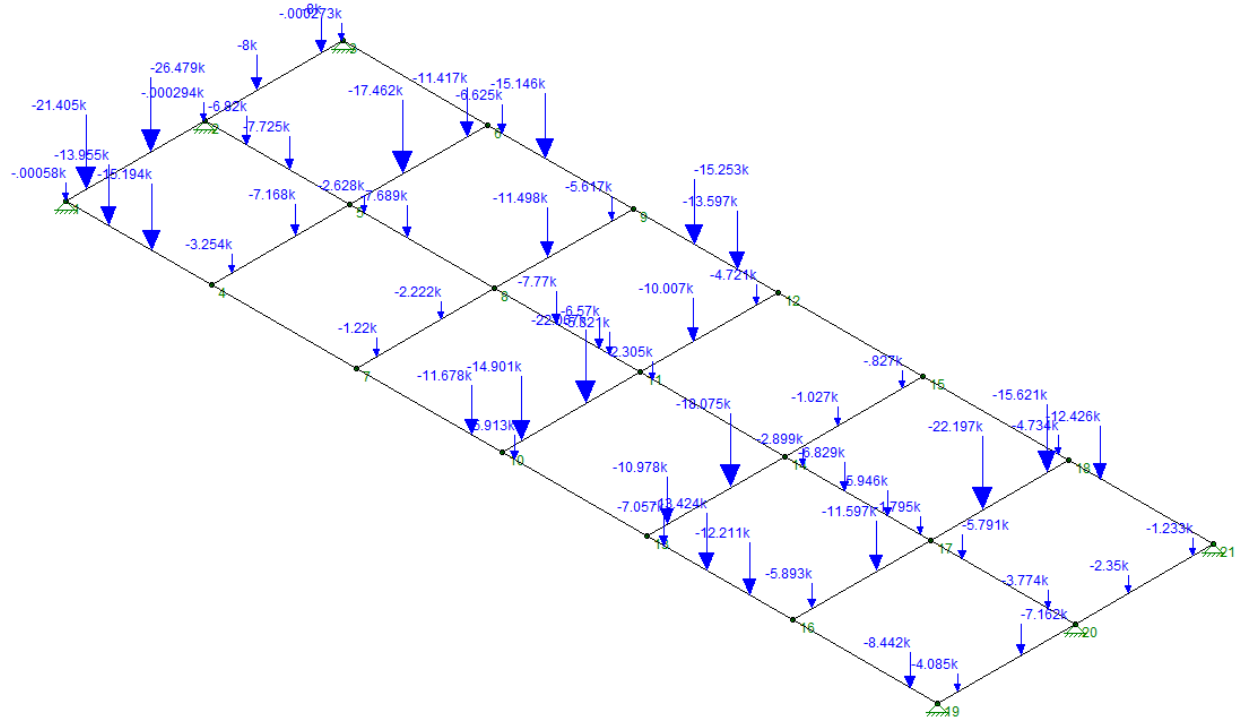


Figure 5-1: Support Reaction Comparison #1: RISA 3D Model

5.2 Capacity: Dead & Live Load Approach

The program was used to analyze the capacity and resulting rating factor of girders using the Dead & Live Load Approach: Methods #1 through #4. These methods produced rating factors which were either too high, too low, or negative. Thus the Dead & Live Load Approach for capacity calculations was discarded.

5.3 Capacity: Friction Load Approach

5.3.1 ABAQUS Setup Confirmation

The ABAQUS models described in section 4.3.9.2 were analyzed to obtain the normal and shear forces at the girder-to-bearing pad interface. One model was selected for initial testing to ensure the ABAQUS setup yielded accurate results. The $12 - 0.4 - 10 - 12$ model was selected where the first number refers to the girder width (in.), b_w , the second number refers to the web width-to-girder height ratio, b_w/h , the third number refers to the height (thickness) of the slab (in.), h_s , and the fourth number refers to the L/h ratio. The subsequent tables, figures, and discussion follow this nomenclature. Figure 5-2 and Figure 5-3 display the normal and shear

force distribution, respectively, in the girder at the girder-to-bearing pad interface for *Model 12 – 0.4 – 10 – 12*. The left edge of the pads represent the outside face of the pad and girder while the right edge of the pads represent the inside face of the pad which is oriented toward the center of the girder. In Figure 5-2, the numbers and lines above the pad midpoint surface represent compressive forces at the interface while the numbers and lines below the midpoint surface represent tensile forces. In Figure 5-3, the numbers and lines above the pad midpoint surface represent shear forces in the girder acting toward the center of the girder while the number and lines below the midpoint surface represent shear forces in the girder acting toward the girder ends. These results show that, at the ends of the girder, the bottom of the girder ‘lifts’ off the pad causing the girder and bearing pad to lose contact so no forces are transferred in this area, leaving the majority of force transfer to take place at the girder-to-bearing pad interface closest to the midpoint of the girder. The uniform load on this girder is 1.92308 psi or 36 kips total. If the load is split evenly between the bearing pads on either end of the girder then the total normal force at one bearing pad should equal 18 kips. Figure 5-2 shows that the ABAQUS model predicts a total normal force of 18.0008 kips on one pad, which is within .039% of the theoretical value.

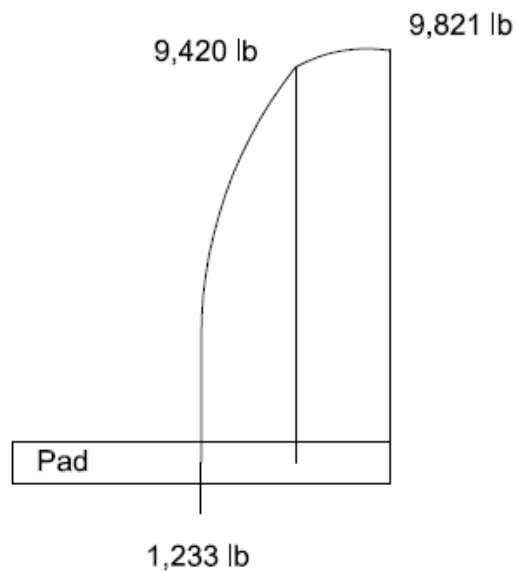


Figure 5-2: Normal Force Distribution in the Girder at the Girder-to-Bearing Pad Interface for Model 12-0.4-10-12

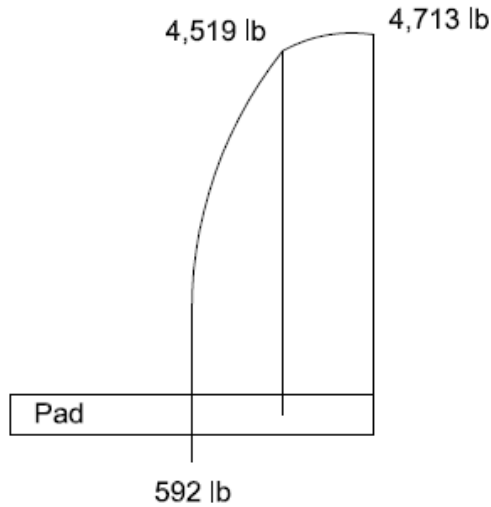


Figure 5-3: Shear Force Distribution in the Girder at the Girder-to-Bearing Pad Interface for Model 12-0.4-10-12

The deflection at the midspan of *Model 12 – 0.4 – 10 – 12* at the bottom face of the web is 0.105162 in. The girder supports in ABAQUS are modeled to act as a partially fixed support. Thus, the midspan deflection should lie somewhere between the values obtained from Equation 5-1 and Equation 5-2, which describe the theoretical maximum deflection for a beam with fully fixed supports and fully pinned supports, respectively. Δ_F equals 0.023156 in. while Δ_P equals 0.115779 in., thus, the measured deflection lies between these extreme values. Based on these deflection results and the normal force at the supports, it is deemed that the ABAQUS setup is accurate and that the models should generate accurate data.

$$\Delta_F = \frac{wL^4}{384(57000\sqrt{f'_c})(I)} = 0.028429 \text{ in.} \quad \text{Equation 5-1}$$

$$\Delta_P = \frac{5wL^4}{384(57000\sqrt{f'_c})(I)} = 0.142147 \text{ in.} \quad \text{Equation 5-2}$$

Where:

Δ_F	=	Displacement @ midspan for fixed girder supports (in.), 0.0232 in.
Δ_P	=	Displacement @ midspan for pinned girder supports (in.), 0.116 in.
w	=	Uniform linear load on girder (psi), 100 lb/in.
L	=	Length of girder (clear span between bearing pads) (in.), 342 in.
I	=	Moment of inertia of girder (in. ⁴), 49280.7 in. ⁴
f'_c	=	Concrete strength (psi), 3000 psi

5.3.2 Girder Length vs S/N ratio

The girder length-to-height ratio (L/h) was recognized as the most crucial parameter varied in the ABAQUS models, so its effect on the shear-to-normal force ratio (S/N) at the girder-to-bearing pad interface was investigated first. Two parameter combinations from Table 4-6 were selected: *Model 12 - 0.4 - 6 - L* and *Model 18 - 0.4 - 6 - L*. ABAQUS models for these two parameter combinations were created for various L/h ratios ranging from 7 to 17 and the resulting S/N (%) ratios are shown in Table 5-4. As shown, the S/N ratio increases for increasing L/h ratios until the S/N ratio reaches 0.57 (57%), at which point the S/N ratio remains constant. 0.57 is the coefficient of friction at the girder-to-bearing pad interface, which is the limiting value before movement of the girder on the bearing pad. It was desired to see if there is any correlation between the L/h and S/N ratios, so the values in Table 5-4 were plotted in Figure 5-4 and Figure 5-5 for *Model 12 - 0.4 - 6 - L* and *Model 18 - 0.4 - 6 - L* respectively. The L/h ratios corresponding to an S/N ratio of 0.57 were excluded. A line of best fit was created for each graph and the coefficient of determination, R^2 , was calculated for the lines. The R^2 values for *Model 12 - 0.4 - 6 - L* and *Model 18 - 0.4 - 6 - L* are 0.9789 and 0.9752 respectively, as shown in Figure 5-4 and Figure 5-5. This indicates that the L/h-to-S/N relationship can accurately be approximated as a linear function. Therefore, throughout the remainder of the parametric analysis, only L/h values of 7 and 12 were modeled. It is assumed that the S/N

relationship between these two values is linear until an S/N ratio of 0.57 is reached, at which point the S/N ratio is constant for every increasing L/h ratio.

Table 5-4: S/N Ratios at Bearing Pad for Various L/h Ratios for ABAQUS Models 12-0.4-6-L & 18-0.4-6-L

L/h ratio	S/N ratio (%)	
	12 - 0.4 - 6 - L	18 - 0.4 - 6 - L
7	14.9	11.4
8	19.5	16.3
9	27	20.4
10	30.1	34
11	36.2	40.4
12	46.9	47.4
13	54.4	57
14	57	57
17	57	57

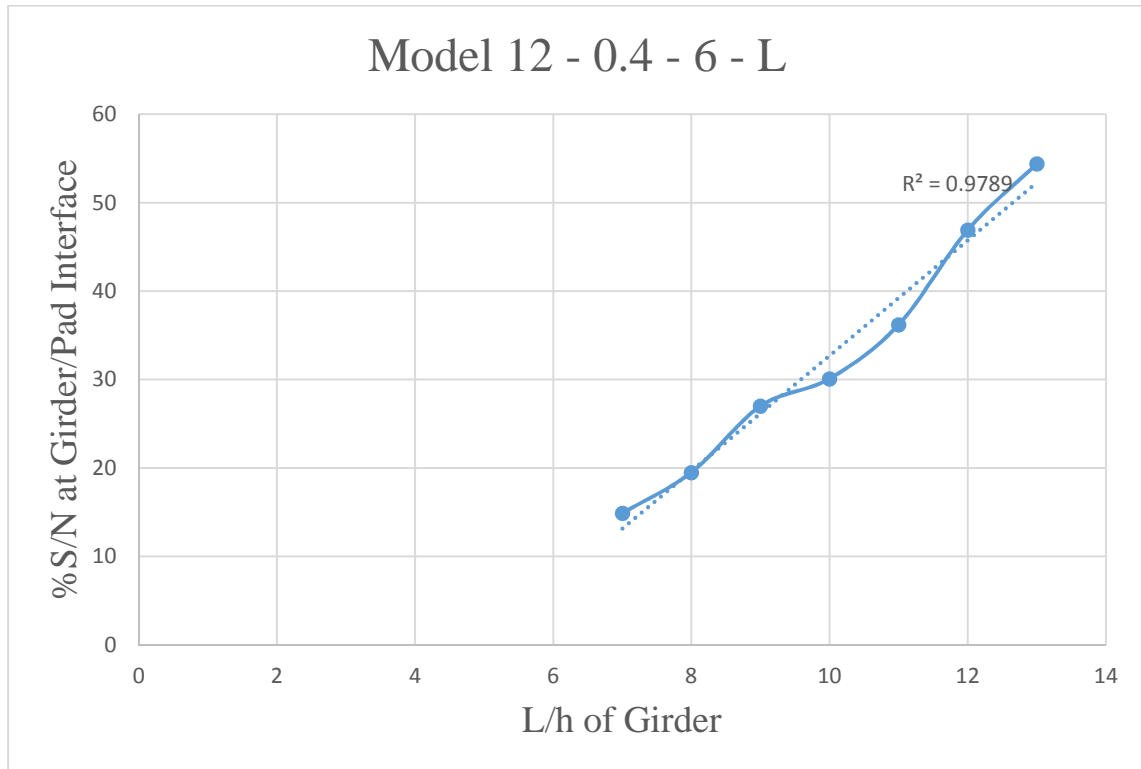


Figure 5-4: L/h Ratio vs. S/N Ratio for Model 12-0.4-6-L

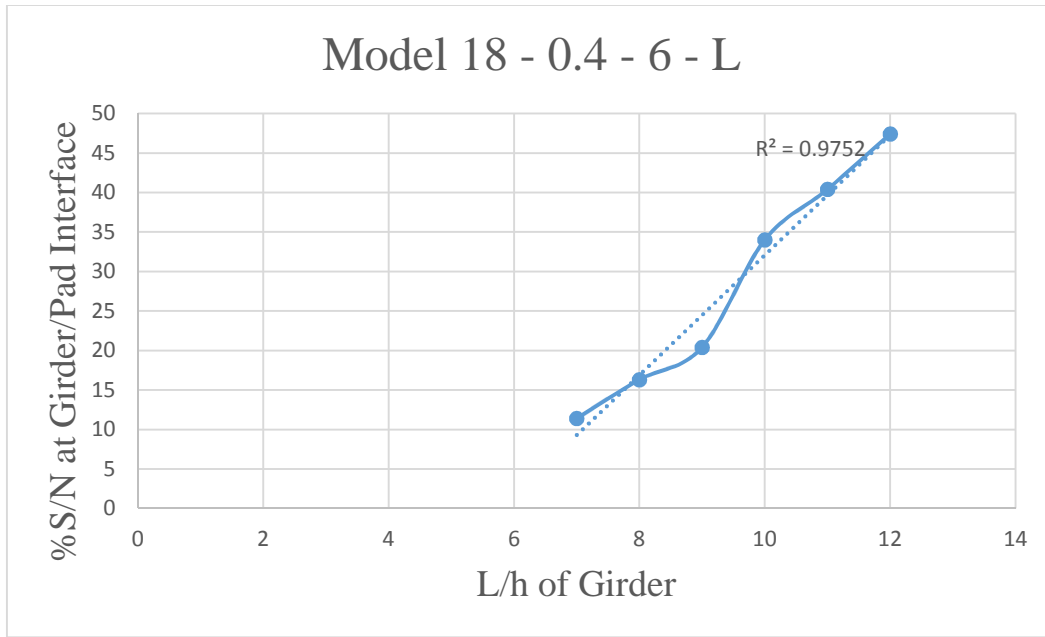


Figure 5-5: L/h Ratio vs. S/N Ratio for Model 18-0.4-6-L

5.3.3 S/N Relationships

Every combination of parameters in Table 4-6, except $L/h = 17$, was modeled in ABAQUS and the shear and normal forces in the girder at the girder-to-bearing pad interface were recorded at one of the supports. The forces for each model are shown in Appendix D. Table 5-6 through Table 5-11 display the resulting S/N ratio for every combination. These tables are color-coded and labeled per Table 5-5 based on the total load applied to the model. As discussed previously, the amount of load applied to a girder is dependent upon the length of the girder.

Table 5-5: Load on Corresponding ABAQUS Models, as Shown in Table 5-6 through Table 5-11

Load on Beam (kips):
¹ 16
² 32
³ 36
⁴ 52
⁵ 68

Table 5-6: S/N Ratio Tables for ABAQUS Models with $b_w = 12''$ & $L/h = 7$

h_s			
$b_w/h:$	6	8	10
0.4	14.9% ^{2*}	15.1% ²	15.1% ²
0.5	14.5% ²	14.6% ²	14.7% ²
0.6	7.4% ¹	7.5% ¹	7.5% ¹

Table 5-7: S/N Ratio Tables for ABAQUS Models with $b_w = 12''$ & $L/h = 12$

h_s			
$b_w/h:$	6	8	10
0.4	46.9% ³	47.4% ^{3*}	48.0% ³
0.5	42.8% ²	43.5% ²	44.0% ²
0.6	42.7% ²	43.6% ²	43.9% ²

Table 5-8: S/N Ratio Tables for ABAQUS Models with $b_w = 15''$ & $L/h = 7$

h_s			
$b_w/h:$	6	8	10
0.4	12.9% ²	12.9% ²	13.0% ²
0.5	12.6% ²	12.7% ²	12.8% ²
0.6	12.3% ²	12.4% ²	12.5% ²

Table 5-9: S/N Ratio Tables for ABAQUS Models with $b_w = 15''$ & $L/h = 12$

h_s			
$b_w/h:$	6	8	10
0.4	53.4% ⁴	53.6% ⁴	54.2% ^{4*}
0.5	40.3% ^{3*}	40.7% ³	41.2% ³
0.6	36.7% ²	37.2% ²	37.7% ²

Table 5-10: S/N Ratio Tables for ABAQUS Models with $b_w = 18''$ & $L/h = 7$

h_s			
$b_w/h:$	6	8	10
0.4	11.4% ²	11.3% ²	11.3% ²
0.5	11.2% ²	11.2% ^{2*}	11.2% ²
0.6	11.0% ²	11.0% ²	11.1% ²

Table 5-11: S/N Ratio Tables for ABAQUS Models with $b_w = 18''$ & $L/h = 12$

h_s	6	8	10
b_w/h :			
0.4	47.4% ⁴	47.2% ⁴	47.4% ⁴
0.5	47.6% ⁴	47.7% ⁴	48.2% ⁴
0.6	35.4% ³	35.8% ³	36.2% ^{3*}

5.3.4 Estimation of Crack Propagation Angle

The principal stresses σ_{\max} and σ_{\min} , maximum shearing stress, $\tau_{xy \max}$, and the angle of the maximum shear plane, θ_s were found for seven of the ABAQUS models (marked with an asterisk (*) in Table 5-6 through Table 5-11) using the transformation of stresses method discussed in section 2.3. These values are displayed in Table 5-12. The maximum shear plane angle is, theoretically, the plane on which the crack should propagate. The angles shown in Table 5-12 are measured clockwise from the bottom of the girder, as displayed in Figure 2-11, thus, the magnitude of these angles is the predicted crack propagation angle. All of these models predict relatively steep angles, which coincide with the observed steep propagation angles for the reverse diagonal cracking shown in inspection report photographs.

Table 5-12: Principal Stresses, Max Shear Stress, and Angle of Maximum Shear Plan for 7 ABAQUS Models.

	Model:						
	12-0.4-6-7	12-0.6-6-7	12-0.4-8-12	15-0.4-10-12	15-0.5-6-12	18-0.5-8-7	18-0.6-10-12
σ_{\max} (psi)	3.24	0.41	31.53	45.68	18.96	1.22	13.04
σ_{\min} (psi)	-151.39	-74.48	-198.19	-238.28	-152.29	-99.98	-124.15
$\theta_{s, \max}$ (°)	-53.32	-49.22	-66.74	-68.65	-64.43	-51.29	-62.96
$\tau_{xy, \max}$ (psi)	77.31	37.44	114.86	141.98	85.62	50.60	68.59

5.3.5 Predicted Crack Propagation Angle vs Actual Propagation Angle

To test how accurately Method #6 predicts the crack angle, 7 girder supports were chosen from Bridge No. 54-104-317.27-(0005). Their location and geometry properties are displayed in Table 5-13. Interpolation was performed within Table 5-6 through Table 5-11 for each girder to determine an estimated interface S/N ratio. Each girder exceeded the limits in the tables so an S/N ratio of 0.57 was used for each girder. This coefficient, along with a reaction force of 26

kips at each support, was used to find the friction force at each support. This friction force is the same for each girder and is 14.82 kips. These forces were converted into stresses and transformed to find the predicted crack propagation angle, which was 69.4° for each girder. The inspection report photos (Special Bridge Inspection Report, 2011) were observed for these supports and an approximate reverse diagonal crack propagation angle was determined. These angles are shown in Table 5-14 and are close to the predicted angle of 69.4° . Thus, it was determined that Method #6 is accurate for estimating the crack propagating angle for use in Equation 4-34.

Table 5-13: Location and Geometry of 7 Girder Supports for Bridge No. 54-104-317.27-(0005)

Support #:	1	2	3	4	5	6	7
Span #:	1	1	2	2	2	4	5
Girder #:	F	F	E	E	F	D	G
Abutment/Pier #:	P1	P1	P2	P2	P2	P4	P4
b_w (in)	15	15	15	15	15	15	15
h (in)	33	33	36	36	36	36	33
h_s (in)	6.5	6.5	6.5	6.5	6.5	6.5	6.5
L (in)	510	510	570	570	570	570	510
b_w/h	0.45	0.45	0.42	0.42	0.42	0.42	0.45
L/h	15.45	15.45	15.83	15.83	15.83	15.83	15.45

Table 5-14: Observed Propagation Angles of Reverse Diagonal Crack for 7 Supports for Bridge No. 54-104-317.27-(0005)

Support #:	1	2	3	4	5	6	7
Observed Crack Angle	73.3	53.4	65.6	66.8	75.1	76.8	68.6

5.3.6 Capacity without Clamping Force

Equation 4-34 requires the capacity of the concrete girder section without consideration of the clamping force. As discussed in section 4.3.9.2.1.3.1, four equations were considered; SMCFT (2006), ACI 318 (2014), Muttoni & Ruiz (2008), and AASHTO (2002). The capacity of a girder with a web width of 15 in., web height (through the deck) of 41 in., and a concrete compressive strength of 3000 psi using each of the four equations are shown in Table 5-15. The SMCFT method is the most conservative. Since the SMCFT method is well tested and is known

as an accurate method for calculating the shear capacity of a beam, it is used in BRIDGE to calculate the shear capacity of the beam without clamping force.

Table 5-15: Capacity of Girder with a Height of 41” & Web Width of 15” using different Capacity Eqn’s

Capacity Equation:	Capacity (kips)
SMCFT (2006)	8.76
ACI 318 (2014)	38.18
Muttoni & Ruiz (2008)	44.18
AASHTO (2002)	51.54

5.4 Analysis of Bridge No. 54-104-15.45

KDOT’s Bridge No. 54-104-15.45 displays the reverse diagonal shear cracking phenomenon and is analyzed by BRIDGE to demonstrate the program’s output and results. This bridge consists of 5 spans. Span #1 and #5 are identical, as are spans #2 and #4. The results for span #1 and #5 are discussed herein. The results for the other three spans are similar and are displayed in Appendix E. Two of each truck are placed on the bridge, one in each lane on the same side of the bridge span. Table 5-16 and Table 5-17 display the operating and inventory rating factors and truck ratings, respectively, for each standard truck option available within the program. The program uses Equation 4-34 and the described procedure to calculate the rating factors in Table 5-16. Equation 2-1 is used to determine the truck ratings shown in Table 5-17. Each truck was analyzed twice; once assuming the entire girder width provided shear resistance, and once assuming that the girder end has deteriorated to the point where only 50% of the girder width is resisting shear. As shown in Table 5-16 and Table 5-17 the girders contributing 100% of their girder width have larger shear capacities and thus larger rating factors, as is intuitive. With few exceptions, the operating RF is larger than 1 while the inventory RF is less than 1, indicating that it is up to the engineer’s judgement whether to load rate this bridge.

Table 5-16: Rating Factors for Spans #1 & #5 for 50% & 100% Girder Width

Rating:	Operating		Inventory	
b_w used:	100%	50%	100%	50%
H Unit	1.22	1.07	0.73	0.64
T 3	1.17	1.04	0.7	0.62
HS	1.11	1.01	0.67	0.6
3S2	1.19	1.06	0.72	0.63
T 3-3	1.25	1.09	0.75	0.65
T-130	1.17	1.05	0.7	0.63
T-170	1.14	1.04	0.68	0.62
HET	1.03	0.97	0.62	0.58
SU4	1.14	1.03	0.68	0.61
SU5	1.12	1.01	0.67	0.61
SU6	1.11	1.01	0.66	0.6
SU7	1.1	1	0.66	0.6
NRL	1.09	1	0.65	0.6

Table 5-17: Truck Ratings for Spans #1 & #5 for 50% & 100% Girder Width

Rating:	Operating		Inventory	
b_w used:	100%	50%	100%	50%
H Unit	15.25	13.375	9.125	8
Type 3	29.25	26	17.5	15.5
HS	24.975	22.725	15.075	13.5
3S2	42.84	38.16	25.92	22.68
Type 3-3	50	43.6	30	26
T-130	76.05	68.25	45.5	40.95
T-170	96.9	88.4	57.8	52.7
HET	113.3	106.7	68.2	63.8
SU4	30.78	27.81	18.36	16.47
SU5	34.72	31.31	20.77	18.91
SU6	38.573	35.0975	22.935	20.85
SU7	42.625	38.75	25.575	23.25
NRL	43.6	40	26	24

Chapter 6 Conclusions

Dozens of KDOT bridges built in the early-to-mid 1900s exhibit a phenomenon known as reverse diagonal shear cracking, shown in Figure 1-1. It is a concern that this cracking will result in a loss of bearing support at the girder ends. Thus, it is important to study this phenomenon to determine the cause of the reverse diagonal cracking and its effects on the capacity of the girder.

It is determined in this study that this cracking is caused by unintended frictional forces acting at the girder-to-bearing pad interface. The girders are supported on steel bearing pads and rockers instead of rubber bearing pads, as is common in new construction. Steel bearing pads and rockers rust and corrode due to decades of exposure to water and deicing salts. This corrosion prevents the rocker from rotating, turning the once pinned connection into a partially-fixed connection. When rotation of the girder is prevented a buildup of shear stress at the girder-to-bearing pad interface occurs caused by the bottom of the girder's tendency to expand towards the ends of the girder when subject to tension during the loading process. This friction force, coupled with the girder reaction, causes the reverse diagonal cracking.

The live and dead load reactions at the support, along with the friction force, act on the reverse diagonal crack as shown in Figure 4-24. These forces cause the crack-driving and crack-clamping forces as shown. From these forces, Equation 4-34 is developed to calculate the rating factor of the bridge at the girder supports. This equation is based on Equation 2-2.

The Simplified Modified Compression Field Theory is used to find the capacity of the girder 'without clamping forces'. This method was chosen because it results in the most conservative capacity estimate and it is widely accepted as a reliable method for finding the shear capacity of cracked concrete beams.

The BRIDGE program was used to load rate Bridge No. 54-104-15.45 and yielded reasonable rating factors for varying trucks and reduced girder widths. The operating rating factors were consistently above 1 while the inventory rating factors were below 1, indicating that the decision to load rate this bridge is based on the engineer's judgement.

References

- AASHTO. (2002). *Standard specifications for highway bridges* (17th ed.). Washington, D.C.: American Association of State Highway and Transportation Officials (AASHTO).
- AASHTO. (2011). Section 6: Load rating. *Manual for bridge evaluation* (2nd ed., pp. 6-i-6-i). Washington, D.C.: American Association of State Highway and Transportation Officials (AASHTO).
- AASHTO. (2014). *LRFD bridge design specifications* (7th ed.). Washington, D.C.: American Association of State Highway and Transportation Officials (AASHTO).
- ACI Committee 318. (2014). *Building code requirements for structural concrete (ACI 318-14)* American Concrete Institute (ACI).
- Al-Mahaidi, R., Taplin, G., & Giufre, A. (2000). Load distribution and shear strength evaluation of an old concrete T-beam bridge. *Transportation Research Record*, 1696
- Azizinamini, A., Boothby, T. E., Shekar, Y., & Barnhill, G. (1994a). Old concrete slab bridges I: Experimental investigation. *Journal of Structural Engineering*, 120(11)
- Azizinamini, A., Boothby, T. E., Shekar, Y., & Barnhill, G. (1994b). Old concrete slab bridges II: Analysis. *Journal of Structural Engineering*, 120(11)
- Azizinamini, A., Elremaily, A., & Choobineh, F. (2004). Advanced methodology for rating concrete slab bridges. *Structures Congress 2000: Advanced Technology in Structural Engineering*, , 103
- Beer, F. P., Johnston Jr., E. R., DeWolf, J. T., & Mazurek, D. F. (2012). Chapter 7: Transformations of stress and strain. *Mechanics of materials* (6th ed., pp. 438-438-445) McGraw-Hill.
- Bentz, E. C., Vecchio, F. J., & Collins, M. P. (2006). Simplified modified compression field theory for calculating shear strength of reinforced concrete elements. *ACI Structural Journal*, July-August, 614-614-624.
- Commander, B., & Schulz, J. (1997). Field verified load rating method for reinforced concrete slab bridges. *Building to Last: Proceedings of Structures Congress XV*, Portland, Oregon. , 2
- Dassault Systemes. (2013). *Abaqus*. Providence, RI: Dassault Systemes Simulia Corp.
- Farny, J. A., Melander, J. M., & Panarese, W. C. (2008). Appendix A: Details of concrete masonry construction. *Concrete masonry handbook* (6th ed., pp. 246) Portland Cement Association.

- KDOT. (2011). *Special bridge inspection report: Special girder end inspection for bridge no. 54-104-317.27-(0005)*. (Inspection). Topeka, KS: KDOT (Kansas Department of Transportation).
- KDOT. (2016). Bridge section - chapter 15: Bridge load rating. *KDOT design manual* (pp. 15-1-15-1 - 15-41) Kansas Department of Transportation (KDOT).
- Kumaraguru, P. (1992). *Strength of dapped-end beams*. Unpublished manuscript.
- Loov, R. E. (1998). Review of A23.3-94 simplified method of shear design and comparison with results using shear friction. *Canadian Journal of Civil Engineering*, 437-437-450.
- Muttoni, A., & Ruiz, M. F. (2008). Shear strength of members without transverse reinforcement as function of critical shear crack width. *ACI Structural Journal*, (March), 163-163-172.
- Muttoni, A., & Thurlimann, B. (1986). *Shear tests on beams and slabs without shear reinforcement*. Unpublished manuscript.
- Rabbat, B. G., & Russell, H. G. (1985). Friction coefficient of steel on concrete or grout. *Journal of Structural Engineering*, 111, 505-505-515.
- Ranasinghe, A. P., & Gottshall, W. L. (2002). Numerical load rating of reinforced concrete compression members: Demonstration with Connecticut arch bridges. *Transportation Research Record*,
- RISA Technologies, L. (2012). *Risa-3d* (10.0.1 ed.) RISA Technologies, LLC.
- Tassios, T. P., & Vintzeleou, E. N. (1987). Concrete - to - concrete friction. *Journal of Structural Engineering*, 113, 832-832-849.
- Vecchio, F. J., & Collins, M. P. (1982). The response of reinforced concrete to in-plane shear and normal stresses. *Department of Civil Engineering, University of Toronto, Ontario, Canada*, 82-03, 332.

Appendix A - Truck Types

Table A-1: Truck Axle Loads and Spacings

Truck Type	Axle #	Axle Load (kips)	Axle Spacing (ft)	
			Minimum	Maximum
H 20	1	8	-	-
	2	32	14	14
Type 3	1	16	-	-
	2	17	15	15
	3	17	4	4
HS 20	1	8	-	-
	2	32	14	14
	3	32	14	30
Type 3S2	1	10	-	-
	2	15.5	11	11
	3	15.5	4	4
	4	15.5	22	22
	5	15.5	4	4
Type 3-3	1	12	-	-
	2	12	15	15
	3	12	4	4
	4	16	15	15
	5	14	16	16
	6	14	4	4
Type T130	1	10	-	-
	2	20	15	15
	3	20	4	4
	4	20	14	14
	5	20	4	4
	6	20	30	30
	7	20	4	4
Type T170	1	16	-	-
	2	18	15	15
	3	18	4	4
	4	18	4	4
	5	20	14	14
	6	20	4	4
	7	20	30	30
	8	20	4	4
	9	20	4	4

Truck Type	Axle #	Axle Load (kips)	Axle Spacing (ft)	
			Minimum	Maximum
HET	1	21.48	-	-
	2	21.35	12.92	12.92
	3	21.16	5	5
	4	19.23	5	5
	5	25.39	15.1	15.1
	6	27.84	5.94	5.94
	7	26.29	5.94	5.94
	8	27.42	5.94	5.94
	9	29.75	5.94	5.94
SU4	1	12	-	-
	2	8	10	10
	3	17	4	4
	4	17	4	4
SU5	1	12	-	-
	2	8	10	10
	3	8	4	4
	4	17	4	4
	5	17	4	4
SU6	1	11.5	-	-
	2	8	10	10
	3	8	4	4
	4	17	4	4
	5	17	4	4
	6	8	4	4
SU7	1	11.5	-	-
	2	8	10	10
	3	8	4	4
	4	17	4	4
	5	17	4	4
	6	8	4	4
	7	8	4	4
NRL	1	6	-	-
	2	8	6	14
	3	8	4	4
	4	17	4	4
	5	17	4	4
	6	8	4	4
	7	8	4	4
	8	8	4	4

Appendix B - Stiffness Matrix

$$[K] = \begin{bmatrix} \frac{12EI}{L^3} & -\frac{6EI}{L^2}S & \frac{6EI}{L^2}C & -\frac{12EI}{L^3} & -\frac{6EI}{L^2}S & \frac{6EI}{L^2}C \\ -\frac{6EI}{L^2}S & \frac{GJ}{L}C^2 + \frac{4EI}{L}S^2 & (\frac{GJ}{L} - \frac{4EI}{L})SC & \frac{6EI}{L^2}S & -\frac{GJ}{L}C^2 + \frac{2EI}{L}S^2 & -(\frac{GJ}{L} + \frac{2EI}{L})SC \\ \frac{6EI}{L^2}C & (\frac{GJ}{L} - \frac{4EI}{L})SC & \frac{GJ}{L}S^2 + \frac{4EI}{L}C^2 & -\frac{6EI}{L^2}C & -(\frac{GJ}{L} + \frac{2EI}{L})SC & -\frac{GJ}{L}S^2 + \frac{2EI}{L}C^2 \\ -\frac{12EI}{L^3} & \frac{6EI}{L^2}S & -\frac{6EI}{L^2}C & \frac{12EI}{L^3} & \frac{6EI}{L^2}S & -\frac{6EI}{L^2}C \\ -\frac{6EI}{L^2}S & -\frac{GJ}{L}C^2 + \frac{2EI}{L}S^2 & -(\frac{GJ}{L} + \frac{2EI}{L})SC & \frac{6EI}{L^2}S & \frac{GJ}{L}C^2 + \frac{4EI}{L}S^2 & (\frac{GJ}{L} - \frac{4EI}{L})SC \\ \frac{6EI}{L^2}C & -(\frac{GJ}{L} + \frac{2EI}{L})SC & -\frac{GJ}{L}S^2 + \frac{2EI}{L}C^2 & -\frac{6EI}{L^2}C & (\frac{GJ}{L} - \frac{4EI}{L})SC & \frac{GJ}{L}S^2 + \frac{4EI}{L}C^2 \end{bmatrix}$$

Figure B-1: Stiffness Matrix as Function Member Properties

Appendix C - Support Reactions: Program vs. RISA

Table C-1: Support Reaction Comparison #2: BRIDGE Input

LOADING:				
		Truck #1:	Truck #2:	
Truck Type:		H Unit	H Unit	
Lane #:		1	2	
Direction of Travel:		Up-station	Down-station	
Truck Location:		Exiting Bridge	Entering Bridge	
Position in Lane:		Center	Center	
Analysis Level:		Inventory	Inventory	
LANE ALIGNMENT:		SECTION GEOMETRY:		
# of Lanes:	2	Girders	Height (in.):	48
Lane Width (ft.):	12		Width (in.):	12
Cantilever Width (ft.):	0	Exterior Diaphragms	Height (in.):	36
Ext. Shld. Width (ft.):	0		Width (in.):	12
Ext. Barrier Width (in.):	12	Interior Diaphragms	Height (in.):	24
Median Shld. Width (ft.):	0		Width (in.):	12
Median Barrier Width (in.):	0	Slab Thickness (in.):		8
BRIDGE MESH:				
# of Girders:	3	# of Interior Diaphragms:		2
Length of Girders (ft.):	50	# of Virtual Diaphragms		3
Tot. # of Diaphragms:	7	Diaphragm Length (ft.):		24
MATERIAL PROPERTIES:		Concrete Strength (psi)		5000

Table C-2: Support Reaction Comparison #2: Results

Reactions at Supporting Nodes: Program vs RISA			
Node:	Program (k)	RISA (k)	% Difference:
1	4.871	4.871	-0.0044%
2	4.400	4.4	0.0092%
3	1.709	1.71	-0.0391%
19	12.143	12.261	-0.9665%
20	41.573	41.336	0.5734%
21	15.304	15.423	-0.7718%

Table C-3: Support Reaction Comparison #3: BRIDGE Input

LOADING:				
		Truck #1:	Truck #2:	
Truck Type:		Heavy Equip. Trans.	H Unit	
Lane #:		1	2	
Direction of Travel:		Up-station	Down-station	
Truck Location:		Exiting Bridge	Entering Bridge	
Position in Lane:		Center	North Edge	
Analysis Level:		Operating Posting	Operating Posting	
LANE ALIGNMENT:		SECTION GEOMETRY:		
# of Lanes:	2	Girders	Height (in.):	48
Lane Width (ft.):	12		Width (in.):	5
Cantilever Width (ft.):	1	Exterior Diaphragms	Height (in.):	36
Ext. Shld. Width (ft.):	6		Width (in.):	12
Ext. Barrier Width (in.):	17	Interior Diaphragms	Height (in.):	24
Median Shld. Width (ft.):	0		Width (in.):	12
Median Barrier Width (in.):	0	Slab Thickness (in.):		8
BRIDGE MESH:				
# of Girders:	3	# of Interior Diaphragms:		2
Length of Girders (ft.):	120	# of Virtual Diaphragms		0
Tot. # of Diaphragms:	4	Diaphragm Length (ft.):		36
MATERIAL PROPERTIES:		Concrete Strength (psi)		4000

Table C-4: Support Reaction Comparison #3: Results

Reactions at Supporting Nodes: Program vs RISA			
Node:	Program (k)	RISA (k)	% Difference:
1	33.185	33.179	0.0186%
2	23.097	23.108	-0.0493%
3	10.153	10.147	0.0547%
10	67.873	67.867	0.0084%
11	86.973	86.984	-0.0124%
12	23.920	23.914	0.0240%

Table C-5: Support Reaction Comparison #4: BRIDGE Input

LOADING:				
		Truck #1:	Truck #2:	
Truck Type:		H Unit	H Unit	
Lane #:		1	2	
Direction of Travel:		Up-station	Down-station	
Truck Location:		Entering Bridge	Entering Bridge	
Position in Lane:		Center	Center	
Analysis Level:		Inventory	Inventory	
LANE ALIGNMENT:		SECTION GEOMETRY:		
# of Lanes:	2	Girders	Height (in.):	36
Lane Width (ft.):	12		Width (in.):	18
Cantilever Width (ft.):	2	Exterior Diaphragms	Height (in.):	24
Ext. Shld. Width (ft.):	6		Width (in.):	12
Ext. Barrier Width (in.):	12	Interior Diaphragms	Height (in.):	18
Median Shld. Width (ft.):	3		Width (in.):	8
Median Barrier Width (in.):	12	Slab Thickness (in.):		10
BRIDGE MESH:				
# of Girders:	4	# of Interior Diaphragms:		1
Length of Girders (ft.):	25	# of Virtual Diaphragms		4
Tot. # of Diaphragms:	7	Diaphragm Length (ft.):		38
MATERIAL PROPERTIES:		Concrete Strength (psi)		4000

Table C-6: Support Reaction Comparison #4: Results

Reactions at Supporting Nodes: Program vs RISA			
Node:	Program (k)	RISA (k)	% Difference:
1	6.567	6.589	-0.3330%
2	30.591	30.533	0.1884%
3	1.926	1.977	-2.5971%
4	0.917	0.902	1.6364%
25	0.917	0.902	1.6364%
26	1.926	1.977	-2.5971%
27	30.591	30.533	0.1884%
28	6.567	6.589	-0.3330%

Table C-7: Support Reaction Comparison #5: BRIDGE Input

LOADING:				
		Truck #1:	Truck #2:	
Truck Type:		Type 3S2 Unit	H Unit	
Lane #:		1	2	
Direction of Travel:		Up-station	Down-station	
Truck Location:		Exiting Bridge	Entering Bridge	
Position in Lane:		North Edge	South Edge	
Analysis Level:		Operating Posting	Operating Posting	
LANE ALIGNMENT:		SECTION GEOMETRY:		
# of Lanes:	2	Girders	Height (in.):	24
Lane Width (ft.):	12		Width (in.):	6
Cantilever Width (ft.):	2	Exterior Diaphragms	Height (in.):	36
Ext. Shld. Width (ft.):	6		Width (in.):	12
Ext. Barrier Width (in.):	12	Interior Diaphragms	Height (in.):	24
Median Shld. Width (ft.):	3		Width (in.):	12
Median Barrier Width (in.):	12	Slab Thickness (in.):		12
BRIDGE MESH:				
# of Girders:	4	# of Interior Diaphragms:		2
Length of Girders (ft.):	200	# of Virtual Diaphragms		3
Tot. # of Diaphragms:	7	Diaphragm Length (ft.):		40
MATERIAL PROPERTIES:		Concrete Strength (psi)		5000

Table C-8: Support Reaction Comparison #5: Results

Reactions at Supporting Nodes: Program vs RISA			
Node:	Program (k)	RISA (k)	% Difference:
1	3.037	3.035	0.0628%
2	2.297	2.302	-0.2170%
3	2.444	2.439	0.2019%
4	0.590	0.592	-0.2763%
25	14.467	14.469	-0.0152%
26	37.972	37.974	-0.0047%
27	32.636	32.624	0.0373%
28	3.557	3.564	-0.2069%

Table C-9: Support Reaction Comparison #6: BRIDGE Input

LOADING:				
	Truck #1:		Truck #2:	
Truck Type:	Type 3S2 Unit		H Unit	
Lane #:	1		2	
Direction of Travel:	Up-station		Down-station	
Truck Location:	Exiting Bridge		Entering Bridge	
Position in Lane:	North Edge		South Edge	
Analysis Level:	Operating Posting		Operating Posting	
LANE ALIGNMENT:		SECTION GEOMETRY:		
# of Lanes:	2	Girders	Height (in.):	36
Lane Width (ft.):	12		Width (in.):	18
Cantilever Width (ft.):	0	Exterior Diaphragms	Height (in.):	36
Ext. Shld. Width (ft.):	3		Width (in.):	12
Ext. Barrier Width (in.):	12	Interior Diaphragms	Height (in.):	24
Median Shld. Width (ft.):	0		Width (in.):	12
Median Barrier Width (in.):	0	Slab Thickness (in.):		8
BRIDGE MESH:				
# of Girders:	4	# of Interior Diaphragms:		2
Length of Girders (ft.):	75	# of Virtual Diaphragms		0
Tot. # of Diaphragms:	4	Diaphragm Length (ft.):		53
MATERIAL PROPERTIES:		Concrete Strength (psi)		4000

Table C-10: Support Reaction Comparison #6: Results

Reactions at Supporting Nodes: Program vs RISA			
Node:	Program (k)	RISA (k)	% Difference:
1	18.009	18.034	-0.1412%
4	7.991	7.988	0.0368%
5	34.088	34.027	0.1783%
8	6.507	6.52	-0.1956%
9	17.701	17.745	-0.2501%
12	6.092	6.075	0.2825%
13	5.887	5.878	0.1581%
16	0.726	0.733	-1.0164%

Table C-11: Support Reaction Comparison #7: BRIDGE Input

LOADING:				
		Truck #1:	Truck #2:	
Truck Type:		Type 3-3 Unit		
Lane #:		1		
Direction of Travel:		Up-station		
Truck Location:		Exiting Bridge		
Position in Lane:		Center		
Analysis Level:		Operating Posting		
LANE ALIGNMENT:		SECTION GEOMETRY:		
# of Lanes:	2	Girders	Height (in.):	24
Lane Width (ft.):	11		Width (in.):	12
Cantilever Width (ft.):	3	Exterior Diaphragms	Height (in.):	36
Ext. Shld. Width (ft.):	6		Width (in.):	12
Ext. Barrier Width (in.):	12	Interior Diaphragms	Height (in.):	24
Median Shld. Width (ft.):	0		Width (in.):	6
Median Barrier Width (in.):	0	Slab Thickness (in.):		12
BRIDGE MESH:				
# of Girders:	5	# of Interior Diaphragms:		1
Length of Girders (ft.):	60	# of Virtual Diaphragms		4
Tot. # of Diaphragms:	7	Diaphragm Length (ft.):		28
MATERIAL PROPERTIES:		Concrete Strength (psi)		5000

Table C-12: Support Reaction Comparison #7: Results

Reactions at Supporting Nodes: Program vs RISA			
Node:	Program (k)	RISA (k)	% Difference:
1	9.695	9.755	-0.6154%
2	14.055	13.943	0.8045%
3	10.591	10.687	-0.9013%
4	6.794	6.698	1.4334%
5	-1.659	-1.608	3.1908%
31	8.890	8.955	-0.7237%
32	16.094	15.955	0.8738%
33	11.023	11.146	-1.1058%
34	5.879	5.789	1.5622%
35	-1.362	-1.322	3.0483%

Table C-13: Support Reaction Comparison #8: BRIDGE Input

LOADING:				
		Truck #1:	Truck #2:	
Truck Type:		HS Unit	Type 3 Unit	
Lane #:		1	2	
Direction of Travel:		Up-station	Down-station	
Truck Location:		Exiting Bridge	Entering Bridge	
Position in Lane:		Center	Center	
Analysis Level:		Inventory	Inventory	
LANE ALIGNMENT:		SECTION GEOMETRY:		
# of Lanes:	2	Girders	Height (in.):	24
Lane Width (ft.):	12		Width (in.):	8
Cantilever Width (ft.):	1	Exterior Diaphragms	Height (in.):	36
Ext. Shld. Width (ft.):	3		Width (in.):	12
Ext. Barrier Width (in.):	8	Interior Diaphragms	Height (in.):	24
Median Shld. Width (ft.):	0		Width (in.):	6
Median Barrier Width (in.):	0	Slab Thickness (in.):		12
BRIDGE MESH:				
# of Girders:	5	# of Interior Diaphragms:		2
Length of Girders (ft.):	40	# of Virtual Diaphragms		3
Tot. # of Diaphragms:	7	Diaphragm Length (ft.):		28
MATERIAL PROPERTIES:		Concrete Strength (psi)		4000

Table C-14: Support Reaction Comparison #8: Results

Reactions at Supporting Nodes: Program vs RISA			
Node:	Program (k)	RISA (k)	% Difference:
1	8.256	8.325	-0.8242%
2	14.412	14.294	0.8288%
3	12.503	12.555	-0.4154%
4	10.304	10.274	0.2945%
5	3.207	3.235	-0.8564%
31	8.288	8.309	-0.2574%
32	18.231	18.155	0.4169%
33	30.655	30.966	-1.0047%
34	45.879	45.403	1.0494%
35	8.264	8.484	-2.5920%

Table C-15: Support Reaction Comparison #9: BRIDGE Input

LOADING:				
	Truck #1:		Truck #2:	
Truck Type:	Type 3-3 Unit		Type 3 Unit	
Lane #:	1		2	
Direction of Travel:	Up-station		Down-station	
Truck Location:	Exiting Bridge		Entering Bridge	
Position in Lane:	North Edge		South Edge	
Analysis Level:	Inventory		Inventory	
LANE ALIGNMENT:		SECTION GEOMETRY:		
# of Lanes:	2	Girders	Height (in.):	30
Lane Width (ft.):	10		Width (in.):	16
Cantilever Width (ft.):	3	Exterior Diaphragms	Height (in.):	36
Ext. Shld. Width (ft.):	3		Width (in.):	12
Ext. Barrier Width (in.):	8	Interior Diaphragms	Height (in.):	36
Median Shld. Width (ft.):	2		Width (in.):	12
Median Barrier Width (in.):	12	Slab Thickness (in.):		12
BRIDGE MESH:				
# of Girders:	5	# of Interior Diaphragms:		2
Length of Girders (ft.):	75	# of Virtual Diaphragms		0
Tot. # of Diaphragms:	4	Diaphragm Length (ft.):		23.6667
MATERIAL PROPERTIES:		Concrete Strength (psi)		4000

Table C-16: Support Reaction Comparison #9: Results

Reactions at Supporting Nodes: Program vs RISA			
Node:	Program (k)	RISA (k)	% Difference:
1	21.891	21.827	0.2919%
4	26.221	26.172	0.1866%
5	12.280	12.407	-1.0226%
8	28.609	28.701	-0.3199%
9	12.698	12.74	-0.3309%
12	41.270	41.333	-0.1522%
13	13.681	13.472	1.5486%
16	47.749	47.546	0.4278%
17	1.451	1.555	-6.6917%
20	16.150	16.249	-0.6078%

Table C-17: Support Reaction Comparison #10: BRIDGE Input

LOADING:				
		Truck #1:	Truck #2:	
Truck Type:		H Unit	HS Unit	
Lane #:		1	2	
Direction of Travel:		Up-station	Up-station	
Truck Location:		Entering Bridge	Entering Bridge	
Position in Lane:		North Edge	South Edge	
Analysis Level:		Operating Posting	Operating Posting	
		Truck #3:	Truck #4:	
Truck Type:		Type 3 Unit	H Unit	
Lane #:		3	4	
Direction of Travel:		Left Bound	Left Bound	
Truck Location:		Exiting Bridge	Exiting Bridge	
Position in Lane:		South Edge	North Edge	
Analysis Level:		Operating Posting	Operating Posting	
LANE ALIGNMENT:		SECTION GEOMETRY:		
# of Lanes:	4	Girders	Height (in.):	48
Lane Width (ft.):	10		Width (in.):	18
Cantilever Width (ft.):	5	Exterior Diaphragms	Height (in.):	24
Ext. Shld. Width (ft.):	3		Width (in.):	12
Ext. Barrier Width (in.):	18	Interior Diaphragms	Height (in.):	12
Median Shld. Width (ft.):	0		Width (in.):	8
Median Barrier Width (in.):	12	Slab Thickness (in.):		4
BRIDGE MESH:				
# of Girders:	3	# of Interior Diaphragms:		1
Length of Girders (ft.):	50	# of Virtual Diaphragms		4
Tot. # of Diaphragms:	7	Diaphragm Length (ft.):		37
MATERIAL PROPERTIES:		Concrete Strength (psi)		5000

Table C-18: Support Reaction Comparison #10: Results

Reactions at Supporting Nodes: Program vs RISA			
Node:	Program (k)	RISA (k)	% Difference:
1	24.483	24.538	-0.2243%
2	77.988	77.877	0.1421%
3	16.098	16.153	-0.3420%
19	2.309	2.315	-0.2594%
20	19.273	19.26	0.0653%
21	4.850	4.857	-0.1433%

Table C-19: Support Reaction Comparison #11: BRIDGE Input

LOADING:				
		Truck #1:	Truck #2:	
Truck Type:		Type T170 Unit	Heavy Equip. Trans.	
Lane #:		1	2	
Direction of Travel:		Up-station	Up-station	
Truck Location:		Entering Bridge	Entering Bridge	
Position in Lane:		Center	Center	
Analysis Level:		Operating Posting	Operating Posting	
		Truck #3:	Truck #4:	
Truck Type:		Type T130 Unit	Heavy Equip. Trans.	
Lane #:		3	4	
Direction of Travel:		Left Bound	Left Bound	
Truck Location:		Exiting Bridge	Exiting Bridge	
Position in Lane:		Center	Center	
Analysis Level:		Operating Posting	Operating Posting	
LANE ALIGNMENT:		SECTION GEOMETRY:		
# of Lanes:	4	Girders	Height (in.):	36
Lane Width (ft.):	12		Width (in.):	12
Cantilever Width (ft.):	6	Exterior Diaphragms	Height (in.):	24
Ext. Shld. Width (ft.):	6		Width (in.):	12
Ext. Barrier Width (in.):	8	Interior Diaphragms	Height (in.):	18
Median Shld. Width (ft.):	0		Width (in.):	8
Median Barrier Width (in.):	0	Slab Thickness (in.):		10
BRIDGE MESH:				
# of Girders:	3	# of Interior Diaphragms:		2
Length of Girders (ft.):	100	# of Virtual Diaphragms		3
Tot. # of Diaphragms:	7	Diaphragm Length (ft.):		47.333
MATERIAL PROPERTIES:		Concrete Strength (psi)		4000

Table C-20: Support Reaction Comparison #11: Results

Reactions at Supporting Nodes: Program vs RISA			
Node:	Program (k)	RISA (k)	% Difference:
1	114.990	115.043	-0.0464%
2	260.107	260.001	0.0408%
3	119.897	119.95	-0.0443%
19	64.663	64.679	-0.0241%
20	105.991	105.96	0.0294%
12	74.752	74.767	-0.0201%

Table C-21: Support Reaction Comparison #12: BRIDGE Input

LOADING:				
		Truck #1:	Truck #2:	
Truck Type:		Type T170 Unit	Heavy Equip. Trans.	
Lane #:		1	2	
Direction of Travel:		Up-station	Up-station	
Truck Location:		Entering Bridge	Entering Bridge	
Position in Lane:		Center	Center	
Analysis Level:		Operating Posting	Operating Posting	
		Truck #3:	Truck #4:	
Truck Type:		Type T130 Unit	Heavy Equip. Trans.	
Lane #:		3	4	
Direction of Travel:		Left Bound	Left Bound	
Truck Location:		Exiting Bridge	Exiting Bridge	
Position in Lane:		Center	Center	
Analysis Level:		Operating Posting	Operating Posting	
LANE ALIGNMENT:		SECTION GEOMETRY:		
# of Lanes:	4	Girders	Height (in.):	36
Lane Width (ft.):	12		Width (in.):	12
Cantilever Width (ft.):	6	Exterior Diaphragms	Height (in.):	24
Ext. Shld. Width (ft.):	6		Width (in.):	12
Ext. Barrier Width (in.):	8	Interior Diaphragms	Height (in.):	18
Median Shld. Width (ft.):	0		Width (in.):	8
Median Barrier Width (in.):	0	Slab Thickness (in.):		10
BRIDGE MESH:				
# of Girders:	3	# of Interior Diaphragms:		2
Length of Girders (ft.):	100	# of Virtual Diaphragms		0
Tot. # of Diaphragms:	2	Diaphragm Length (ft.):		47.333
MATERIAL PROPERTIES:		Concrete Strength (psi)		4000

Table C-22: Support Reaction Comparison #12: Results

Reactions at Supporting Nodes: Program vs RISA			
Node:	Program (k)	RISA (k)	% Difference:
1	120.519	120.543	-0.0197%
2	249.081	249.034	0.0188%
3	125.393	125.417	-0.0188%
10	66.528	66.534	-0.0091%
11	102.229	102.215	0.0135%
12	76.650	76.657	-0.0095%

Table C-23: Support Reaction Comparison #13: BRIDGE Input

LOADING:				
		Truck #1:	Truck #2:	
Truck Type:		Type 3S2 Unit	H Unit	
Lane #:		1	2	
Direction of Travel:		Up-station	Up-station	
Truck Location:		Entering Bridge	Exiting Bridge	
Position in Lane:		Center	Center	
Analysis Level:		Inventory	Inventory	
		Truck #3:	Truck #4:	
Truck Type:		Type T130 Unit	Type T170 Unit	
Lane #:		3	4	
Direction of Travel:		Left Bound	Left Bound	
Truck Location:		Entering Bridge	Exiting Bridge	
Position in Lane:		Center	Center	
Analysis Level:		Inventory	Inventory	
LANE ALIGNMENT:		SECTION GEOMETRY:		
# of Lanes:	4	Girders	Height (in.):	24
Lane Width (ft.):	12		Width (in.):	8
Cantilever Width (ft.):	0	Exterior Diaphragms	Height (in.):	24
Ext. Shld. Width (ft.):	3		Width (in.):	8
Ext. Barrier Width (in.):	8	Interior Diaphragms	Height (in.):	16
Median Shld. Width (ft.):	3		Width (in.):	8
Median Barrier Width (in.):	12	Slab Thickness (in.):		6
BRIDGE MESH:				
# of Girders:	4	# of Interior Diaphragms:		1
Length of Girders (ft.):	125	# of Virtual Diaphragms		4
Tot. # of Diaphragms:	7	Diaphragm Length (ft.):		61
MATERIAL PROPERTIES:		Concrete Strength (psi)		4000

Table C-24: Support Reaction Comparison #13: Results

Reactions at Supporting Nodes: Program vs RISA			
Node:	Program (k)	RISA (k)	% Difference:
1	45.792	45.793	-0.0014%
2	86.691	86.693	-0.0029%
3	104.374	104.367	0.0063%
4	118.311	118.314	-0.0029%
25	4.042	4.046	-0.0869%
26	86.718	86.718	-0.0004%
27	141.489	141.479	0.0074%
28	78.583	78.590	-0.0084%

Table C-25: Support Reaction Comparison #14: BRIDGE Input

LOADING:				
		Truck #1:	Truck #2:	
Truck Type:		Type 3-3 Unit	Type T130 Unit	
Lane #:		1	2	
Direction of Travel:		Up-station	Up-station	
Truck Location:		Exiting Bridge	Exiting Bridge	
Position in Lane:		Center	Center	
Analysis Level:		Inventory	Inventory	
		Truck #3:	Truck #4:	
Truck Type:				
Lane #:				
Direction of Travel:				
Truck Location:				
Position in Lane:				
Analysis Level:				
LANE ALIGNMENT:		SECTION GEOMETRY:		
# of Lanes:	4	Girders	Height (in.):	24
Lane Width (ft.):	10		Width (in.):	8
Cantilever Width (ft.):	1	Exterior Diaphragms	Height (in.):	24
Ext. Shld. Width (ft.):	3		Width (in.):	8
Ext. Barrier Width (in.):	8	Interior Diaphragms	Height (in.):	16
Median Shld. Width (ft.):	0		Width (in.):	8
Median Barrier Width (in.):	0	Slab Thickness (in.):		6
BRIDGE MESH:				
# of Girders:	4	# of Interior Diaphragms:		2
Length of Girders (ft.):	125	# of Virtual Diaphragms		3
Tot. # of Diaphragms:	7	Diaphragm Length (ft.):		44
MATERIAL PROPERTIES:		Concrete Strength (psi)		5000

Table C-26: Support Reaction Comparison #14: Results

Reactions at Supporting Nodes: Program vs RISA			
Node:	Program (k)	RISA (k)	% Difference:
1	39.775	39.767	0.0201%
2	26.594	26.619	-0.0951%
3	28.497	28.472	0.0878%
4	2.917	2.925	-0.2708%
25	82.263	82.289	-0.0312%
26	117.950	117.897	0.0448%
27	56.182	56.209	-0.0486%
28	-0.178	-0.178	-0.2407%

Table C-27: Support Reaction Comparison #15: BRIDGE Input

LOADING:				
		Truck #1:	Truck #2:	
Truck Type:		Type 3-3 Unit	Type 3-3 Unit	
Lane #:		1	2	
Direction of Travel:		Up-station	Up-station	
Truck Location:		Exiting Bridge	Exiting Bridge	
Position in Lane:		Center	Center	
Analysis Level:		Inventory	Inventory	
		Truck #3:	Truck #4:	
Truck Type:		Type 3 Unit	H Unit	
Lane #:		3	4	
Direction of Travel:		Left Bound	Left Bound	
Truck Location:		Entering Bridge	Entering Bridge	
Position in Lane:		South Edge	North Edge	
Analysis Level:		Inventory	Inventory	
LANE ALIGNMENT:		SECTION GEOMETRY:		
# of Lanes:	4	Girders	Height (in.):	36
Lane Width (ft.):	12		Width (in.):	12
Cantilever Width (ft.):	3	Exterior Diaphragms	Height (in.):	36
Ext. Shld. Width (ft.):	3		Width (in.):	12
Ext. Barrier Width (in.):	8	Interior Diaphragms	Height (in.):	16
Median Shld. Width (ft.):	3		Width (in.):	12
Median Barrier Width (in.):	12	Slab Thickness (in.):		8
BRIDGE MESH:				
# of Girders:	4	# of Interior Diaphragms:		2
Length of Girders (ft.):	60	# of Virtual Diaphragms		0
Tot. # of Diaphragms:	4	Diaphragm Length (ft.):		54.333
MATERIAL PROPERTIES:		Concrete Strength (psi)		5000

Table C-28: Support Reaction Comparison #15: Results

Reactions at Supporting Nodes: Program vs RISA			
Node:	Program (k)	RISA (k)	% Difference:
1	52.812	52.844	-0.0602%
4	49.858	49.911	-0.1066%
5	73.042	72.967	0.1030%
8	88.513	88.415	0.1112%
9	19.670	19.725	-0.2775%
12	84.281	84.318	-0.0439%
13	0.115	0.104	10.8286%
16	27.708	27.716	-0.0290%

Table C-29: Support Reaction Comparison #16: BRIDGE Input

LOADING:				
		Truck #1:	Truck #2:	
Truck Type:		Heavy Equip. Trans.	Type T170 Unit	
Lane #:		1	2	
Direction of Travel:		Up-station	Up-station	
Truck Location:		Exiting Bridge	Exiting Bridge	
Position in Lane:		North Edge	South Edge	
Analysis Level:		Inventory	Inventory	
		Truck #3:	Truck #4:	
Truck Type:		Type 3-3 Unit	Type T130 Unit	
Lane #:		3	4	
Direction of Travel:		Left Bound	Left Bound	
Truck Location:		Entering Bridge	Entering Bridge	
Position in Lane:		South Edge	North Edge	
Analysis Level:		Inventory	Inventory	
LANE ALIGNMENT:		SECTION GEOMETRY:		
# of Lanes:	4	Girders	Height (in.):	36
Lane Width (ft.):	12		Width (in.):	18
Cantilever Width (ft.):	3	Exterior Diaphragms	Height (in.):	24
Ext. Shld. Width (ft.):	3		Width (in.):	12
Ext. Barrier Width (in.):	12	Interior Diaphragms	Height (in.):	24
Median Shld. Width (ft.):	3		Width (in.):	12
Median Barrier Width (in.):	12	Slab Thickness (in.):		8
BRIDGE MESH:				
# of Girders:	5	# of Interior Diaphragms:		1
Length of Girders (ft.):	90	# of Virtual Diaphragms		4
Tot. # of Diaphragms:	7	Diaphragm Length (ft.):		54
MATERIAL PROPERTIES:		Concrete Strength (psi)		5000

Table C-30: Support Reaction Comparison #16: Results

Reactions at Supporting Nodes: Program vs RISA			
Node:	Program (k)	RISA (k)	% Difference:
1	84.409	84.48	-0.0837%
2	132.906	132.735	0.1290%
3	75.796	75.912	-0.1524%
4	54.987	54.988	-0.0014%
5	46.302	46.285	0.0365%
31	107.212	107.322	-0.1029%
32	206.007	205.719	0.1398%
33	108.477	108.756	-0.2563%
34	105.658	105.520	0.1310%
35	86.045	86.083	-0.0436%

Table C-31: Support Reaction Comparison #17: BRIDGE Input

LOADING:				
		Truck #1:	Truck #2:	
Truck Type:		H Unit	Type 3 Unit	
Lane #:		1	2	
Direction of Travel:		Up-station	Up-station	
Truck Location:		Exiting Bridge	Exiting Bridge	
Position in Lane:		North Edge	South Edge	
Analysis Level:		Inventory	Inventory	
		Truck #3:	Truck #4:	
Truck Type:		HS Unit	Type 3 Unit	
Lane #:		3	4	
Direction of Travel:		Left Bound	Left Bound	
Truck Location:		Entering Bridge	Entering Bridge	
Position in Lane:		South Edge	North Edge	
Analysis Level:		Inventory	Inventory	
LANE ALIGNMENT:		SECTION GEOMETRY:		
# of Lanes:	4	Girders	Height (in.):	36
Lane Width (ft.):	12		Width (in.):	18
Cantilever Width (ft.):	3	Exterior Diaphragms	Height (in.):	24
Ext. Shld. Width (ft.):	3		Width (in.):	12
Ext. Barrier Width (in.):	12	Interior Diaphragms	Height (in.):	24
Median Shld. Width (ft.):	3		Width (in.):	12
Median Barrier Width (in.):	12	Slab Thickness (in.):		8
BRIDGE MESH:				
# of Girders:	5	# of Interior Diaphragms:		2
Length of Girders (ft.):	90	# of Virtual Diaphragms		3
Tot. # of Diaphragms:	7	Diaphragm Length (ft.):		54
MATERIAL PROPERTIES:		Concrete Strength (psi)		5000

Table C-32: Support Reaction Comparison #17: Results

Reactions at Supporting Nodes: Program vs RISA			
Node:	Program (k)	RISA (k)	% Difference:
1	5.164	5.167	-0.0501%
2	6.975	6.968	0.0998%
3	6.652	6.661	-0.1372%
4	7.026	7.021	0.0739%
5	4.864	4.866	-0.0378%
31	17.424	17.453	-0.1662%
32	77.635	77.564	0.0919%
33	48.463	48.556	-0.1914%
34	58.055	57.965	0.1557%
35	55.741	55.780	-0.0702%

Table C-33: Support Reaction Comparison #18: BRIDGE Input

LOADING:				
		Truck #1:	Truck #2:	
Truck Type:		H Unit	Type T170 Unit	
Lane #:		1	2	
Direction of Travel:		Up-station	Up-station	
Truck Location:		Exiting Bridge	Exiting Bridge	
Position in Lane:		North Edge	South Edge	
Analysis Level:		Inventory	Inventory	
LANE ALIGNMENT:		SECTION GEOMETRY:		
# of Lanes:	4	Girders	Height (in.):	36
Lane Width (ft.):	12		Width (in.):	18
Cantilever Width (ft.):	3	Exterior Diaphragms	Height (in.):	24
Ext. Shld. Width (ft.):	3		Width (in.):	12
Ext. Barrier Width (in.):	12	Interior Diaphragms	Height (in.):	24
Median Shld. Width (ft.):	3		Width (in.):	12
Median Barrier Width (in.):	12	Slab Thickness (in.):		8
BRIDGE MESH:				
# of Girders:	5	# of Interior Diaphragms:		2
Length of Girders (ft.):	90	# of Virtual Diaphragms		0
Tot. # of Diaphragms:	4	Diaphragm Length (ft.):		54
MATERIAL PROPERTIES:		Concrete Strength (psi)		5000

Table C-34: Support Reaction Comparison #18: Results

Reactions at Supporting Nodes: Program vs RISA			
Node:	Program (k)	RISA (k)	% Difference:
1	31.984	31.991	-0.0226%
4	45.123	45.138	-0.0338%
5	65.260	65.247	0.0203%
8	98.490	98.462	0.0282%
9	29.926	29.942	-0.0544%
12	35.817	35.836	-0.0522%
13	15.736	15.713	0.1477%
16	16.093	16.078	0.0922%
17	-5.983	-5.971	0.1939%
20	-6.446	-6.437	0.1391%

Appendix D - ABAQUS Models: Shear & Normal Forces

Table D-1: Forces at One Support for ABAQUS Models with a Girder Width of 12 in.

Beam Model	Normal Force (lbs.)	Shear Force (lbs.)
12-0.4-6-7	15999.7	2391.6
12-0.4-6-8	16001	3115.2
12-0.4-6-9	18002.2	4865
12-0.4-6-10	16002.5	4815.5
12-0.4-6-11	16003.5	5788.9
12-0.4-6-12	18006.9	8438.3
12-0.4-6-13	18009.2	9803.3
12-0.4-6-14	26024	14834
12-0.4-6-17	26042.4	14842
12-0.4-8-7	15980.7	2406.1
12-0.4-8-12	18006.9	8537.2
12-0.4-8-17	26038.7	14842
12-0.4-10-7	16000.63	2417.6
12-0.4-10-12	18007.1	8639.2
12-0.5-6-7	16000.74	2321.3
12-0.5-6-12	16006.54	6856.4
12-0.5-8-7	16000.77	2344
12-0.5-8-12	16006.82	6969.4
12-0.5-10-7	16000.76	2348
12-0.5-10-12	16007.02	7044.3
12-0.6-6-7	8000.11	593.26
12-0.6-6-12	16008	6842.8
12-0.6-8-7	8000.125	599.09
12-0.6-8-12	15988.45	6966.7
12-0.6-10-7	8000.133	599.24
12-0.6-10-12	16008.95	7022

Table D-2: Forces at One Support for ABAQUS Models with a Girder Width of 15 in.

Beam Model	Normal Force (lbs.)	Shear Force (lbs.)
15-0.4-6-7	16000.38	2067.6
15-0.4-6-12	26010.25	13897
15-0.4-8-7	16000.4	2066.2
15-0.4-8-12	26010.06	13949
15-0.4-10-7	16000.43	2076.5
15-0.4-10-12	26010.22	14085
15-0.5-6-7	16000.43	2020.5
15-0.5-6-12	18005.22	7253.5
15-0.5-8-7	16000.49	2030.6
15-0.5-8-12	18005.24	7328.8
15-0.5-10-7	16000.44	2042
15-0.5-10-12	18005.4	7420.2
15-0.6-6-7	16000.56	1969.2
15-0.6-6-12	16004.75	5866.1
15-0.6-8-7	16000.54	1981.3
15-0.6-8-12	16004.86	5950.4
15-0.6-10-7	16000.54	1996
15-0.6-10-12	16005.04	6031.4

Table D-3: Forces at One Support for ABAQUS Models with a Girder Width of 18 in.

Beam Model	Normal Force (lbs.)	Shear Force (lbs.)
18-0.4-6-7	16000.3	1826.9
18-0.4-6-8	18000.7	2936.3
18-0.4-6-9	18000.9	3685.5
18-0.4-6-10	26157.5	8900.4
18-0.4-6-11	26005	10518
18-0.4-6-12	26006.9	12317
18-0.4-6-13	34016.6	19389
18-0.4-8-7	16000.28	1814.3
18-0.4-8-12	26006.61	12275
18-0.4-10-7	16000.23	1815.4
18-0.4-10-12	26006.58	12333
18-0.5-6-7	16000.28	1788.5
18-0.5-6-12	26008.83	12376
18-0.5-8-7	16000.28	1786.7
18-0.5-8-12	26008.84	12417
18-0.5-10-7	16000.32	1794
18-0.5-10-12	26008.84	12535
18-0.6-6-7	16000.34	1755.4
18-0.6-6-12	18004.13	6380.4
18-0.6-8-7	16000.37	1762.2
18-0.6-8-12	18004.16	6438.1
18-0.6-10-7	16000.39	1772.3
18-0.6-10-12	18004.31	6518

Appendix E - RF and Truck Ratings for Bridge # 54-104-15.45

Table E-1: Rating Factors for Spans #2 & #4 for 50% & 100% Girder Width

Rating:	Operating		Inventory	
b_w used:	100%	50%	100%	50%
H Unit	1.24	1.09	0.74	0.65
T 3	1.19	1.05	0.71	0.63
HS	1.12	1.01	0.67	0.61
3S2	1.19	1.05	0.71	0.63
T 3-3	1.24	1.09	0.74	0.66
T-130	1.18	1.06	0.71	0.64
T-170	1.13	1.04	0.68	0.62
HET	0.97	1.03	0.58	0.62
SU4	1.16	1.04	0.69	0.62
SU5	1.13	1.02	0.68	0.61
SU6	1.12	1.01	0.67	0.61
SU7	1.1	1.01	0.66	0.6
NRL	1.1	1	0.66	0.6

Table E-2: Truck Ratings for Spans #2 & #4 for 50% & 100% Girder Width

Rating:	Operating		Inventory	
b_w used:	100%	50%	100%	50%
H Unit	15.5	13.625	9.25	8.125
Type 3	29.75	26.25	17.75	15.75
HS	40.32	36.36	24.12	21.96
3S2	42.84	37.8	25.56	22.68
Type 3-3	49.6	43.6	29.6	26.4
T-130	76.7	68.9	46.15	41.6
T-170	96.05	88.4	57.8	52.7
HET	106.7	113.3	63.8	68.2
SU4	31.32	28.08	18.63	16.74
SU5	35.03	31.62	21.08	18.91
SU6	38.92	35.0975	23.2825	21.198
SU7	42.625	39.1375	25.575	23.25
NRL	44	40	26.4	24

Table E-3: Rating Factors for Span #3 for 50% & 100% Girder Width

Rating:	Operating		Inventory	
b_w used:	100%	50%	100%	50%
H Unit	1.28	1.11	0.77	0.67
T 3	1.21	1.07	0.73	0.64
HS	1.13	1.02	0.68	0.61
3S2	1.19	1.06	0.71	0.64
T 3-3	1.25	1.11	0.75	0.66
T-130	1.19	1.07	0.71	0.64
T-170	1.14	1.04	0.68	0.62
HET	1.03	0.97	0.62	0.58
SU4	1.18	1.05	0.71	0.63
SU5	1.15	1.04	0.69	0.62
SU6	1.13	1.03	0.68	0.61
SU7	1.12	1.02	0.67	0.61
NRL	1.11	1.01	0.66	0.61

Table E-4: Truck Ratings for Span #3 for 50% & 100% Girder Width

Rating:	Operating		Inventory	
b_w used:	100%	50%	100%	50%
H Unit	16	13.875	9.625	8.375
Type 3	30.25	26.75	18.25	16
HS	40.68	36.72	24.48	21.96
3S2	42.84	38.16	25.56	23.04
Type 3-3	50	44.4	30	26.4
T-130	77.35	69.55	46.15	41.6
T-170	96.9	88.4	57.8	52.7
HET	113.3	106.7	68.2	63.8
SU4	31.86	28.35	19.17	17.01
SU5	35.65	32.24	21.39	19.22
SU6	39.268	35.7925	23.63	21.198
SU7	43.4	39.525	25.9625	23.638
NRL	44.4	40.4	26.4	24.4